**ALI RIAZ**

# FUNCTIONALIZED POLYHEDRAL OLIGOMERIC SILSESQUIOXANE (POSS) FOR INCORPORATION OF CHEMICALLY PENDANT CHAINS

# UTILIZAÇÃO DE SILSESQUIOXANOS OLIGOMÉRICOS POLIÉDRICOS FUNCIONALIZADOS (POSS) NO ANCORAMENTO DE CADEIAS ORGÂNICAS À SUPERFÍCIE

**CAMPINAS**

**2014**

**UNIVERSIDADE ESTADUAL DE CAMPINAS**

**INSTITUTO DE QUÍMICA**

**ALI RIAZ**

# FUNCTIONALIZED POLYHEDRAL OLIGOMERIC SILSESQUIOXANE (POSS) FOR INCORPORATION OF CHEMICALLY PENDANT CHAINS

**ORIENTADOR / SUPERVISOR: PROF. DR. JOSÉ DE ALENCAR SIMONI**

# UTILIZAÇÃO DE SILSESQUIOXANOS OLIGOMÉRICOS POLIÉDRICOS FUNCIONALIZADOS (POSS) NO ANCORAMENTO DE CADEIAS ORGÂNICAS À SUPERFÍCIE

TESE DE DOUTORADO APRESENTADA AO INSTITUTO DE QUÍMICA DA UNICAMP PARA OBTENÇÃO DO TÍTULO DE DOUTOR EM CIÊNCIAS.

Doctorate thesis presented to the Institute of Chemistry of the University of Campinas to obtain the Ph.D. in Sciences.

**ESTE EXEMPLAR CORRESPONDE À VERSÃO FINAL DA TESE DEFENDIDA POR ALI RIAZ E ORIENTADA PELO PROF. DR. JOSÉ DE ALENCAR SIMONI.**

_____

**Assinatura do Orientador**

**CAMPINAS**

**2014**

Ficha catalográfica
Universidade Estadual de Campinas
Biblioteca do Instituto de Química
Simone Lucas Gonçalves de Oliveira - CRB 8/8144

Riaz, Ali, 1981-
R351f Functionalized polyhedral oligomeric silsesquioxane (POSS) for incorporation of chemically pendant chains / Ali Riaz. – Campinas, SP : [s.n.], 2014.

Orientador: José de Alencar Simoni.
Tese (doutorado) – Universidade Estadual de Campinas, Instituto de Química.

1. Silsesquioxanos oligoméricos. 2. Dióxido de carbono. 3. Calorimetria. I. Simoni, José de Alencar. II. Universidade Estadual de Campinas. Instituto de Química. III. Título.

Informações para Biblioteca Digital

**Título em outro idioma:** Utilização de silsesquioxanos oligoméricos poliédricos funcionalizados (POSS) no ancoramento de cadeias orgânicas à superfície
**Palavras-chave em inglês:**
Oligomeric silsesquioxanes
Carbon dioxid
Calorimetry
**Área de concentração:** Química Inorgânica
**Titulação:** Doutor em Ciências
**Banca examinadora:**
José de Alencar Simoni [Orientador]
Alzira Maria Serpa Lucho
Oyrton Azevedo de Castro Monteiro Junior
Pedro Luiz Onófrio Volpe
Pedro Paulo Corbi
**Data de defesa:** 27-03-2014
**Programa de Pós-Graduação:** Química

Dedicated to my Family and Teachers

**ACKNOWLEDGEMENT**

First of all I would like to thank Allah for giving me the opportunity to come to Brazil for PhD and have kept me close to many people with whom I have learned a lot about life.

I would like to thank to those people who made it possible for me the realization of this thesis.

- To my parents and my family, for their endless affection, support, encouragement, without demanding anything in return.
- To Professor José de Alencar Simoni, for being an excellent supervisor and mentor, for all his valuable advices, patience and endless help.
- Special thanks to Professor Claudio Airoldi for his full cooperation as an advisor during my studies.
- To my laboratory colleagues for providing a stimulating environment to learn and grow. I am especially grateful to all my Pakistani, Brazilian and Indian friends for their support and well wishes.
- It is a pleasure for me to thank those professors who were the members of my doctoral general examination committee: Pedro Paulo Corbi, Carlos Henrique Inacio Ramos and Italo Odone Mazali.
- Teachers who participated in my thesis qualification; José de Alencar Simoni, Pedro Luiz Onófrio Volpe, Claudio Airoldi, Italo Odone Mazali, for their valuable contributions in discussions to complete this thesis.
- I would like to thank the technical staff of the Institute of Chemistry, UNICAMP, Raquel (CHN), Fabiana (TG), Anderson (NMR), Renata (XRD-ICP), Daniel (SEM), Alice (Lab A1-100) CPG staff especially Isabel, which greatly helped me during the course of my studies and all others who directly or indirectly contributed to the completion of my work.
- I owe my deepest gratitude to TWAS (The World Academy of Sciences) and CNPq (National Council for Scientific and Technological Development) for their financial support.

Ali Riaz

*Curriculum Vitae*

# Ali Riaz

## ACADEMICS

| | | | |
|---|---|---|---|
| **Ph.D** | | | **03/2010 – 03/2014** |
| Chemical Sciences | **UNICAMP** | -Universidade Estadual de Campinas | SP - Brazil |
| **M.Sc** | | | **09/2002 – 02/2005** |
| Inorganic Chemistry | **UOP** | -University of Peshawar | KPK - Pakistan |
| **B.Sc** | | | **09/2000 – 02/2002** |
| Biological Sciences | **GPGCC** | -Govt Pos-Grad. College CHD. | KPK - Pakistan |
| **F.Sc** | | | **03/1997 – 02/1999** |
| Pre-Medical | **GPGCC** | -Govt Pos-Grad. College CHD. | KPK - Pakistan |

## Articles

1. **RIAZ, A.**, AIROLDI, C., SIMONI, J. A. "*Functionalized polyhedral oligomeric silesquioxane for incorporation of chemically pendant chains."* Journal of Materials Research (Internal assessment)

2. **RIAZ, A.**, AIROLDI, C., SIMONI, J. A. "*Polyhedral oligomeric silsesquioxanes loaded with polyethylenamine: as filter for $CO_2$ at low pressure."* International Journal of Greenhouse Gas Control (Internal Assessment)

3. **RIAZ, A.**, AIROLDI, C., SIMONI, J. A. "*Polyethylenamine, Phenyl and Methacrylate anchored Polyhedral Oligomeric Silsesquioxanes: Synthesis, Characterization and its sorption capacity for heavy metals."* Journal of Environmental Protection (Internal Assessment)

## Presentations in Events

1. **RIAZ, A.**, AHMED, K., AIROLDI, C., SIMONI, J. A.
*Polyhedral oligomeric silsesquioxanes loaded with polyethyleneimine: synthesis, spectral characterization and comparison.* (Congress) "**Pure and Applied Chemistry International Conference (PACCON)**, 2013, Thailand.

2. **RIAZ, A.**, AIROLDI, C., SIMONI, J. A.
*Amino-Functionalized Silsesquioxanes and their derivatives as filters for heavy metals and $CO_2$.* (Congress) "**Pittcon**", 2013, USA.

3. **RIAZ, A.**, AIROLDI, C., SIMONI, J. A.
   *Glycidoxy, Phenyl and Methacrylate anchored Polyhedral Oligomeric Silsesquioxanes: Synthesis and Characterization.* (Congress) "**12th Annual UNESCO / IUPAC Workshop and Conference on Macromolecules & Materials**," 2013, South Africa.

4. **RIAZ, A.**, CORREA, A. C., AHMED, K., AHMAD, A., ULLAH, I., RASHID, H. U.
   *Gamma irradiation a safe way to extend shelf life of dired Figs*. (Meeting) "**IX Brazilian Meeting on Chemistry of Food and Beverages"**, 2012, Brazil.

5. **RIAZ, A.**, AIROLDI, C., SIMONI, J. A.
   *Silsesquioxanos Poliédricos Oligoméricos carregados com Polietilenoimina: Síntese, Caracterização e Comparações Espectrais*. (Workshop) "**X Workshop em Fisica Molecular e Espectrooscopia"**, 2012, Brazil.

6. CORREA, A. C., **RIAZ, A.**
   *Desenvolvimento de metodologia para determinação de gordura e proteína em bebidas lácteas utilizando calibração multivariada e infravermelho próximo. (Symposium)* "**9 SLACA - Simpósio Latino Americano De Ciência De Alimentos"**, 2011, Brazil.

7. **RIAZ, A.**, CORREA, A. C., AIROLDI, C., ULLAH, H., SIMONI, J. A.
   *Functionalized polyhedral oligomeric silesquioxane for incorporation of chemically pendant chains*. (Meeting) **"X Encontro da SBPMat Gramado-RS"**, 2011, Brazil.

8. ULLAH, H., CURTI, G. J., **RIAZ, A.**, SIMONI, J. A.
   *Metabolismo no solo e calorimetria isotérmica: uma combinação única.* (Congress) "**34ª Reunião Anual da Sociedade Brasileira de Química"**, 2011, Brazil.

9. **RIAZ, A.**, CORREA, A. C., SHAH, Z.
   *Time dependent radiolytic changes in ficus carica using $^{60}$Co as a Gamma radiation source., (Symposium)* "**9 SLACA - Simpósio Latino Americano De Ciência De Alimentos"**, 2011, Brazil.

Abstract

This report presents the synthesis and characterization of POSS compounds having cubic silsesquioxane cage to which the organic pendant chains are anchored. The project was started with the idea to synthesize the cubic silsesquioxanes with organofunctionalized pendant chains, which are able to capture heavy metals, dyes and some acids like $CO_2$. But in the beginning the hurdles like low % yields (30-37 %) and long reaction times (5-35 days) were to be faced. The reactions were worked out to enhance the % yields as well as to reduce the reaction time. Some modifications in reaction routes have been introduced, which brought up remarkable improvements in the results, where yield was increased upto 64 % and reaction time was reduced to 1 day. All the synthesized products were then characterized for their structure elucidations using different physical techniques like FTIR, CHN, TGA, $^{13}$CNMR & $^{29}$SiNMR in solid state, where Si—O cages of all compounds were elaborated through $^{29}$Si-NMR in solid state as well as through their respective FTIR patterns, while the pendant chains anchored to the POSS cages were confirmed using $^{13}$C-NMR results along with their respective FTIR spectra. The synthesized compounds were then tested for their thermal stability using the TGA technique. After optimizing the synthesis of cubic silsesquioxanes, hybrids PAA-13-3, PAA-MTC and PAA-Ph were worked out for their abilities of capturing divalent cations like $Cu^{2+}$, $Cd^{2+}$ and $Pb^{2+}$ from their aqueous solutions, where $Cu^{2+}$ showed higher affinity of sorption than other two bivalent metals. These sorption systems were analyzed using the ICP-OES. To explain the sorption behaviour of these samples some statistical models like Langmuir, Freundlich, Sips, Temkin and Redlich-Peterson were applied to the sorption data, where the data for $Cu^{2+}$ on to PAA-13-3 was best fitted by Langmuir adsorption isotherm model showing the sorption to be monolayer, while in case of PAA-MTC and PAA-Ph Freundlich model was found to be a best fit, confirming multilayer sorption. One of the synthesized materials (PAA-13-3) was also evaluated for its ability to adsorb gaseous $CO_2$ and was proved to be promising in removing $CO_2$, even at low pressures (max. 100 mmHg). The adsorption of $CO_2$ in the material is also studied by solid-gas adsorption calorimetry through a calorimeter especially developed for this system, where enthalpy of adsorption values were found to be between -7 and -36 kJ mol$^{-1}$.

Resumo:

Este trabalho apresenta a síntese e caracterização de compostos silsesquioxanos gaiola cúbica (POSS) com cadeias orgânicas pendentes. O projeto foi iniciado com a idéia de sintetizar os silsesquioxanos cúbicos com cadeias organofuncionalizadas ancoradas, capazes de capturar os metais pesados, corantes e $CO_2$. Mas foram enfrentadas algumas dificuldades como baixo rendimento (30-37%) e longo tempo de reação (5-35 dias). As reações foram investigadas para melhorar o rendimento, bem como para reduzir o tempo de reação. Algumas modificações em rotas de reação foram introduzidas, o que trouxe melhorias notáveis nos resultados, onde o rendimento aumentou cerca de 64 % e o tempo de reação foi reduzido para 24 horas em média. Na sequência, os produtos sintetizados foram caracterizados para elucidar suas estruturas, utilizando diferentes técnicas físicas tais como FTIR, CHN, XRD, MEV, TGA, $^{13}$CNMR e $^{29}$SiNMR no estado sólido, onde as gaiolas Si-O de todos os compostos foram evidenciadas por meio de $^{29}$SiRMN e dos seus espectros de FTIR, enquanto as cadeias ancorados às gaiolas de POSS foram confirmadas utilizando os resultados de $^{13}$CRMN, juntamente com seus respectivos espectros de FTIR. Os compostos sintetizados também foram testados quanto à sua estabilidade térmica utilizando a técnica de TGA. Após a otimização da síntese de silsesquioxanos cúbicos, os híbridos PAA-13-3, PAA-MTC e PAA-Ph foram avaliados por suas habilidades de captação de cátions bivalentes, tais como $Cu^{2+}$, $Cd^{2+}$ e $Pb^{2+}$ de suas soluções aquosas, sendo que o $Cu^{2+}$ apresentou maior afinidade de sorção em relação aos dois metais. Estes sistemas de sorção foram analisados através ICP-OES. Para explicar o comportamento de sorção destas amostras alguns modelos estatísticos como Langmuir, Freundlich, Temkin e Redlich-Peterson foram aplicadas, onde os dados de sorção de $Cu^{2+}$ em PAA-13-3 foram melhor ajustados pelo modelo Langmuir, mostrando ser uma sorção monocamada, enquanto que no caso do PAA-MTC e PAA-Ph modelo de melhor ajuste foi o Freundlich, confirmando a sorção de múlti camadas. Um dos materiais sintetizados (PAA-13-3) foi avaliado quanto à sua capacidade de adsorver $CO_2$ gasoso, mostrando-se promissor na remoção de $CO_2$, mesmo a baixas pressões (máx. 100 mm Hg). A adsorção de $CO_2$ no material também foi estudada por calorimetria de adsorção gás-sólido, em um calorímetro especialmente desenvolvido para tal, observando-se valores de entalpia de adsorção entre -36 e -7 kJ $mol^{-1}$.

Contents

# List of Figures:

# List of Tables:

# Abbreviations:

| Abbreviation | Detailed Terminology |
|---|---|
| $a_R$ | Redlich–Peterson isotherm constant (1/mg) |
| $a_S$ | Sips isotherm model constant (L/mg) |
| $A_T$ | Tempkin isotherm equilibrium binding constant (L/g) |
| $Q_L$ | maximum monolayer coverage capacities (mg/g) |
| $b_T$ | Tempkin isotherm constant |
| $C_e$ | equilibrium concentration (mg/L) |
| **B** | Redlich– Peterson isotherm exponent |
| $K_F$ | Freundlich isotherm constant (mg/g) |
| $K_L$ | Langmuir isotherm constant (L/mg) |
| $K_{RP}$ | Redlich–Peterson isotherm constant (L/g) |
| $K_S$ | Sips isotherm model constant (L/g) |
| **N** | adsorption intensity |
| $q_e$ | Amount of adsorbate in the adsorbent at equilibrium (mg/g) |
| **R** | universal gas constant (8.314J/molK) |
| $R^2$ | correlation coefficient |
| **T** | temperature (K) |
| $\beta_S$ | Sips isotherm model exponent |
| $Q_s$ | Sips maximum capacity parameter ($dm^3$/mg) |
| **POSS** | Polyhedral oligomeric silsesquioxane |
| $T_n$ | $[RSiO_{3/2}]_n$ |
| **NMR** | Nuclear magnetic resonance spectroscopy |
| **TGA** | Thermogravimetric analysis |
| **PAA-12** | $Si_8O_{12}[(CH_2)_3Cl]_8$ |
| **PAA-13** | $Si_8O_{12}[(CH_2)_3NH_2]_8$ |
| **PAA-13-2** | $Si_8O_{12}[(CH_2)_2NH(CH_2)_2NH_2]_8$ |
| **PAA-13-3** | $Si_8O_{12}[(CH_2)_2NH(CH_2)_2NH(CH_2)_2NH_2]_8$ |
| **PAA-GDP** | $Si_8O_{12}[(CH_2)_3O(CH_2)_2O]_8$ |
| **PAA-MTC** | $Si_8O_{12}[(CH_2)_3O(CO)C(CH_2)CH_3]_8$ |
| **PAA-Ph** | $Si_8O_{12}Ph_8$ |
| **GDS** | Gas Dosing System |
| **FTIR** | Fourier Transformed Infra-red Spectroscopy |
| **WPXRD** | Wide angel Powder X-Ray Diffraction |
| **SEM** | Scanning Electron microscopy |
| **X@$T_nR_n$** | X is entrapped in POSS endohedral cage |
| **Ppm** | Parts per million |
| **$cm^{-1}$** | IR spectral unit |
| **Nm** | Nanometer |
| **Å** | Angstrom |
| **Θ** | Angle of reflection |
| **IUPAC** | International Union of pure and applied chemisty |
| **M** | Mass of the adsorbent |
| **ICP-OES** | Inductively coupled plasma optical emission spectroscopy |
| **Mmol** | Millimole |
| $R_L$ | Langmuir dimensionless constant |

# 1. Introduction:

## 1.1. Hybrid Materials:

The rise of technological human civilization is directly tied to the development of more advanced materials. Until the 20th century, this meant making stronger materials, a process that generally meant higher temperature of processing. However, with the progress in higher temperature processing materials and the limitations of the available energy, was need to see how Nature has solved the same challenges, without using high temperatures at all. One result of this new approach is the class of materials called hybrid organic-inorganic materials.

Nature uses organic materials derived from biological sources to organize the formation of complex hierarchical structures that are often dramatically stronger than the inorganic material would normally be expected. Animals use proteins to template the formation of complex hierarchical structures with amazing improvements to strength and to complex function. Calcium carbonate is the most commonly used material along with calcium phosphate in bone and silica in sponges. Calcium carbonate is generally very weak (chalk), however as a hybrid organic-inorganic composite it can be very strong, as in nacre or mother of pearl. In nacre the thin plate-like bricks of aragonite are glued together with elastic protein to give a strong tough material. Cracks oriented perpendicular to the plates into the nacre has to expend energy at all of the interfaces in order to propagate. The small size of the plates and their organization gives rise to the opalescence typical of mother of pearl.

In plants, silica is more commonly used than calcium carbonate. In many grasses and leafy plants, silica structures called “phytoliths” are templated by carbohydrates to provide structural materials when located inside the plant and to

defense against herbivores, when at the surface. The saw tooth structure on the grass blade makes eating the plant less appetizing.

***Figure 1:*** *Maya blue used by ancient Mayans, Structure of the hybrid organic-inorganic dye.*

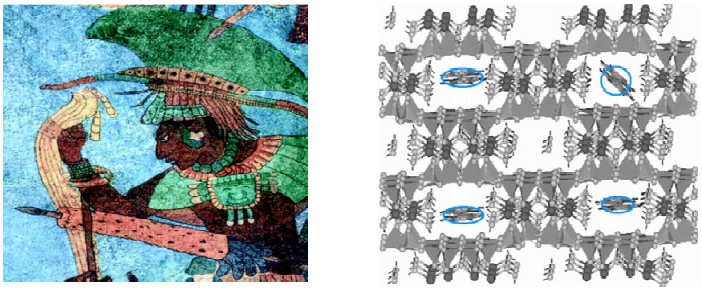

(a) (b)

Ancient Mayans used a hybrid organic-inorganic material made from the organic dye indigo and clay, where in the flat dye fits into pores in the clay, normally occupied by water molecules. There it is protected from oxidation and leaching, making this the longest lived organic based dye. Another blue dye (Han blue) also survives from ancient times, but it is solely based on a transition metal in clay without any organics. Some of the earliest hybrids in modern times are based on dyes encapsulated into a metal oxide matrix. This can be viewed as a step beyond using alumina mordants or fixing agents to prevent the color in dyed cloth from running.

As far as man-made materials are concerned, the possibility to combine properties of organic and inorganic components for materials design and processing is a very old challenge that likely started since ages (Egyptian inks, green bodies of ceramics, prehistoric frescos are some of the examples). However, the so-called hybrid organic–inorganic materials are not simply physical mixtures. They can be broadly defined as nanocomposites with organic and inorganic components, intimately mixed. Indeed, hybrids are either homogeneous systems derived from monomers and miscible organic and inorganic components, or heterogeneous

systems (nanocomposites) where at least one of the components domains has a dimension ranging from some angstroms to several nanometers.[1]

At first glance, these materials are considered as biphasic materials, where the organic and inorganic phases are mixed at the nanometer to sub-micrometer scales. However, it is obvious that the properties of these materials are not just the sum of the individual contributions from both phases. These materials may be divided into two distinct classes. In class-I, organic and inorganic compounds are embedded and only weak bonds (hydrogen, van der waals forces) give the cohesion to the whole structure. In class-II, the two phases are linked together through strong chemical bonds (covalent or ionic-covalent bonds).[2]

The introduction of these hybrid materials has led the researchers towards the development of new materials, mainly when covalent molecules are incorporated on inorganic or organometallic polymers, which investigations are devoted to improve properties of these surfaces. Among a series of them, there are amorphous silicas, which play an important role in many different fields of the chemistry; there are other siliceous material used, for example, as adsorbents and fillers in acid-catalyzed reactions or as catalyst supports. The silica properties are strongly affected by the nature and number of their surface silanol groups, which effectively varied using different calcination conditions. Thus, silica and other similar siliceous materials can react with various organic and inorganic substrates, which make possible to change the properties of the original material, where immobilizing process drives to desirable molecules.[3-7]

In principle, a lot of molecules can be immobilized, with specific intentions, onto a variety of inorganic surfaces. For this purpose, efforts are progressively improved to design new materials, in order to embrace characteristics having significant practical advantages, such as those related to structural and thermal stability,

swelling behavior, accessibility to the reactive centers, and insolubility in organic and aqueous solvents.[9-13] The main feature is the search of new silylating agents to improve the characteristics of the surface chemistry for enhancing immobilization procedures, by employing the homogeneous and the heterogeneous synthetic routes, whose the principal focus is to apply the new surface in academic or technological applications.[9-11]

As it is known, the success of a synthetic process for any class of organofunctionalized surfaces is based on new silylating agents, which can be used to obtain chemically modified surfaces through immobilization via sol-gel process in mesoporous silica and hybrids containing lamellar arrangements. In principle, all of these new surfaces display the silylating moieties covalently bonded to the inorganic framework. The availability of basic centers attached to the pendant chains is the desired agent to develop many practical utilities.[4,6,7,9-13]

One of the most fashionable feature research fields was recently expanded for inorganic polymers, containing silicon atoms disposed in well-established arrangement. This class of compounds, named polyhedral oligomeric silesquioxane (POSS), can act as monomers of polymers for applications in new chemical technology for the nanoreinforced inorganic-organic hybrids.[14-20] Thus, the polymeric incorporating POSS monomers are becoming the focus of many studies due to the simplicity in processing and the excellent comprehensive properties of this class of hybrid materials, consisting of rigid silica cores surrounded by symmetrically distributed functional groups.[11]

The recent development of several families of functional hybrids based on POSS affords a tremendous potential for modification of inorganic-organic hybrid polymers, mainly when are associated with convenient molecules covalently bonded to the inorganic structure. The typical POSS monomers possess the

structure of cube-octameric frameworks with eight organic corner groups, one or more of which can, in principle, be reactive or polymerizable.[17] Therefore, the appropriated design permits obtaining covalent inorganic-organic links on the nanoscale dimension.[21] The cubic octafunctional molecule are an ideal nanosized starting material for the synthesis of dendritic-like polymers, which application depends on their composition and, first of all, on the type of organic substituents bonded on any silicon atoms.[22] The choice of an appropriated pendant organic molecule proceeding from the original silylating agent, in which are attached basic groups, or even the possibility in expanding the covalent chain through other reactions, is a convenient way to enrich the resulting final pendant molecules to use such new material in extracting many adsorption species from a liquid fluid.[12]

The potential applicability of these inorganic materials for removal and pre-concentration of metal ions, as well as textile dyes from solutions is of fundamental importance, especially in environmental studies. Thus, the monitoring and removing these species from natural water are essential to reduce the possible effects of these contaminants on the normal life of a given community, due to the fact that the presence of high concentrations can affect water and foods, to cause many risks to mankind.[23-25]

## 1.2. Introduction to Silsesquioxanes:

Polyhedral oligomeric silsesquioxanes (POSS) are one type of hybrid inorganic/organic material of the form $(RSiO_{3/2})_n$, abbreviated $R_nT_n$, where organic substituents ($R_n$) are attached to a silicon-oxygen cage. The most common POSS cage is the $R_8T_8$, a molecule with a cubic array of silicon atoms and bridging oxygen atoms with eight R groups at the vertexes of the cube; other cages with well-defined geometries include $n$ = 6, 10, 12, 14, 16, and 18, as shown is Fig 2.[26]

***Figure 2:*** *Structures of silsesquioxanes with n = 6, 8, 10 and 12*

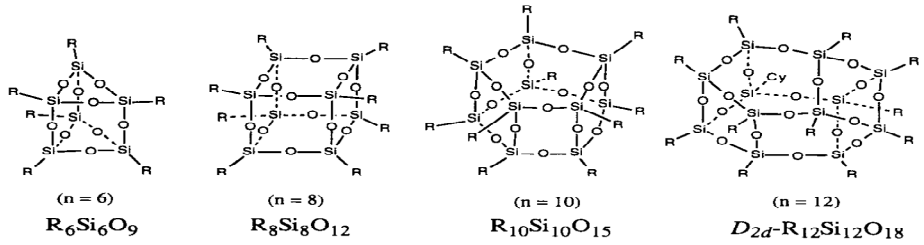


## 1.2.1. Types of Silsesquioxanes:

On the bases of structure, silsesquioxanes may be divided into two main groups. a) Completely condensed silsesquioxanes, in which the cage is completely closed through silicon oxygen bonding as shown in Fig. 3(a). In these compounds, oxygen just acts as bridge between two silicon atoms, and no hydroxyl group is present. b) Incompletely condensed silsesquioxanes contain silanol groups (Si–OH) that make them available as ligands for metal coordination, as shown In Fig. 3(b).

***Figure 3:*** *silsesquioxanes completely condensed (a), incompletely condensed (b).*

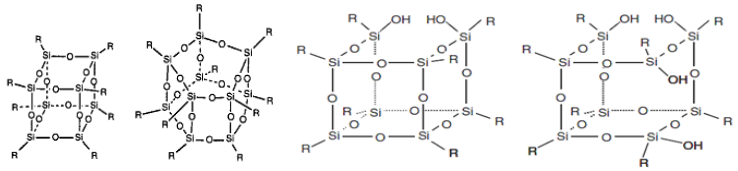

**(a)** **(b)**

## 1.2.2. Nomenclature:

The etymology of the term "silsesquioxane" (Sil = "Silicon", Sesqui = "a half" and ane = "organic pendat chain") [$(RSiO_{1.5})_n$] refers to the 1:5 ratio between silicon and oxygen atoms (from the Latin semisque – "and a half "). Structurally, silsesquioxanes consists of $sp^3$ hybridized Si atoms bound to three oxygen atoms and one R group, where in R is typically an organic moiety as mentioned above. When n = 4, 6, 8, 10, or 12, the resulting compounds are called polyhedral

oligomeric silsesquioxanes and possess three dimensional, symmetrical structures. In the specific instance where n = 8, the silsesquioxane octamers are referred to as cubic silsesquioxanes or simply "cubes." Alternatively they are called "POSS" (trademarked by Hybrid Plastics, Inc., but here after referred to as cubes). Cubes have been the focus of many studies due to their nanometer size, high degree of symmetry, and numerous preparative routes to useful quantities.[27-29] When n = ∞ the compounds are polymeric and known simply as polysilsesquioxanes. While the actual structure of polysilsesquioxanes [typically referred to as "T Resins" (see below for nomenclature)] has been the subject of much debate,[30,31] it is believed that the polymer chains contain a variety of structures including linear chain, open-caged, and ladder-like structures, depending on the reaction conditions employed.[32-35]

The shorthand notation for silicon atoms in a silicon-oxygen framework uses letters to denote the types of silicon and numerical subscripts and optional superscripts to denote the number and type of functional groups, respectively. Silicon bound to three oxygen atoms is commonly referred to as a "T" unit. Similarly, an "M" unit consists of silicon bound to one oxygen, a "D" unit has a silicon atom bound to two oxygen atoms, and a "Q" unit is silicon bound to four oxygen atoms (Table 1). The number of Si atoms is denoted by a subscript and the symbol for additional valences occupied by organic substituents is appended to the letter designation as a superscript. For example, $T_8H$ ($H_8Si_8O_{12}$) refers to a silsesquioxane cage structure containing eight silicon atoms, each connected to three oxygen atoms and one hydrido group. For simplicity, this is often shortened to "hydrido $T_8$" or "octahydrido" with understanding by those in the field.

*Table 1. Description of the Silicon Structures*

| **Silicon Species** | General Formula | Valency | Nomenclature |
|---|---|---|---|
| Siloxy | $[R_3SiO_{1/2}]$ | Mono | M |
| Siloxane | $[R_2SiO_{2/2}]$ | Di | D |
| Silsesquioxane | $[RSiO_{3/2}]$ | Tri | T |
| Silicate | $[SiO_{4/2}]$ | Quaternary | Q |

### 1.2.3. Silsesquioxanes as Nanoplatforms:

Since the ability to precisely tailor the macroscopic properties of a material requires manipulating component organization at the finest (nanometer) length scales, highly symmetrical nanobuilding blocks are required to minimize structural defects and maximize periodicity from the nanometer to the macroscopic length scales. These nanobuilding blocks should be easily prepared and modifiable (via chemical synthesis) to tailor to the property needs of the material. Clearly, nanocomponents that are easily made and whose properties and assembly can be closely controlled with high homogeneity could have a significant impact on the development of new nanomaterials. The polyhedral octameric ($T_8$), decameric ($T_{10}$), and dodecameric ($T_{12}$) cages are shown above in Figures 2a and 2b. The $T_8$, $T_{10}$, and $T_{12}$ silsesquioxanes have Oh, D5h, and D2d symmetry, respectively. The $T_{10}$ and $T_{12}$ cages are typically never found as the only products, but usually as by-products in the synthesis of $T_8$ cages.[36] Of particular interest are the highly symmetric cubic silsesquioxanes (Figure 3a), which are unique spherical organic/inorganic molecules consisting of rigid silica cores with eight vertices (vertex body diagonal = 0.53 nm) each containing an organic moiety. They are 1-2 nm in diameter with volumes < 2 $nm^3$ with each organic functional group located in a separate octant in Cartesian space, orthogonal or in opposition to each other. The positioning of the functional groups, the variety possible, and their size

provide unique opportunities to build nanocomposites in 2- or 3-D. In addition, the silica core makes these compounds thermally quite robust, adding to their utility in applications where in typical organics fail.

***Figure 4:*** *Dimensions of Octahydral oligomeric silsesauioxanes*

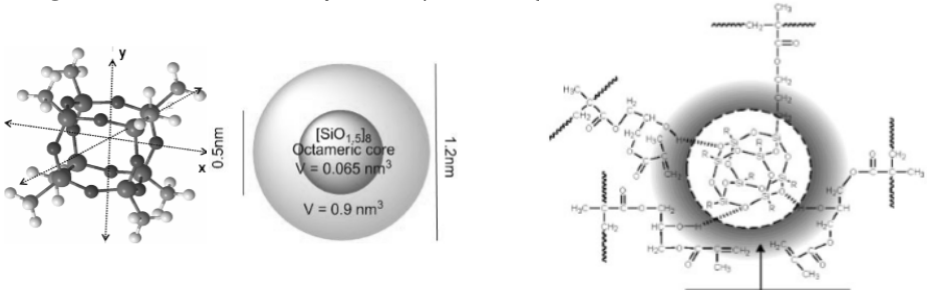


The construction of materials nanometer-by-nanometer should lead to the design of a variety of materials with well-defined nanoarchitectures and novel predictable behaviors. As "ideal" nanobuilding blocks, polyhedral silsesquioxanes allow for subsequent and selective chemical modification to provide a wide variety of derivatives, thus permitting specific assembly of these molecular components into larger, well-defined structures with tailorable properties. The synthesis, functionalization, characterization and application of cubic silsesquioxanes are the focus of this thesis.

### 1.2.4. History of Silsesquioxane:

The history of the POSS materials describes that Buff, Wohler[37] and Ladenburg[38] were attempting to synthesize silicon analogs of carboxylic acids, XSiOOH and were mistaken for anhydrides of the latter, $(XSiO)_2O$. Later on, Friedel and Ladenburg[39] and other researchers[40-42] reported such types of compounds, but these authors did not suspect that the obtained solids of the general formula $(XSiO_{1.5})_n$ might contain volatile polyhedral oligosilsesquioxanes. The first successful synthesis of well-defined POSS structure $(CH_3SiO_{1.5})_n$ was reported by Scott in 1946.[43] After decades of inactivity, the research on POSS was started again since

the discovery of preparing polymerizable POSS in the 1990s. Meanwhile, much attention has been given to polyhedral oligomeric silsesquioxanes (POSS), especially to octahedral octasilsesquioxanes ($T_8$), having an octacyclic inorganic silicon and oxygen framework covered externally by various organic substituents. Among all the reported types of POSS, the octasilsesquioxanes have shown a great potential for many applications such as electronics, optics, surface-modified supports and catalyst.[44-47]

## 1.3. Formation of Silsesquioxanes:

### 1.3.1. Hydrolytic Condensation of $RSiX_3$:

The most common synthetic route to obtain octameric silsesquioxanes is the hydrolytic condensation of monosilanes $RSiX_3$ (X = Cl, OMe, OEt)[48] , the general reaction is shown as under.

$$RSiX_3 + 3H_2O \rightarrow RSi(OH)_3 + 3HX \qquad \text{equation 1}$$

$$a RSi(OH)_3 \rightarrow (RSiO1.5)_a(H_2O)_{0.5b} + (1.5_a – 0.5_b)H_2O \qquad \text{equation 2}$$

This is a two step reaction. In the first step hydrolysis of the monosilane precursor occurs to give the corresponding trisilanol[49]. The first step is usually fast. The second step is the condensation of the trisilanol to yield different silsesquioxane species.

During the synthesis of the cube a control of the reaction conditions must be made to avoid the formation of polysilsesquioxanes and to favor the formation of cube.[50,53,55,56] The main conditions for the synthetic preparation of the silsesquioxanes is the initial monomer concentration, the solvent used, the nature of the substituent "R" of the starting monomer, the temperature reaction, the addition of water and the solubility of polyhedral oligomer formed.

In accordance with the high reactivity of the trifunctional organosilicates, the synthesis of these oligomers should be in inorganic or organic solvent along with the presence of water or some acid or base. A high concentration of monomer favors the formation of polysilsesquioxane while dilute solutions are used in order to favor the intramolecular cyclization, leading to formation of polyhedral oligomer.

The silsesquioxanes can be formed in both polar and nonpolar solvents. However, the concentration of monomer depends on the solvent. In an alcoholic medium, a diluted concentration is favorable, while in solvents such as benzene, toluene, cyclohexane and many more, this value should be greater, as reported.[50, 55] The smaller and less branched substituent X favors the conditions for the hydrolytic condensation of $XSiY_3$ forming the cube.[56]

Condensation reaction is a multistep process involving the formation of many different intermediate structures, as illustrated in Fig 5.[50]

***Figure 5:*** *Proposed mechanism of formation for the completely condensed silsesquioxane*

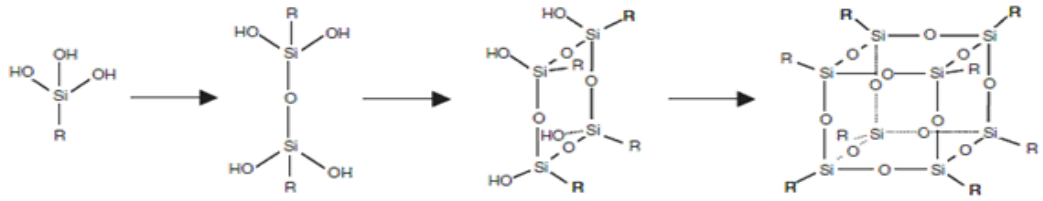

For instance, Brown[58] et al. explained this process in the case of the synthesis of completely condensed phenylsilsesquioxanes ($Ph_8Si_8O_{12}$), they proposed the reaction to proceed by the consecutive formation of the dimer, the cyclic tetramer and, finally, the cubic silsesquioxane. A standard acid hydrolysis is characterized by a very long reaction time (5 weeks) and low yield (from 27 to 31%).[22, 57] Another method makes use of the hydrolysis in acidic medium (HCl), but with the subsequent condensation conducted in basic medium ($NH_4OH$). This method leads

to yields of condensation products exceeding 90 %. However, the reaction product is a mixture of various oligomeric silsesquioxanes, and the selectivity for the target product $(T\text{-}PrCl)_8$ is very low.[59, 60]

### 1.3.2. Corner-Capping Reactions

This method was used by Feher and coworkers to obtain the cubic silsesquioxane from the incompletely condensed structure (Fig. 6).[61] The reaction of the cyclohexyl silsesquioxane $(c\text{-}C_6H_{11})_7Si_7O_9(OH)_3$ with an organotrichlorosilane $RSiCl_3$ in the presence of an amine offers a straightforward route to various monosubstituted octa- silsesquioxanes.

***Figure 6:*** *Corner-capping reaction. Chex = c-$C_6H_{11}$*

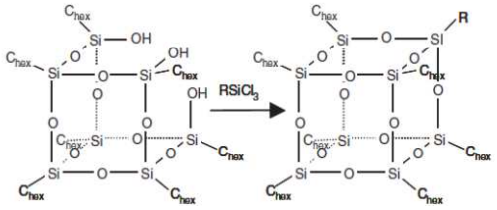


The syntheses of $T_8R_7R'$ derivatives from partially condensed silsesquioxanes all follow the same general reaction scheme shown as under,

$$R_7Si_7O_9(OH)_3 + RSiX_3 \xrightarrow{\text{base}} T_8R_7R' \quad X = Cl, \text{O-alkyl} \qquad \text{Scheme1}$$

where a partially condensed silsesquioxane, $R_7Si_7O_9(OH)_3$, or its sodium salt, $Na_3[R_7Si_7O_9(O)_3]$, reacts with a chloro- or alkoxysilane, often in the presence of a base such as $NEt_3$ or a tetraalkylammonium hydroxide.

Gießmann[62] and coworkers used $Cy_7Si_7O_9(OH)_3$ (where Cy = c-$C_6H_{11}$) Hexachloro-disilane, $Si_2Cl_6$, and hexachlorodisiloxane, $Si_2OCl_6$, reagents for the synthesis of novel functional silsesquioxanes. Reactions between $Cy_7Si_7O_9(OH)_3$ (where Cy = c-$C_6H_{11}$) and either $Si_2Cl_6$ or $Si_2OCl_6$, respectively, were carried out in toluene solution. Reactions in a 1:1 mole ratio in the presence of 3 equivalents

of triethylamine afforded their respective novel trichlorosilanes products as is illustrated in Fig 7**.**

***Figure 7:*** *Preparation of $Cy_7Si_8O_{12}SiCl_3$ and $Cy_7Si_8O_{12}OSiCl_3$*

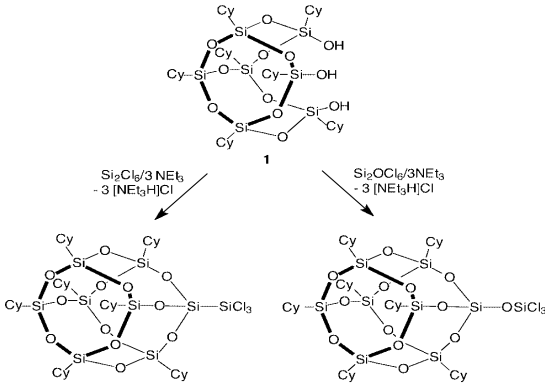


## 1.3.3. Synthesis of POSS Compounds by Hydrosilylation

A type of reaction in which the reaction between Si-H and an unsaturated compound such as an alkene or alkyne, occurs in the presence of a catalyst, often platinum, is called hydrosilylation. In case of POSS derivatives, the hydrosilylation reaction can be summarized in general as follows.

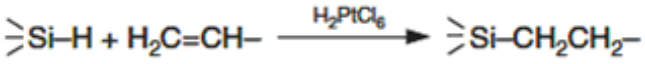


Equatio 3,

The yields of such a reaction are often high, especially in the cases of simple alkyl-functionalized alkenes.[26] Kim and coworkers[63] reported the synthesis of octa(2-(p-chloro-benzyl)ethyl)-octasilsesquioxane using hydrosilylation method. They treated octa(hydridosi1sesquioxane) with vinylbenzyl chloride in the presence of 1,2-dimethoxy- ethane solution of $H_2PtCl_6H_2O$ as a catalyst. The reaction is shown in the Fig 8.

***Figure 8:*** *Synthesis of octa(2-(p-chloro-benzyl)ethyl)-octasilsesquioxane*

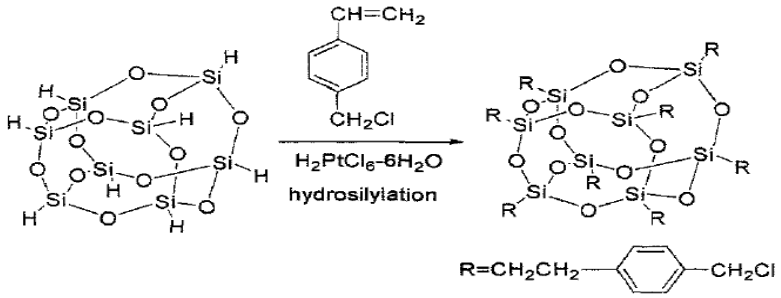


Fu and coworkers[64] in 2004 carried out a hydrosilation reaction by treating $T_8R_7CH_2CH{=}CH_2$ with 1,4-bis (dimethyl-silyl) benzene to synthesis the POSS complex $(c\text{-}C_5H_9)_7[Si_8O_{12}]\text{-}((CH_2)_3SiMe_2(C_6H_4)SiMe_2H)$. The schematic reaction is shown in Fig 9.

***Figure 9:*** *Preparation of* $(c\text{-}C_5H_9)_7[Si_8O_{12}]\text{-}((CH_2)_3SiMe_2(C_6H_4)SiMe_2H)$

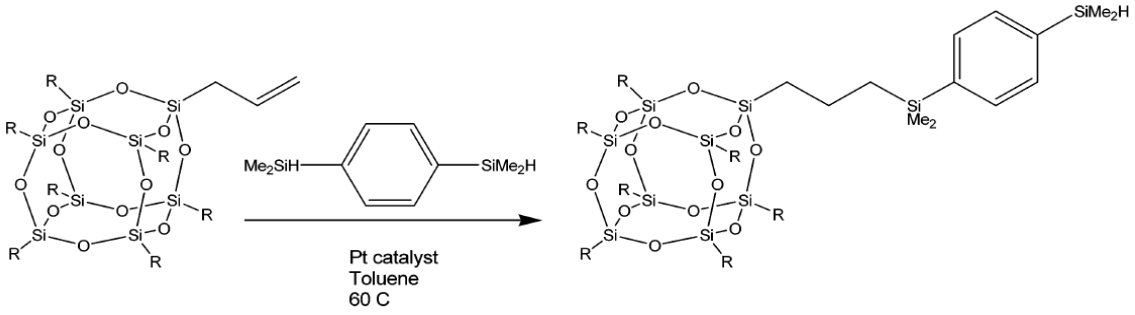


## 1.3.4. Synthesis of Bridged POSS Compounds:

Such reactions have been used to form linked multi-$T_8$ species, both in cases with simple oxygen bridges between two $T_8$ derivatives and in cases partially condensed silsesquioxane bridges.

Anderson and coworkers[65] synthesized cyclohexyl POSS dimer $[(c\text{-}C_6H_{11})_7Si_8O_{12}]_2O$ and cyclohexyl POSS trimer $[Cy_7Si_8O_{12}]_2[exo,exo\text{-}Cy_8Si_8O_{13}]$, shown in Fig 10 and 11.

***Figure 10:*** *Synthesis of POSS Dimers*

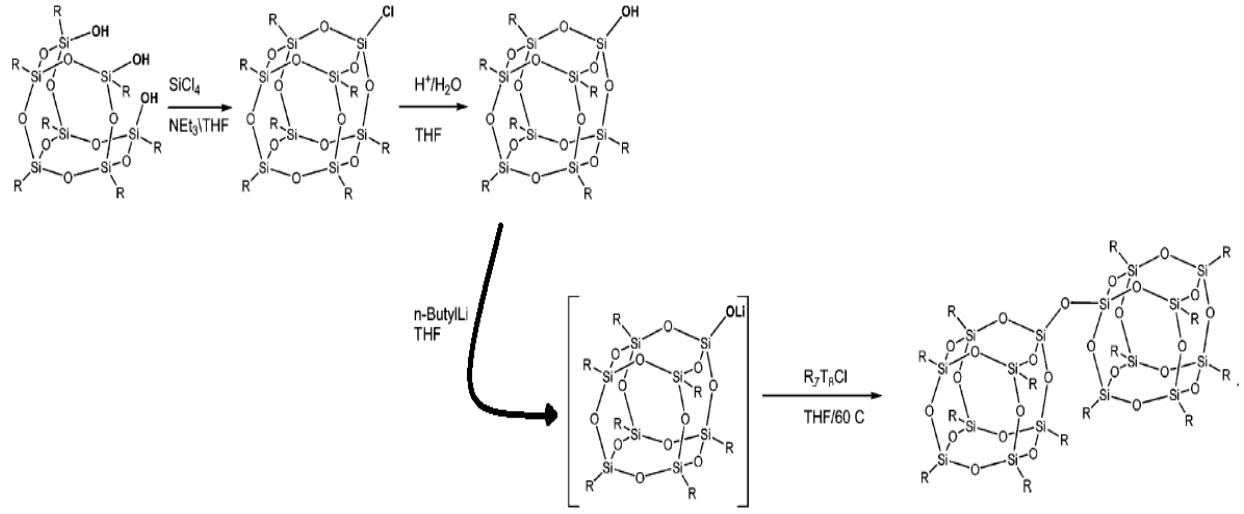


***Figure 11:*** *Synthesis of the Cyclohexyl POSS Trimer*

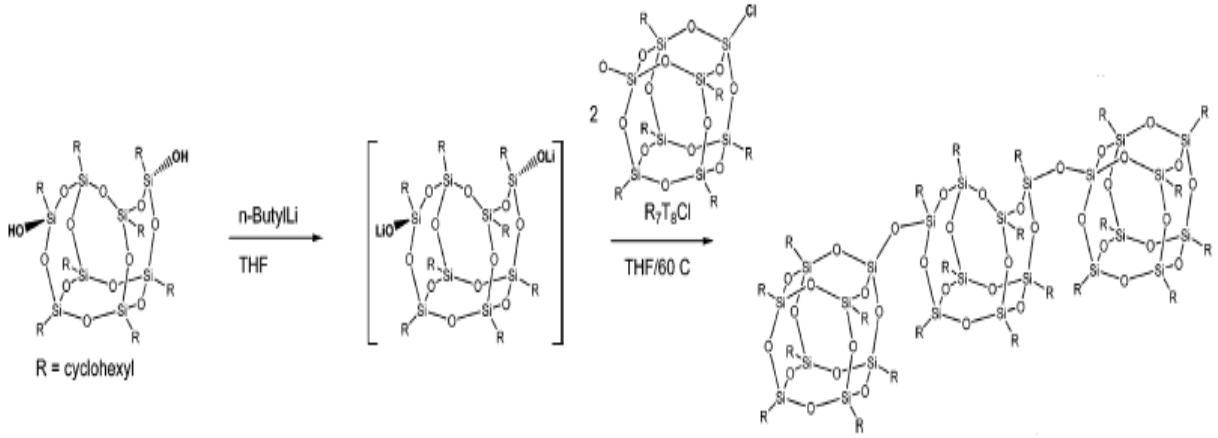


## 1.3.5. Synthesis of Endohedral POSS Compounds

POSS derivatives in which an atom or ion is encapsulated inside the POSS cage thus forming endohedral complex are called endohedral POSS compounds as shown in Fig 12. Such atom or ion may be introduced either during the initial synthesis of the POSS or as a post-synthetic modification.

***Figure 12:*** *Endohedral POSS Compounds*

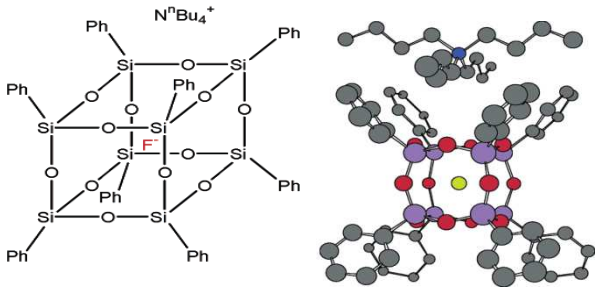


Fluoride anions are among the most commonly introduced species and it can be done by two methods. Bassindale and coworkers[67] reported fluoride ion entrapment in octasilsesquioxane cages endohedral species. They prepared $[NBu_4][F@T_8\text{-}(CH{=}CH_2)_8]$, tetrabutylammonium octavinyloctasilsesquioxane fluoride, by treating vinyltriethoxysilane with tetrabutylammonium fluoride. Similarly $[NBu_4][F@T_8\text{-}(C_6H_4\text{-}4\text{-}Me)_8]$, tetrabutylammonium octa-p-tolyloctasilsesquioxane, Fluoride was synthesized from p-Tolyltriethoxysilane and then tetrabutylammonium fluoride.[66, 67] The presence of the fluoride anion within the POSS cage has been confirmed both by $^{19}F$ NMR spectroscopy and single-crystal X-ray diffraction studies.

Similar endohedral complexes have also been prepared by the reaction of $T_8R_8$ compounds with tetrabutylammonium fluoride, with varying results.[26] For the reaction of $T_8$ species with electron-withdrawing functional groups, the endohedral complexes $[NMe_4][F@T_8Ph_8]$, $[NMe_4][F@T_8\text{-}(CH{=}CH_2)_8]$, $[NMe_4]$-$[F@T_8(CH{=}CHPh)_8]$, $[NMe_4]\{F@T_8\text{-}[(CH_2)_2CF_3]_8\}$, $[NMe_4]\{F@T_8[(CH_2)_2(CF_2)_3$-$CF3]_8\}$, and $[NMe_4][F@T_8[(CH_2)_2(CF_2)_5CF_3]_8]$ could be prepared and isolated, whereas for $T_8$ species containing solely electrondonating functional groups, such as $T_8Me_8$, $T_8Et_8$, $T_8Cy_8$, and $T_8(i\text{-}Bu)_8$, no reaction was observed.[26]

Atomic hydrogen has also been encapsulated within the $T_8$ cage, forming the endohedral complex $H@T_8(OSiMe_3)_8$, by $\gamma$-irradiation of the empty $T_8(OSiMe_3)_8$

cage in air.[68] Studies of the trapping and detrapping of H atoms in a variety of POSS cages, including $T_8$, $T_{10}$, and $T_{12}$ species, and ESR spectra of the endohedral complexes have recently been reviewed.[69]

### 1.3.6. Modification of Substituents To Prepare POSS Compounds

There has been significant efforts in systematically investigating the modification of $T_8$ POSS compounds by organic synthetic reactions. A wide range of substitution reactions such as nitration, bromination, sulfunation, Suzuki reactions, organic ring substitution reaction and many more has been attempted with $T_8$ POSS compounds.

Nitration[70] is a general chemical process for the introduction of a nitro group into a chemical compound. Takahashi et al (2006) prepared an aminophenyl-silsesquioxanes, dodecaamino- phenylsilsesquioxane $(NH_2PhSiO_{1.5})_{12}$ (DAPS), and hexadecaaminooctaphenylsilsesquioxane $((NH2)_2PhSiO_{1.5})_8$ (HDAPS), from dodecaphenylsilsesquioxane $(PhSiO_{1.5})_{12}$ (DPS), and octa- phenylsilsesquioxane $(PhSiO_{1.5})_8$ (OPS), by nitration in fuming $HNO_3$, followed by reduction with $HCO_2H$ /$Et_3N$/Pd/C. The scheme of the reactions are shown in Fig 13 and 14 as under.

***Figure 13:*** *schematic reaction for the synthesis of DAPS*

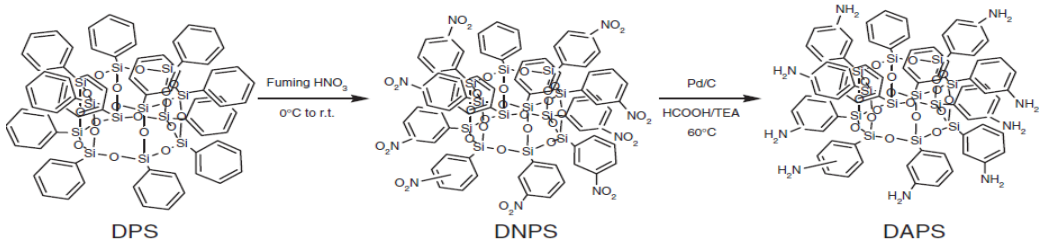

***Figure 14:*** *Schematic reaction for the synthesis of HDAPS*

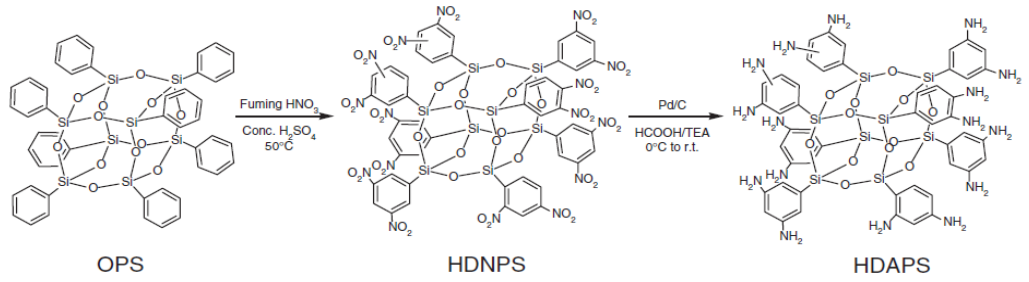


Liu and coworkers[71] synthesized octabenzenesulphonate polyhedral oligomeric silsesquioxanes. The authors performed substitution at the aromatic ring attached to the POSS molecule as shown in Fig 15.

***Figure 15:*** *Schematic synthesis of Octabenzenesulphonate Polyhedral Oligomeric Silsesquioxanes*

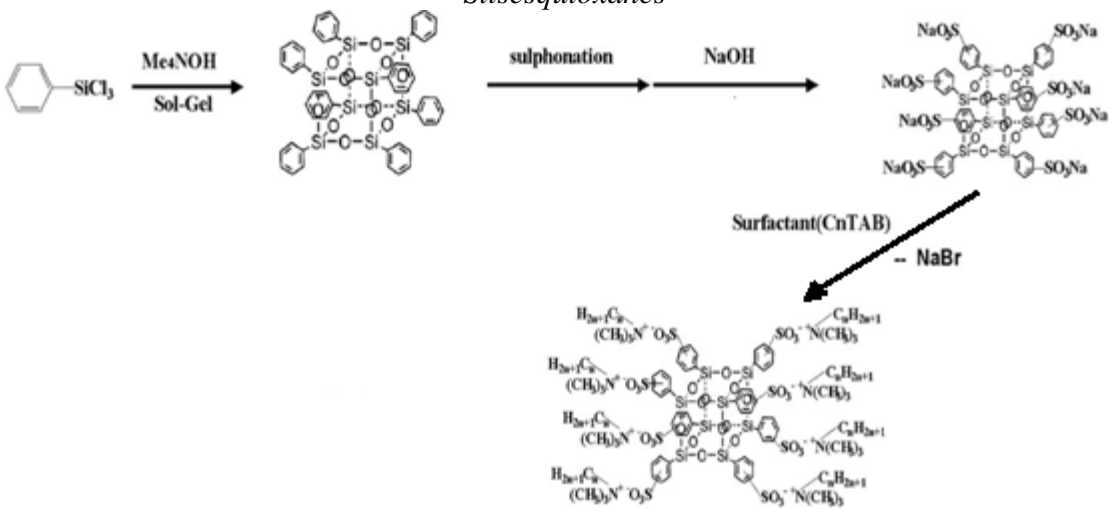


Other reactions in which the modification at the substituent attached to the POSS are present in a wide range of research papers.

## 1.4 Applications of POSS compounds:

The fundamental aspect of this work is the application of POSS based materials. Much research has focused on obtaining polymers with custom-made properties. POSS monomers are unique because they contain relatively large and robust Si-O cages that can be functionalized according to the intended incorporation in the

thermoplastic resin, mainly in large-scale preparations. This would be feasible without modification of the manufacturing process.

POSS based polymers are known to increase glass transition and decomposition temperatures, a fantastic oxygen permeability and reduced flammability and heat evolution. This makes them excellent candidates for enhancing polymers, such as polyurethanes by increasing wear-and-tear resistance. Other applications of these materials are also pursued by both US Air Force and National Aeronautics and Space Administration.[113]

The US Air Force has identified the atomic oxygen resistance of POSS polymers (they form a glassy, passivating $SiO_2$ layer that prevents further decay of the underlying polymer in the hyperthermal presence of atomic oxygen / Low Earth Orbit condition simulations). NASA is also researching their properties as flame retardants and is considering using these materials as film coatings for cabin items during space missions.

Epoxy resins based on POSS analogues are being studied for their potential as insulating "glues" to hold together the several metal layers of substrate printed circuit boards. These resins would also offer a response to the demand for materials with coefficients of thermal expansions between the values of the Si chip and the circuit board (to minimize shear stress). Silsesquioxanes based resins are expected to offer an alternative to the expensive doping of the traditional epoxy resin with silica nanoparticles.[114]

The safety of the use of silicone-containing materials in the context of biomedical devices needs to be addressed. Proteins have been known to bind to silicone surfaces; therefore compromising results of silicone based medical devices. Along with this, protein deposition on silicone-based contact lenses is known to reduce

both their comfort and medical performance. The nature of these interactions has been deemed somewhat controversial, but a solution to address this issue is necessary. Functionalized silsesquioxane polymer coatings allow for inferences to correlate POSS/silicone–protein interactions and offer information about the distinct nature of this week, but important interactions.[115]

The different mechanical and chemical properties bring the POSS cages forward as a solution to the problem of higher temperature and oxidation resistance materials that the industry is currently seeking. POSS monomers offer a simple alternative to forming high-resistance and tough hybrid materials (between ceramics and polymers). They are also available as both blendable resins (ceramics), as well as simple organic monomers (polymers). They are easily soluble in most organic solvents and are thermally stable. They can be easily polymerized using radical, condensation, ring opening polymerizations (standard organic polymerization reactions).

On the other hand, a porous three-dimensional array of cubes may harbor extensive catalytic properties. Metal organic frameworks are being explored for their ability to participate in chemical reactions[116] because of their catalyst encapsulation properties. It may be that the extended framework structures based on POSS allow for a more efficient entrapment of the desired catalyst. These properties need to be further investigated.

One of the current trends in research involving metal-organic frameworks is their exploration towards gas sorption, storage and separation.[117-119] While their sorption rates may be promising,[120] optimal structural, thermal, and mechanical stability has not yet been achieved. It is believed that the coordination and hydrogen bonded POSS polymeric materials[121] may produce a more efficient gas storage material,

due to the high porosity and stability of the Si-O cages incorporated in the frameworks.

## 1.5 Heavy Metal sorption:

From very beginning human being considered metals as important materials in different aspects. In the present, metals are important in infrastructure, transport and different goods such as electronics, batteries, photographic films and many more, in our day to day life. Although the metals are useful for human being, but on other side heavy metals is one of the main environmental pollution sources as well.

The term "Heavy metals" is used for a group of metals and metalloids that have atomic density greater than 5.0 g $cm^{-3}$.[123] Generally, cadmium, copper, chromium, mercury, cobalt, nickel, lead and zinc are called as heavy metals.

In human health, the effects of the metal ion accumulation may be classified as: acute and chronic. Acute effects are associated with the sensory disturbances as well as with the digestive system disorders. Nervous systems break down and cardiac damages are related to chronic heavy metals effects.

Heavy metals are different in nature than other environmental pollutants because they are non-biodegradable and may cause long run problems in soil, flora and fauna both in terrestrial as well as in marine environment.[124] They are also responsible for toxicity in humans.[125] Humans have faced some serious problems due to these heavy metals in the past. The accident in Aznalcollar, Spain,[126] Minimata disease in Japan[127] and arsenic contamination of subsoil water in Bangladesh[128] are a few examples which caused serious environmental disasters due to the release of heavy metals through effluents directly to water resources.

These metals may be classified as essential and non-essential elements.[129] Essential elements are those present in biological fluids with concentration lower than 1µg per gram.[130] Iron, copper, zinc and magnesium are the elements that are present in different enzymes, controlling different metabolic processes as well as maintaining health in different organisms.[131] But access of these metals may cause problems to human health as well as to the environment. For example, in patients of Wilson's disease, copper accumulates in excess amounts in the liver, the brain, the kidneys, the cornea, and other tissues, thereby damaging them.[132]

Non-essential elements are pollutants with potential risks to the health and environment. These elements include aluminum, cadmium, mercury and lead.[133] The presence of these metals in water, even at lower concentration, is still dangerous to human health as well as to the environment.[134] Some of the non-essential elements are capable of replacing essential elements in organisms. Lead and cadmium, for example, may substitute calcium in enzymatic reactions, causing serious health troubles.[133] These heavy metals may produce some reactive radicals that may damage cellular structures including DNA and cellular membranes.[131] Lead may interfere bone and teeth metabolism altering permeability of blood vessels.[135]

The presence of these heavy metals and their respective ions are therefore highly toxic pollutants in our environment. The most common techniques that are used to remove these heavy metals from aqueous medium are chemical precipitation, electrodeposition, sorption processes and similar processes.[136]

Adsorption processes are very important in many areas of interest such as complex synthesis with catalytic properties, in the decontamination of waters by heavy metals and in chromatographic processes. In catalytic processes after the formation of the metal surface, the catalytic properties of the metal are significantly changed,

not only as the electron density of the metal, but also imposing steric constraints for catalysis.

In environmental applications, the type of adsorption and their study is of great interest and motivation for the researchers nowadays. The mechanisms and control of the properties of adsorbent materials, the types of solvents and some other factors are of great importance, in order to achieve good planning for sorption processes. This area is a focus of many current studies, and there is still much to be discovered, especially with the emergence of new materials, such as silsesquioxanes. The molecular interphase interaction between two sites, the surface of the adsorbent material and the metal in solution can be of two types, chemisorption and physisorption.

According to the IUPAC rules, adsorption can be defined, as the enrichment of one or more components of an interfacial layer.[112] Adsorption processes as stated earlier, can be classified into physisorption and chemisorptions. Physisorption is a process where Van der Waals type attractions occur, and in chemisorption the interactions between substrate and adsorbate are ionic and /or of covalent type.[137]

The enthalpy values for the two types of adsorption is about 20 kJ $mol^{-1}$ for physical adsorption and between 250-500 kJ $mol^{-1}$ for the chemical adsorption, demonstrating that the latter is much more stronger type of interaction. The components of an adsorption process can be called adsorbent, which is the surface that will bind to the metal and metal adsorptive that is collected by the adsorbent thus forming the adsorbate. It is very common nowadays to use the term adsorbate for the adsorptive, ie, the metal.[138, 139] The adsorption on solid surfaces, such as the chemically modified silsesquioxanes can be of various types of coordination, depending on the adsorbate. To have a better understanding, a revision of the types of adsorption is required.

## 1.6 Soft and hard Acid Bases:

Some types of donor atoms in the adsorbent material forms strong bonds with some metal ions. This interaction shows different stability constant in accordance with the type of metal ions used. Metal ions thus can be classified according to the type of binder to which it is aligned.

Metals that form stronger bonds with the oxygen atom donor, belongs to class A, and are called hard metal ions. While the ions that form stronger bonds with sulfur or phosphorus donors belong to class B and are known as soft metal ions. Generally, the metal ions of the class A (hard) are smaller and with its larger cationic charge. These ions form stronger bonds with hard bases which contain smaller and more electronegative atoms, such as O, N and F.

On the other side of the metal ions Class B (soft) are larger and more polarizable, mostly are in its lowest oxidation state. These are considered soft acids and forms stronger bonds with soft bases that contain more polarizable atoms and less electronegative donors such as S, Se, P, or As. Such classification is very useful in order to make a prediction of the chelating power of the group that will be used in the organofuncionalization of the material (silsesquioxane this case), with the purpose of adsorbing a certain specific type of metallic ion.

## 1.7. Adsorption isotherms models:

An adsorption isotherm is a thermodynamic model to study quantitative and qualitatively the behavior of the retention or mobility of a substance from one media (liquid/gaseous media) to a solid phase at a constant temperature and pH.

Generally, the adsorption results are usually presented through a graphical expression, where the quantity of the adsorbed material is plotted against its residual concentration (or pressure). Physicochemical parameters of these graphs may provide an insight into the adsorption mechanism, surface properties as well

as the degree of affinity of the adsorbents. For complete interpretation of these graphs a wide variety of equilibrium isotherm models including Langmuir, Freundlich, Temkin, Redlich-Peterson, Sips, and some other models have been formulated.

## 1.7.1.Two Parameter isotherm models:

### 1.7.1.1. Langmuir isotherm

The Langmuir adsorption isotherm is based on monolayer, uniform, and finite adsorption site assumptions, therefore a saturation value is reached beyond which no further adsorption takes place. It also assumes that there is no interaction between the molecules adsorbed on neighboring sites. The Langmuir equation which is valid for a monolayer adsorption onto a surface with a finite number of identical sites is given by:

$$q_e = \frac{Q_L K_L C_e}{1 + K_L C_e} \qquad \text{Equation 4}$$

where *Ce* is the concentration of the adsorbate solution at equilibrium, qe is the adsorbate amount at surface sorbent, and $K_L$ is the constant related to the free energy of adsorption (L/mg) and $Q_L$ is the maximum adsorption capacity.

### 1.7.1.2. Freundlich isotherm

Freundlich isotherm is an empirical equation for multilayer, heterogeneous adsorption sites. The Freundlich equation is commonly given by:

$$q_e = K_F C_e^{1/n_F} \qquad \text{Equation 5}$$

This is the earliest model that describes non-ideal and reversible adsorption systems. According to this model the amount adsorbed is the sum of adsorption on all sites, with the stronger binding sites firstly occupied. The slope ranges between 0 and 1 is a measure of adsorption intensity or surface heterogeneity, becoming

more heterogeneous as its value gets closer to zero. Recently, Freundlich isotherm is criticized for its limitation of lacking fundamental thermodynamic basis, not approaching the Henry's law at vanishing concentrations.

### 1.7.1.3. Temkin Isotherm:

Temkin isotherm is the early model describing the adsorption of hydrogen onto platinum electrodes within the acidic solutions. The expression is as follows:

$$q_e = \frac{RT}{b_T} \ln A_T\, C_e \qquad \text{Equation 6}$$

The isotherm is taking into account the adsorbent–adsorbate interactions. This model ignores extremely low and large value of concentrations, and assumes that heat of adsorption of all molecules in the layer would decrease linearly rather than logarithmic with coverage. As implied in the equation, its derivation is characterized by a uniform distribution of binding energies.

## 1.7.2.Three Parameter Models:

### 1.7.2.1. Redlich–Peterson isotherm

Redlich–Peterson equation included three adjustable parameters into an empirical isotherm. This equation is widely used as a compromise between Langmuir and Freundlich systems. The equation for this model is:

$$q_e = \frac{K_{RP} C_e}{1 + a_R\, C_e^{\beta}} \qquad \text{Equation 7}$$

where $K_{RP}$ and $\beta$ are constants. When the value of $\beta$ is equal to 1, the above equation is reduced to the Langmuir isotherm, while it reduced to a Freundlich isotherm, in case the value of the parameter $a_R\, C_e^{\beta}$ is much bigger than 1. The ratio of $K_{RP}/a_{RP}$ indicates the adsorption capacity.

Redlich–Peterson isotherm is a hybrid isotherm featuring both Langmuir and Freundlich isotherms, which incorporate three parameters into an empirical equation. The model has a linear dependence on concentration in the numerator and an exponential function in the denominator to represent the adsorption equilibria over a wide concentration range, that can be applied either in homogeneous or heterogeneous systems due to its versatility.

### 1.7.2.2. Sips isotherm

The nonlinear Sips (Freundlich–Langmuir) isotherm equation can be represented as:

$$q_e = \frac{Q_S K_S C_e^{n_S}}{1 + K_S C_e^{n_S}} \qquad \text{Equation 8}$$

Where, $K_S$ is equilibrium constant. If the value of $n_S$ is equal to 1, then this equation will become a Langmuir equation. Alternatively, as either $C_e$ or $K_S$ approaches 0, this isotherm reduces to the Freundlich isotherm.

Sips isotherm is a combined form of Langmuir and Freundlich expressions, deduced for predicting the heterogeneous adsorption systems and to reduce the limitation of the Freundlich isotherm model to the rising of the adsorbate concentration. At low adsorbate concentrations, it reduces to Freundlich isotherm; while at high concentrations, it predicts a monolayer adsorption capacity characteristic of the Langmuir isotherm. As a general rule, the equation parameters are governed mainly by the experimental conditions such as the alteration of pH, temperature and concentration.

## 2. Aim of the Study:

The aim of this study is to synthesize, characterize and apply cubic oligomeric silsesquioxanes, having different pendant chains, which are either be able to coordinate with metals and $CO_2$, or to be able to allow further modification in their pendant chains for producing nano composites for the above mentioned applications.

## 2.1. Specific Objectives:

- Synthesize organic-inorganic hybrid materials, polyherdral oligomeric silsesquioxanes (POSS), functionalized with different organic pendant chains, through hydrolytic condensation reaction.
- Characterize all the synthesized POSS hybrids using different physical techniques like elemental analysis (CHN), vibrational spectroscopy in infrared region (FTIR), wide angle powder X-ray diffraction (WPXRD), thermogravimetric analysis (TGA), scanning electron microscopy (SEM) and nuclear nagnetic nesonance (NMR) in solid state for the nuclei $^{13}C$ and $^{29}Si$.
- Modify the synthesized hybrid precursors through substitution in functional group of pendant chain in order to introduce new heteroatom like N, S, O.
- Apply these hybrid materials for:
    - Solid/gas sorption of $CO_2$ at low pressure and at room temperature.
    - Sorption of divalent cations like $Cu^{2+}$, $Cd^{2+}$ and $Pb^{2+}$ from their aqueous solutions.

# 3. Experimental:

After a short discussion about silsesquioxanes in earlier sections of this thesis and defining our objectives, strategy was designed to obtain silsesquioxanes. The detailed description of the experiments performed during our research is given in the following sections.

## 3.1. Materials:

Reagents used in the present work are summarized in table 2:

***Table 2. Reagent used in the present work***

| No | **Reagent** | **Company** |
|---|---|---|
| 1 | (3-Chloropropyl)tri-methoxysilane | Aldrich |
| 2 | γ-Amino-propyltriethoxysilane | Aldrich |
| 3 | N-[3-(Trimethoxysilyl)porpyl]ethylenediamine | Aldrich |
| 4 | 3-Trimethoxysilylpropyl)diethylene-triamine | Aldrich |
| 5 | (Glycidoxypropyl)trimethoxysilane | Aldrich |
| 6 | (Phenyl)triethoxysilane | Aldrich |
| 7 | (Propylmethacrylate)triethoxysilane | Aldrich |
| 8 | Diethanolamine | Aldrich |
| 9 | Acrilonitril | Aldrich |
| 10 | Methanol | Synth |
| 11 | Ethanol | Synth |
| 12 | Acetone | Synth |
| 13 | Hydrochloric acid | Aldrich |
| 14 | di-n-Butyltin dilaurate | Aldrich |
| 15 | Lead nitrate | Vetec |
| 16 | Cadmium nitrate | Vetec |
| 17 | Copper Nitrate | Vetec |

All of the reagents given in table 2 were of analytical grade and were used without any purification. In all of the experiments deionized water was used.

## 3.2. Synthesis:

Among of all polyhedral oligomeric silsesquioxanes, cubic POSS have gained attention for the past 60 years, because of its spontaneous $T_8$ cage formation from its chloro or alkoxy silanes. Due to the stability of the $Si_4O_4$ ring structure, cubic POSS species are preferred when compared to the other POSS species such as $T_{10}$, $T_{12}$ and others. The polyhedral oligomeric silsesquioxanes are mostly synthesized by following methods:

1. Hydrolytic Condensation of $RSiX_3$;
2. Corner-Capping Reactions;
3. Synthesis of POSS Compounds by Hydrosilylation;
4. Synthesis of Bridged POSS Compounds;
5. Synthesis of Endohedral POSS Compounds;
6. Modification of Substituents To Prepare POSS Compounds;

Among all of these methods, hydrolytic condensation route is used by a significant number of researchers. Hydrolytic condensation route have certain inherent disadvantages, including the long reaction times and less than 50 % yields of the product. On the other hand, it usually affords symmetrical $T_8R_8$ compounds as well. These inherent low yields of the hydrolytic condensation route to the POSS species are due to the formation of other types of silsesquioxanes, such as ladder and other non-polyhedral silsesquioxane polymers as byproduct as well as by the formation of other oligomers with higher order of the desired POSS species, such as the $T_{10}$ and $T_{12}$ derivatives. In order to improve the yields of these simple

preparations, study is ongoing with changes in solvent systems, type of hydrolysis, and addition of other compounds as catalysts to the reactions.

Keeping in view our project objectives, the research journey begun with the synthesis of PAA-12 following the literature.[21] The procedure was reproduced without any further modification and the results obtained were according to the reported ones.

### 3.2.1.Synthesis of PAA-12: $Si_8O_{12}[(CH_2)_3Cl]_8$

A solution of 150 $cm^3$ of dry methanol and 5 $cm^3$ of concentrated hydrochloric acid was placed in a three-necked, round bottom flask equipped with a condenser, an addition funnel, and a magnetic stirrer bar. To this solution was added dropwise a portion of (3-chloropropyl) trimethoxysilane (15 g, 75 mmol) through the addition funnel over a period of 10 min with vigorous stirring. The stirring was continued for two hours until the solution had cooled to room temperature. The reaction mixture was kept at room temperature for another 48 h without stirring. After two days, di-n-butyltin dilaurate (0.15 g, 0.24 mmol), as a condensation catalyst, was added with stirring. The reaction mixture was maintained at room temperature for two days until a white crystalline precipitate appear. The solution was filtered of and the crystals were collected, then washed several times with methanol, and dried under vacuum. The final product was obtained in 30 % (1.96g) yield.

***Figure 16:*** *Two-Step Synthesis of Octakis(3-chloropropyl)silsesquioxane.*

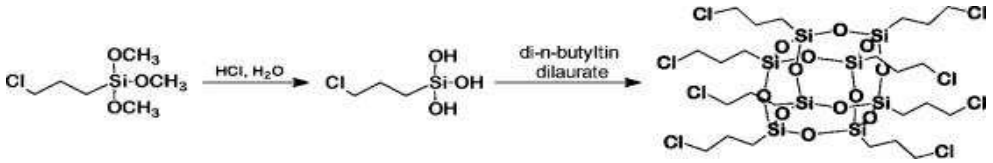


The reaction was repeated again and again with slight modifications, substituting solvent in some while catalyst in others, but neither the reaction time nor yield was improved. The reaction was reproduced using ethanol, n-hexane and benzene as a

solvent, individually, but the results were more or less the same as that of the first one and no improvement was observed in the yield of the product.

***Figure 17:*** *Structure of catalyst di-n-butyltin dilaurate*

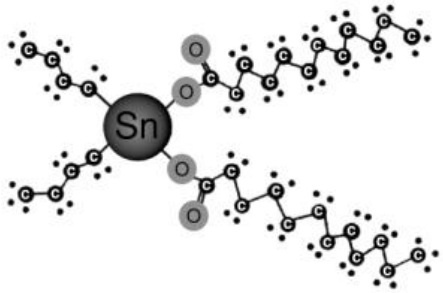


From the structure and mode of action of the catalyst di-n-butyltin dilaurate, it was assumed that using acetone in abundance could improve the yield. The reaction was reproduced using acetone as a solvent and in the absence of the catalyst di-n-butyltin dilaurate, but did not bring any improvement in the yield. The results obtained were almost similar to those obtained by the previous reports, where Ibrahim et. al, and other researchers[15, 22, 140-143] reported 31-37 % yield.

The amount 1.96 g of the synthesized product obtained was supposed to be improved in yield and then be modified by substitution reaction, but due to the longer reaction time and low yield, some modification in the project was made. Instead of using the PAA-12 as a precursor for further hybrid material, the decision was to synthesize the PAA-13 starting directly from 3-(trimethoxysilyl) propylamin.

### 3.2.2. Synthesis of PAA-13: $Si_8O_{12}[(CH_2)_3NH_2]_8$:

For the synthesis of PAA-13 the procedure in the literature[144] was followed with slight modification, and the results obtained were compared to the reported ones, which were quite close to the expected results.

A 150 $cm^3$ syringe containing γ-amino-propyltriethoxysilane was slowly added to methanol anhydrous (250 $cm^3$) in a 500 $cm^3$ three-neck round bottom flask.

Concentrated HCl (9 $cm^3$) was carefully added, under stirring, to the above mentioned solution. The product began to crystallize from the reaction mixture after 30 days. The reaction mixture was kept in refrigerator for next 2 week for the condensation process to complete. Octahydrochloride salt in 35 % yield was obtained and washed with methanol and then dried at room temperature under vacuum. The resulting product, the octahydrochloride slat, was then subjected to structure elucidation.[144]

***Figure 18:*** *Synthesis of Octakis(3-aminopropyl)silsesquioxane*

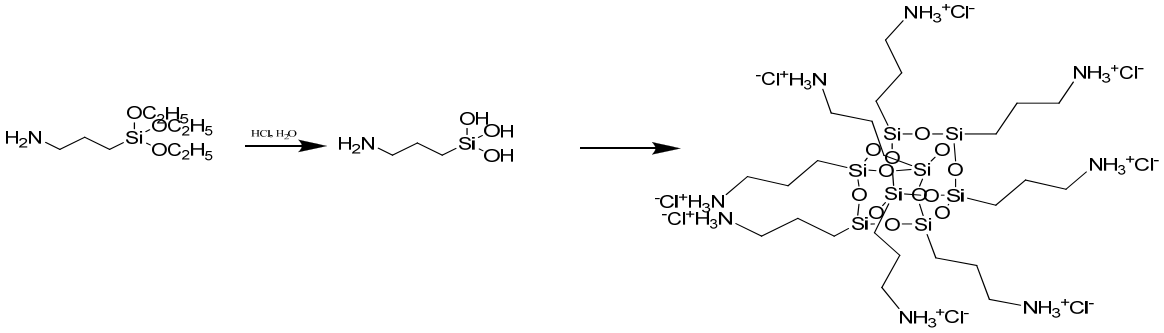


This time, the low yield and even the longer reaction time were accompanied by another barrier, the crystal handling. The crystals obtained were too much hygroscopic and had to be handled with much care and kept at a very low temperature in an airtight system. To solve the long reaction time problem, the procedure was repeated with a slight modification. The reaction was repeated with the addition of the di-n-butyltin-dilaurate, but the catalyst did not affect the long reaction time and the product was again obtained in 4 weeks with more or less the same yield. The same reaction was repeated using different acids, such as $H_2SO_4$ and $HNO_3$, with or without adding the catalyst, but again no improvements in reaction time were observed. Analyzing the literature, [105, 106, 145-152] it was revealed that the low yields and the long reaction times are common with such type of silsesquioxanes, where 4-30 % yield has been reported. Several attempts were made to improve the yield and reaction time for PAA-13, but these attempts did

not bring any remarkable change. The decision was made to move forward for the synthesis of PAA13-2.

### 3.2.3.Synthesis of PAA-13-2: $Si_8O_{12}[(CH_2)_2NH(CH_2)_2NH_2]_8$

The literature mentioned for PAA-13 was followed to synthesize PAA-13-2. About 10 $cm^3$ concentrated HCl was carefully and slowly added to a solution of 250 $cm^3$ methanol anhydrous and 10 $cm^3$ of N-[3-(trimethoxysilyl)porpyl]ethylenediamine. The reaction was conducted in a 500 $cm^3$ three-neck round bottom flask. The reaction mixture was kept at room temperature and was allowed to stir for 35 days. On 35$^{th}$ day, the product has begun to crystallize. A total of 2.08 g product was obtained, which corresponds to 36 % yield. The product obtained was then washed with methanol several times and then dried in vacuum. The resultant product, the octahydrochloride salt, was subjected to the physical characterization.[27]

***Figure 19:*** *Two-Step Synthesis of Octakis(3-ethylenediamine-propyl)silsesquioxane*

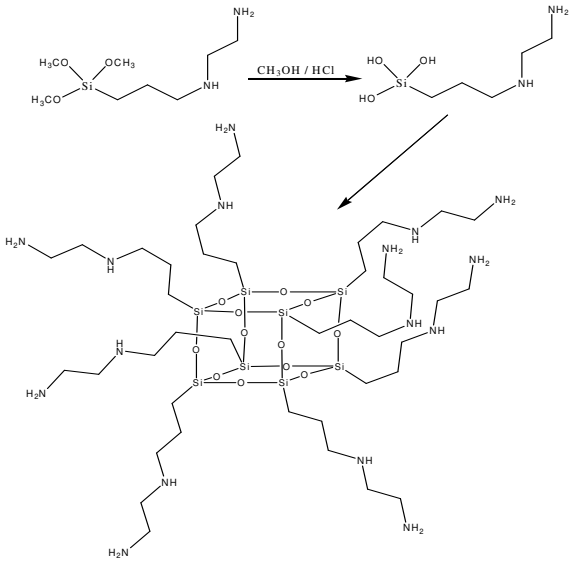


Observing the results of the last 3 preparations, the research was still far away to fulfill the objective of the project. The precursors for the next steps were presenting some serious problems like long reaction times and low yields. Looking back to the past attempts, it was decided to move forward towards the

synthesis of PAA-13-3. But, for PAA-13-3, some changes were made in the reaction procedure. Analyzing the literature, the following mechanism has been reported for the synthesis of POSS.[103]

***Figure 20:*** *Proposed reaction mechanism for the POSS synthesis through hydrolytic condensation.*

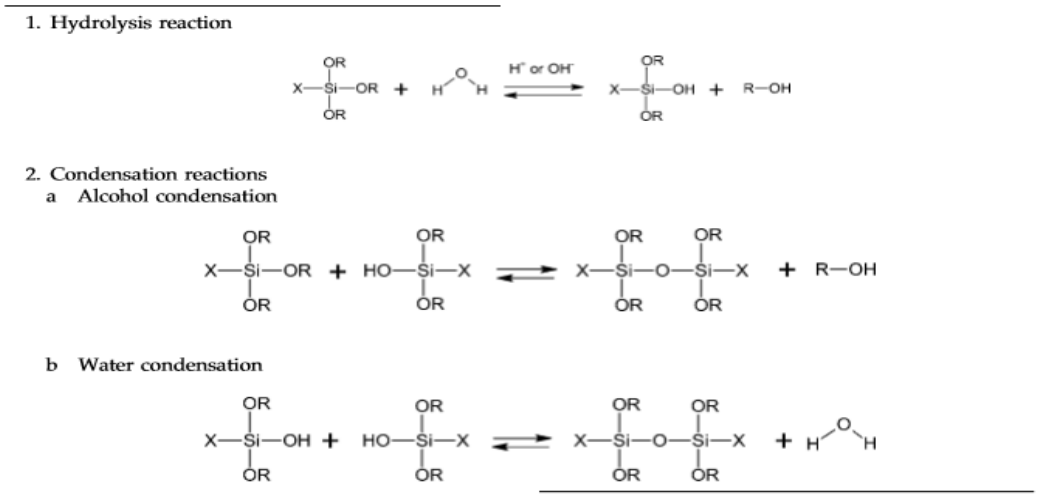


The above mechanism reveals an alcohol generation during the reaction course. This generated alcohol in the presence of alcoholic solvent further dilutes the reaction mixture and hence imbalance the stoichiometry of reaction, which favors the reverse reaction in hydrolysis as well as alcohol condensation steps.

After discussions with the field experts it was supposed that reaction without solvent may enhance the rate of the forward reaction and hence to reduce the reaction time. To test the hypothesis, in a small round bottom flask, 2 $cm^3$ of the N'-[3-(trimethoxysilyl)propyl]diethylene-triamine was taken and a few drops of concentrated HCl, under vigorous stirring, was added to it, which result the formation of some brown color precipitation. Temperature was controlled in an ice-bath. The precipitate was analyzed and was found to be a polymer. But this test based reaction opened a window towards the better results. A close analysis of the test reaction data revealed that the availability of more siloxane sites for a fewer

acid molecules may favor the polymer formation. In light of these finding some modification in the reaction course was introduced. These modifications have brought some wonderful results. The test reaction was successful and the procedure was optimized for the synthesis of PAA-13-3.

### 3.2.4.Synthesis of PAA-13-3: $Si_8O_{12}[(CH_2)_2NH(CH_2)_2NH(CH_2)_2NH_2]_8$

A 250 $cm^3$ round bottom flask equipped with a refluxing condenser, a magnetic stirrer and a three-way cock was at first evacuated and charged with $N_2$. The operation was repeated three times. Then, to the flask was added 9 $cm^3$ of concentrated HCl. and then 10 $cm^3$ of N'-[3-(trimethoxysilyl)propyl] diethylenetriamine was added drop wise. The resulting mixture was allowed to stir and subsequently cooled using ice-bath for 30 min. The reaction flask was then transferred to the freezer for 6 h to get maximum condensation. Most volatile components were removed at reduced pressure below 40 $^oC$ and then were further vacuum dried for 8 h. The dried, light brown solid, was then washed with diethanolamine followed by washing with acetone in vacuum using a closed system. Final dark brown solid obtained was subjected to characterization.

***Figure 21.*** *Synthesis of Octakis-[3-(diethylenetriamine)propyl]silsesquioxane*

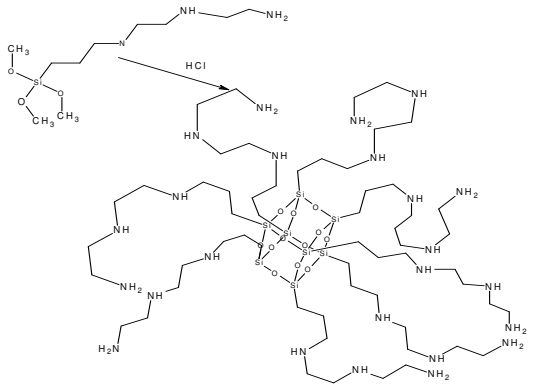

PAA-13-3 was synthesized without any solvent. The product was obtained in a short time. The yield was reasonably high with a total of 3.12 grams (64 %) of the product, which is much higher than other members of the group, discussed above

(30-37 %). The reaction was repeated again and again with much care and the results obtained were surprisingly reproduced at each time the reaction was repeated. In order to be sure about success of the process, the synthesis was tested using different acids and the results obtained were similar. The synthetic procedure for PAA-13-3, was followed to synthesize other POSS compounds like PPA-GDP, PAA-Ph, and PAA-MTC, within a shortest reported time.

## 3.2.5.Synthesis of PAA-GDP: $Si_8O_{12}[(CH_2)_3O(CH_2)_2O]_8$

In a 250 $cm^3$ round bottom flask equipped with a refluxing condenser, a magnetic stirrer, was added 9 $cm^3$ of concentrated HCl and then 10 ml of (glycidoxypropyl)triethoxysilane was added drop wise. The resulting mixture was allowed to stir and subsequently cooled using ice-bath for 30 min. The reaction flask was then transferred to the freezer for 6 h to get maximum condensation. The resulting light brown, viscous liquid was then dried in vacuum for 10 h. The dried solid was then washed with acetone. Final light brown solid obtained was subjected to characterization.

***Figure 22:*** *Synthesis of Octakis-(3-glycidoxypropyl)silsesquioxane*

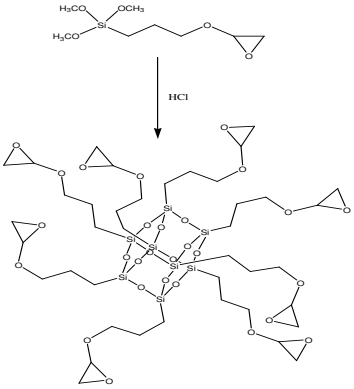


## 3.2.6. Synthesis of PAA-MTC: $Si_8O_{12}[(CH_2)_3O(CO)C(CH_2)CH_3]_8$

In a 250 $cm^3$ round bottomed flask, about 10 $cm^3$ of concentrated HCl was added with care, then 10 $cm^3$ of (3-propylmethacrylate)triethoxysilane was added drop wise. The resulting mixture was allowed to stir and subsequently cooled using ice-

bath for 30 min. The reaction flask was then transferred to the freezer for 6 h to get a maximum condensation. Most volatile components were removed at reduced pressure below 40 $^{o}$C and then were further vacuum dried for 8 h. The dried solid crystals were then washed with acetone. Final dirty brown solid crystals obtained was subjected to characterization

***Figure 23:*** *Synthesis of Octakis-[3-propylmethacrylate]silsesquioxane.*

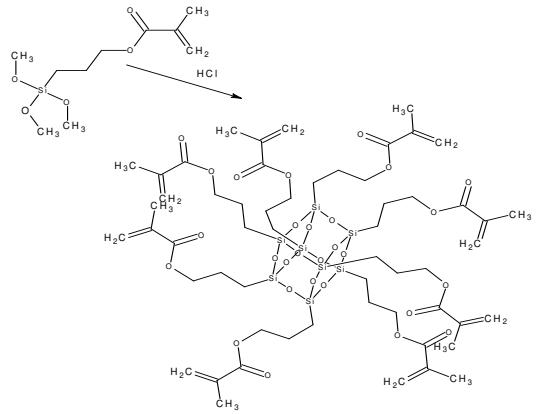


## 3.2.7.Synthesis of PAA-Ph: $Si_8O_{12}Ph_8$:

A 250 cm$^3$ round bottom flask equipped with a refluxing condenser, a magnetic stirrer and a three-way cock was, at first, evacuated and charged with $N_2$. The operation was repeated three times. Then the flask was added with 9 cm$^3$ of concentrated HCl, and then 10 cm$^3$ of (phenyl)triethoxysilane was added drop wise. The resulting mixture was allowed to stir and subsequently cooled using ice-bath for 30 min. The reaction flask was then transferred to the freezer for 6 h to get maximum condensation. The most volatile components were removed at reduced pressure below 40 $^{o}$C and then were further vacuum dried for 8 h. The dried solid was then washed with acetone in nitrogen atmosphere in a closed system. The final white solid obtained was subjected to characterization.

***Figure 24:*** *Synthesis of Octakis-[phenyl]silsesquioxane.*

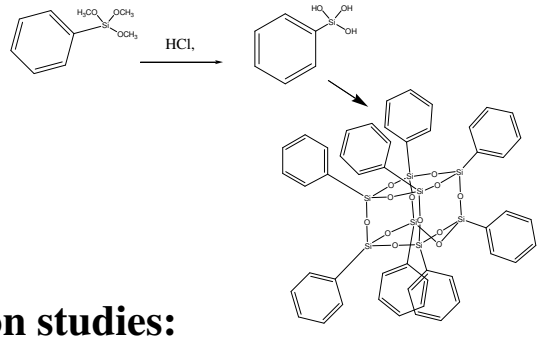


## 3.3. Adsorption studies:

### 3.3.1. $CO_2$ Adsorption using Gas Dosing System (GDS) for the sample PAA-13-3:

#### 3.3.1.1. Description of Gas Dosing System:

The gas dosing system (GDS), Figure 25, developed by the Drs. Nilton de Oliveira Junior and José de Alencar Simoni, was used to determine the adsorption of $CO_2$ using the hybrid PAA-13-3. This system has an internal compartment of fixed and known volume, made up of stainless steel 316 L, with four major connections linking: a vacuum pump, a pressure sensor, entrance for the adsorbent gas and a reaction cell. All these three connections linking are controlled by respective valves. The system is fully automated and is operated by licensed software.

***Figure 25:*** *Gas Dosing System (GDS)*

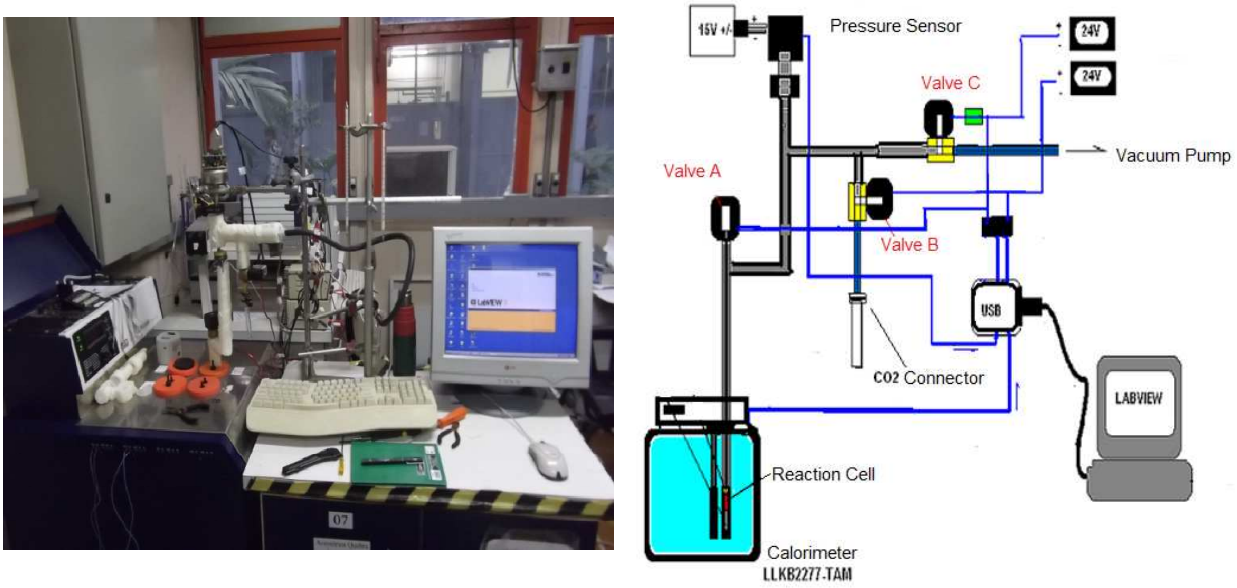

### 3.3.1.2. Experimental Procedure:

For measuring the amount of gas sorbed by PAA-13-3, sample was taken in a reaction cell, which was then placed inside calorimeter (Thermometric 2277), valve C was opened while keeping valves A and B closed, meanwhile the vacuum in system was created using the vacuum pump followed by the opening of valve A, to make sure the drainage of the air and other gases present in the reaction cell. When it was assured that all the gasses are being exhausted from the reaction cell, valve A and C were closed. To charge up the internal chamber with $CO_2$, valve B was then opened until the pressure of the chamber reached 10 mmHg.

In order to start the sorption process, the valve B was closed and the valve A was opened, the gas was allowed to enter into the reaction cell. The gas pressure inside the chamber dropped down from 10 mmHg, representing the equilibrium after the gas adsorption. The energy released during sorption process was simultaneously measured by the calorimeter, which helps in understanding the sorption process such as surface properties of the solid, sorption mechanism, gas sorption selectivity etc. The system was then charged with 20, 30, 40….100 mmHg of $CO_2$ for repeating the adsorption phenomenon under different pressures. Data collected by the system, was then treated by using an integrator program, developed in SciLab® software. This integrator generates a detailed analysis of the sorption process through different graphs and tables.[213]

## 3.3.2.Divalent Metal Cation sorption:

For metal sorption studies, $Cu^{2+}$, $Cd^{2+}$ and $Pb^{2+}$ were used as sorbate, while three hybrid materials PAA-13-3, PAA-MTC and PAA-Ph were used as sorbents. For these sorption studies two different protocols were used. In the first experiment sorbent PAA-13-3 was tested for the sorption capacity of divalent cations $Cu^{2+}$,

$Cd^{2+}$ and $Pb^{2+}$. While in the second experiment the hybrid materials PAA-13-3, PAA-MTC and PAA-Ph were tested for their sorption ability of divalent $Cu^{2+}$.

### 3.3.2.1. PAA-13-3 Sorption Capacities for $Cu^{2+}$, $Cd^{2+}$ and $Pb^{2+}$:

The capacity of PAA-13-3 to extract divalent metals from aqueous solution was determined in duplicate runs, using a batch process with aqueous solutions of nitrates of the divalent copper, cadmium and lead, using a mass of approximately 5 to 20 mg of PAA-13-3 suspended in 10 $cm^3$ of metal solutions with concentrations ranging from 0.70 to 7.0 mmol $dm^{-3}$. The suspensions were shaken for 24 h in an orbital bath at (298±1) K. At the end of this process, the solid was separated by filtration, aliquots of the supernatant were removed and the cation concentrations were determined by ICP-OES. The sorption capacities ($q_e$) were calculated by Eq.(9),

$$q_e = \frac{ni - ns}{m} \qquad \text{Equation 9}$$

Where $_{Qe}$ is the cation adsorbed quantity, $n_i$ and $n_s$ are the cation quantities in the initial and the supernatant solutions after reaching equilibrium, respectively, and $m$ is the mass of the adsorbent used in each adsorption process.

### 3.3.2.2. PAA-13-3, PAA-MTC and PAA-Ph Sorption Capacities for $Cu^{2+}$:

The procedure mentioned above for the sorption of PAA-13-3, was repeated for the three hybrid materials using divalent $Cu^{2+}$ solutions with different concentrations. The solutions were shaken, filtered and were analyzed using ICP-OES. Sorption capacities for all three hybrid materials were calculated and were subjected to further statistical treatments.

# 4. Characterization Techniques

## 4.1. Elemental Analysis (CHN):

The major elements of an organic substance, namely, carbon, hydrogen, and nitrogen, are commonly determined using commercially available CHN and CHNS analyzers, in which the organic substance undergoes oxidative decomposition and the subsequent reduction of nitrogen and sulphur oxides with the formation of the final products: carbon dioxide, water, elemental nitrogen, and sulphur dioxide. Currently, both old types of Analyzers (Carlo Erba, models 1106 and 1108; Hewlett-Packard, model 185; Perkin Elmer, model 240; etc.) and new types (Euro EA 3000; Perkin Elmer 2400, series II; CE 440; Varian EL III; etc.) are used in the practice of organic elemental analysis.

Here in this study using Perkin Elmer 2400, series II, Carbon, Hydrogen and Nitrogen elemental Analyzer, synthesized samples were analyzed in order to investigate the samples for their organic pedant chain contents.

## 4.2. Infrared Spectroscopy:

Vibrational spectroscopy has been used extensively for the characterization of $T_8$ compounds. The stretching band due to the Si-O-Si linkages are usually strong and occurs at circa of 1100 $cm^{-1}$, but it is also broad, and this has led to a range of values being quoted for the same compound by different authors.[79] The analogous bands in ladder silsesquioxanes also occur in the region of 1030-1055 $cm^{-1}$,[80,19] so they may be used to distinguish cage from ladder compounds. Chomel and coworkers used this characteristic band, generated by Si-O-Si bond vibration, to distinguish POSS cage derivatives from ladder siloxanes.[80]

IR spectroscopy has also been used for checking that the characteristic Si-O-Si band in the IR spectrum of a monomeric $T_8$ compound is present in a material in

which the monomer was incorporated, which is usually assumed to indicate that the processing of the monomer has not destroyed the $T_8$ cage. The appearance of the band at 1103-1110 $cm^{-1}$ in the spectrum of $T_8[(CH_2)_3OCH_2CH(O)CH_2]_8$ was reported to confirm that POSS cage stays intact during polymerization process. Other researchers have also reported the same band in their findings.[81-84]

On other side the disappearance of the band at 1130 $cm^{-1}$ due to the photoxidation of copolymer poly(N-dodecylacrylamide-co-3-methacryloxypropyl-heptaphenyl)-POSS and its replacement by another band at 1065 $cm^{-1}$ due to the formation of $SiO_2$ film on breakdown of cage has also been reported.[85] In another study, similar $SiO_2$ layers have also been reported, which were formed by the reaction of the polymer with oxygen plasmas.[86]

Other characteristic bands present in the IR spectrum of POSS hybrids are being reported by different researchers are O-Si-O symmetric vibrations at 558$cm^{-1}$ and O-Si-O asymmetric vibrations at 390 $cm^{-1}$.[87]

In the present work the spectra have been taken by using Bomen-FTIR MB series, collecting 32 scans with 4 $cm^{-1}$ resolution in 4000 to 400 $cm^{-1}$ region. All the spectra were recorded through KBr disk.

## 4.3. Solid State Nuclear Magnetic Resonance (NMR):

### 4.3.1. $^{29}$Si-NMR:

The solid state $^{29}$Si NMR spectroscopy has become a widely used tool for the analysis of POSS species. Relatively narrow chemical shift ranges for alkyl (-65 to -70 ppm), aryl (-75 to -81 ppm), and siloxy (-95 to -120 ppm) substituted POSS cages appears as their characteristic peaks. This technique is being used to find out the status of POSS cage in final product, when cage is one of the starting components, while preparing new composite material through polymerization or

mechanical process. The solid state $^{29}$Si NMR spectra have been used to confirm the integrity of the $T_8$ cage on the formation of organic-inorganic hybrid materials. For example, the $^{29}$Si NMR solid state data for nanocomposites derived from $T_8[OSiMe_2(CH_2)_4CH(O)CH_2]_8$ or from $T_8(C_6H_4NH_2)_8$ indicate that the POSS cores remain largely intact.[74]

The solid state $^{29}$Si NMR technique has also been used to determine the degree of substitution in the reaction between $T_8(OSnMe_3)_8$ and chlorosilanes to give materials in which the POSS cages are cross-linked by Si-O-Si linkages.[170] The solid-state $^{29}$Si NMR signal from $\{T_8[(CH_2)_3NH_3]_8\}Cl_8$ in the presence of Pd nanoparticles is broadened, but the chemical shift is not significantly altered indicating that the cage is not cleaved by the particles and that there is a weak interaction between the POSS species and the Pd.[47]

The chemical shift values of the solid state molecular species can be useful, when is required to confirm that cage is still intact in the polymerization process. For example, the reaction of $T_8[CH_2CH(O)CH_2]_8$ with diamines[72] and the radical induced polymerization of methyl methacrylate[73] with $T_8(OSiMe_2H)_8$ results in both cases indicated that cages remained intact.

Similarly, the $^{29}$Si NMR spectra of hybrid materials $T_8[OSiMe_2(CH_2)_4CH(O)CH_2]_8$ or $T_8(C_6H_4NH_2)_8$ indicated that POSS cages remained unchanged.[74] In case of $\{T_8[(CH_2)_3NH_3]_8\}$ the signal became broadened but the chemical shift not changed too much, which meant that the POSS core was not cleaved.[75]

## 4.3.2. $^{13}$C-NMR:

The $^{13}$C NMR spectra in solid state for $T_8$ derivatives ranging from simplest to the complex ones, has been reported by different authors and is found to be a useful characterization technique. The solid- state $^{13}$C spectra for $T_8[OSiMe_2(CH_2)_3CN]_8$

and $T_8(SiMe_2$- t-Bu$)_8$ have also been recorded.[163, 112] Chan and coworkers reported that the solid state $^{13}C$ spectra of star polymers comprising a $T_8$ core and poly(ε-caprolactone) substituents show that they can form inclusion complexes with cyclodextrins.[75] A comparison of the solid state $^{13}C$ NMR spectrum of $T_8$(i-Bu$)_7C_6H_4$-4-CH=$CH_2$ and its copolymers with vinylpyrrolidine demonstrated that the POSS cage is indeed incorporated into the polymer.[77]

Although solid state $^{13}C$ NMR is a useful technique in material sciences, it is rarely recorded in case of POSS compounds, most probably due to the complicated spectra and the lack of information about the POSS core. However, Xu. et. al reported solid state $^{13}C$ NMR spectrum of copolymers of vinylpyrrolidine with $T_8$(i-Bu$)_7C_6H_4$-4-CH=$CH_2$ and explained that the POSS cage was incorporated intact into the polymer.[76] The spectrum of $T_8(CH=CH_2)_8$ was used to set up the Hartmann-Hahn conditions for magic angle spinning $^{29}Si \rightarrow ^{13}C$ cross polarization transfer,[77] and a detailed $^{13}C$-NMR study of $T_8$(i-Bu$)_8$ was used to investigate the motion of the substituents as a function of temperature.[78]

For all the synthesized samples, $^{29}Si$ and $^{13}C$ spectra in solid state were recorded using Bruker 300 & 400 MHz spectrometers. The spectra were recorded using HPDEC and CP/MAS techniques. Samples were analyzed in 75-100 MHz frequencies. Pulse interval for all the samples was 3 s with acquisition time of 0.05 s and pulse sequence with 4000 μs. For all the samples tetramethylsilane was used as a reference.

## 4.4. Thermogravimetry:

Thermal stability and decomposition pathways of POSS compounds have been reported in numerous publications. TGA analysis of POSS compounds such as $T_8R_8$ (R = H, Me, i-Bu, i-Oct, Ph) are somehow complicated due to their complete

sublimation in the presence of nitrogen and partial sublimation in air. For $T_8H_8$ and $T_8Me_8$ both in air and in nitrogen atmosphere, incomplete evaporation has been reported. But $T_8(i\text{-}Bu)_8$ and $T_8(i\text{-}Oct)_8$ evaporates completely in inert atmosphere, whereas oxidizes to silica in air.[101]

However POSS compounds containing higher alkyl groups show thermal stability to a higher temperature.[102] Different researchers have reported TGA analysis of $T_8[(CH_2)_3NH_2]_8$ with certain variations, which is perhaps due to its hygroscopic nature. Its degradation is reported at onset temperatures i.e. 320, 350 and 425 ºC respectively at different occasions.[103-105]

TGA of $\{T_8[(CH_2)_3NH_3]_8\}Cl_8$ shows a two-step decomposition. Initial decomposition of the alkylammonium chloride group occurs between 305 and 420 ºC in the first step and at 420-650 ºC degradation of the propyl chains occur in second step.[105] TGA of the aryl-POSS compounds $T_8R_8$ (R = Ph, $C_6H_4$-2-Me, $C_6H_4$-3-Me, $C_6H_4$-4-Me) show onsets for decomposition at 486, 435, 431 and 413 ºC, respectively.[107]

Thermogravimetric curves for all the synthesized hybrids were recorded using model 2050 TGA of TA instruments. The experiments were conducted in synthetic air as well as in inert atmosphere with a flux rate of 100 $cm^3\ min^{-1}$. The samples were weighed in the range of 10-15 mg. All the experiments were conducted with a temperature range increase of 10 $^oC\ min^{-1}$.

## 4.5. Scanning Electron Microscopy:

SEM and TEM have been used to monitor the progress of siloxane formation upon hydrolysis of $MeSi(OEt)_3$ and $EtSi(OEt)_3$ and show that self assembly of the final cubic crystalline material occurs via initial spherical particle formation, followed

by chains of spherical particles and bundles of rod-like structures, resulting in regular cubic crystals smaller than 5 μm.[94, 95, 108]

SEM of $T_8Me_8$ prepared from swollen poly(2-hydroxyethylmethacrylate) shows that cubic crystals having edges up to 20-30 μm long may be formed [91]. SEM of poly(ε-caprolactam) blended with $T_8Ph_8$ shows that the POSS molecules adhere poorly to the polymer and instead form POSS domains of 1-20 μm across.[110]

SEM of $\{T_8[(CH_2)_3NH_3]_8\}Cl_8$ shows it to form crystalline microrods and particles ranging in size from 1–80 μm.[111] SEM of $T_8(OSiMe_2H)_8$ shows that well defined cubic particles with a porous structure and of 100 μm size may be formed from the reaction of $[T_8O_8]_8$ with $HMe_2SiCl$,[112] but the related derivatives $T_8[OSiMe_2(CH_2)_3CN]_8$ and $T_8[OSiMe_2(CH_2)_3Cl]_8$ show a much lower degree of porosity.[112, 109]

In the present work scanning electron microscopic analysis were performed in a scanning electron microscope JEOL-JSM 6360-LV. Analysis were performed on a double faced carbon ribbon adhered on a gold support. In these analyses the software Bal-Tec MD20 was used. Samples were prepared without any grinding of the products.

## 4.6. X-ray Diffraction Studies on Powders:

Powder X-ray diffraction technique has been extensively used to determine the structure and nature of the POSS particles. The similarity between XRD pattern of POSS both in monomeric species as well as in polymeric materials makes the XRD technique very useful to show that the POSS cage has remained intact in polymerization.

There are several common observations in the XRD spectra of POSS based compounds. Diffraction peaks at 2θ values of 8.3°, 18.9°, and 24.4°, which

corresponds to d-spacings of 11, 5, and 3 Å. These findings have been typically attributed to the overall dimensions of the POSS molecule, the body diagonal of the POSS cage, and the distance between opposite $Si_4O_4$ faces, respectively.[88] Special care is needed to analyze the diffraction patterns of POSS compounds, because the ideal cubic cage of $T_8R_8$ compounds are somehow distorted. This distortion results some variations in data for face diagonal, body diagonal and face to face distances across the POSS cage. That is why the crystal dimensions vary among rhombohedral,[90] triclinic and monoclinic.[89] The diffraction patterns of several alkyl substituted POSS compounds have been reported in the literature[177] along with their respective indexed reflection data. This data shows that POSS may be regarded as spheres packed in a hexagonal ABCA format, which gives hexagonal or rhomobohedral geometry. Most of the publications have referred the POSS structure to be rhombohedral. According to the Cambridge Crystallographic Database 55% is in triclinic, 26% are monoclinic and 23% are rhombohedral in nature. The XRD pattern for $T_8(CH{=}CH_2)_8$ shows several sharp peaks at $2\theta$ = 9.8, 20.1 and 29.9º,[178-180] while the XRD pattern of $T_8[(CH_2)_3NH_2]_8$ shows several sharp peaks indicative of crystallinity and consistent with a rhombohedral unit cell, with a = 11.57 Å and $\alpha$ = 95.1º.[103-105, 145]

The powder X-ray diffraction pattern for $T_8H_8$ shows characteristic peaks at $2\theta$ = 7.9, 8.4, 11.04, 18.9 and 24.13 º, [16] while the pattern for $T_8Me_8$ is indicative of a rhombohedral structure,[91, 92, 94] and has a characteristic peak at ca. $2\theta$ = 10.8º,[93, 95] which is also present in diffraction patterns for POSS polyethylene nanocomposites containing >1 wt % POSS, indicating that the $T_8Me_8$ crystallizes when dispersed in the polyethylene.[94, 95, 97]

The WAXD pattern of $T_8(i\text{-}Bu)_8$ shows several sharp peaks, e.g. at ca. 2θ =7.96, 8.84, and 10.86 ° corresponding to d-spacings of 11.1, 10.0 and 8.1 Å. This is an indicative of POSS phase segregation.[98]

WAXD studies of $T_8(OSiMe_2H)_8$ provide evidence for the presence of small disordered POSS domains.[99] Conversely, although the XRD pattern for $T_8[OSiMe_2(CH_2)_3OH]_8$ is indicative of crystallinity, upon incorporation into a POSS- polyimide film the crystallinity is lost.[44, 100]

## 4.7. ICP-OES:

Inductively coupled plasma optical emission spectroscopy is based on emission spectroscopic concept. The plasma is used to heat up the sample for breaking the chemical bonds in order to get free atoms and ions. This way, the characteristic electromagnetic radiation corresponding to each atom may be emitted. From these emitted electromagnetic radiations the concentration of the species are measured.

In the present work, an optical emission spectrometer Perkin Elmer 3000DV was used for the quantitative determination of the cations in solutions.

## 5. Results and Discussion:

In the present study, different characterization techniques have been used to analyze the synthesized hybrid materials. These characterizations explain the structure of the synthesized compounds through solid state NMR ($^{13}C$ & $^{29}$ Si) and FTIR, crystallinity using WAPX, thermal resistance through TGA and morphology using SEM.

After synthesizing the hybrid materials, sorption experiments were conducted for which analytical techniques like ICP, microcalorimetry and UV-visible spectroscopy have been utilized.

### 5.1. Elemental Analysis for CHN:

Here in this study using Perkin Elmer 2400, series II, Carbon, Hydrogen and Nitrogen Elemental Analyser, our synthesized samples were analyzed in order to investigate the samples for their organic pedant chain contents. The results are given in table 3 and table 4. The values of each element are also expressed in terms of mmoles of each element per gram of compound (mmol $g^{-1}$) and in terms of the mole ratio between hydrogen and carbon (H / C) in table 3 and carbon and nitrogen (C / N) in table 4. The values of the quantities of each component (Q) incorporated in the pendant chains in mmol per gram of the material for carbon, hydrogen and nitrogen were calculated using equation 10 considering the percentage of the element and its respective atomic mass.

$$Q = \frac{\%of\ Element \times 10}{Atomic\ mass\ of\ the\ element} \qquad \text{Equation 10}$$

The product PAA-12 obtained was submitted to the elemental analysis to measure the quantities of carbon, hydrogen and nitrogen. The results in percentage 25.9 ± 0.2 for carbon, 4.22 ± 0.20 for Hydrogen and 0.20 ± 0.19 for Nitrogen may be observed. The expected theoretical percentage of the organic material was 59 %

(including Cl percentage), in which carbon is 27.8 % and Hydrogen was 4.67 %, while the experimental results are 56 % (from TGA results), 25.9 % and 4.22 % for carbon and hydrogen respectively, which are very close to the expected results. Out of 56 % organic content of the sample, 25.9 % carbon represents 21.6 mmol of carbon per gram of the sample, which is a good amount available for further substitutions in the sample.

*Table 3. CHN results for the synthesized silsequioxanes.*

| Material | Experimental | | | | | Calculated | | | | |
|---|---|---|---|---|---|---|---|---|---|---|
| | **C/%** | **H/%** | **C/mmol $g^{-1}$** | **H/mmol$g^{-1}$** | **H/C** | **C/%** | **H/%** | **C/mmol$g^{-1}$** | **H/mmol$g^{-1}$** | **H/C** |
| PAA-12 | 25.9 | 4.22 | 21.6 | 41.9 | 1.9 | 27.8 | 4.67 | 23.2 | 46. 3 | 2.0 |
| PAA-GDP | 5.74 | 29.0 | 57.0 | 24.1 | 0.4 | 5.88 | 39.0 | 58.4 | 32.5 | 0.6 |
| PAA-MTC | 29.9 | 5.75 | 24.9 | 57.2 | 2.3 | * | * | * | * | * |
| PAA-Ph | 4.06 | 56.2 | 46.8 | 40.4 | 0.9 | 3.87 | 55.4 | 46.1 | 38.5 | 0.8 |

** In case of PAA-MTC some segnifican difference in calculated and experimental values were observed, where analysis of other characterization results for the hybrid PAA-MTC, for instance the bands (1500 – 1550$cm^{-1}$) in IR spectrum (Figure 28b), indicates the presence of unexpected –OH functional group, which in turn affects the calculations and hence end up with a difference in expected and actual values.*

PAA-MTC was also analyzed for its CHN content. The results may be confirmed from table 3, where the percentage of carbon may be observed to be 29.9 % and hydrogen 5.75 %. These values correspond to the 24.9 mmol $g^{-1}$ and the 57.2 mmol $g^{-1}$ for carbon and hydrogen respectively. The expected results for these elements were 41.3 % carbon, 5.76 % hydrogen, 34.4 mmol$g^{-1}$ of carbon and 57.3 mmol$g^{-1}$ of hydrogen.

For the product PAA-GDP, the elemental analysis results are given in table 3. From the table we may observe that the sample is consisted of 5.74 % carbon, and 29.0 % of hydrogen. From the table it may be noted that the 5.74 % of carbon content are in a close relation to that of the expected 5.88 % while in case hydrogen 29.0 % was found experimentally, which were expected to be 39.0 %. The 5.74 % carbon content of the sample corresponds to the 57.0 mmol $g^{-1}$ while 29.0 % of hydrogen gives 24.1 mmol$g^{-1}$ of hydrogen in the sample.

In case of PAA-Ph, the CHN elemental analysis reveals that the compound is consisted of 4.06 % of carbon and 56.2 % of hydrogen. Converting 4.06% of carbon to the mmol $g^{-1}$ gives a total of 46.8 which is in a close agreement to the expected one, while in case of hydrogen the 56.2 % corresponds to 40.4 mmol $g^{-1}$ of the sample. The calculated value for the hydrogen is 46.1%, which is 38.5 mmol $g^{-1}$.

*Table 4. CHN results for the the synthesized silsequioxanes with nitrogen content.*

| Material | Experimental | | | | | Calculated | | | | |
|---|---|---|---|---|---|---|---|---|---|---|
| | C/% | N/% | C/m.molg$^{-1}$ | N/m.molg$^{-1}$ | C/N | C/% | N/% | C/m.molg$^{-1}$ | N/m.molg$^{-1}$ | C/N |
| **PAA-13** | 25.8 | 8.73 | 21.5 | 6.24 | 3.4 | 24.4 | 9.49 | 20.3 | 6.78 | 3.0 |
| **PAA-13-2** | 22.3 | 10.5 | 18.6 | 7.49 | 2.5 | 26.4 | 12.3 | 22.0 | 8.81 | 2.5 |
| **PAA-13-3** | 23.0 | 11.2 | 19.2 | 8.00 | 2.4 | 27.4 | 13.7 | 22.9 | 9.78 | 2.3 |

In the above table the experimental values from the elemental analysis for C and N are compared with those of the calculated ones for PAA-13 sample. The 25.8 % (carbon) and 8.73% (nitrogen) are in a close relation to the calculated ones, i.e., 24.4 % (carbon) and 9.49 % (nitrogen). From these percentages the mmol $g^{-1}$ of carbon and nitrogen were being calculated, which were 21.5 mmol $g^{-1}$ for carbon and 6.24 mmol $g^{-1}$ for nitrogen, while their expected quantities were 20.3 mmol $g^{-1}$ for carbon and 6.78 mmol $g^{-1}$ for nitrogen. These results of the elemental percentages show that the organic pendant chain comprises of the 64 % of the total mass of the synthesized POSS.

Similarly for the compound PAA-13-2, CHN results are 22.3 % for carbon and 10.5 % for nitrogen, while the expected results were 26.4 % of carbon and 12.3 % of nitrogen. These results show the incorporation of the pendant chain to the cage of the silsesquioxane. That is a step towards the confirmation of the pendant chain in main framework. The calculations of the elemental percentages show that the

organic pendant chain comprises of the 77 % of the total mass of the synthesized POSS and it is in a close relationship with TGA results of the compound.

From the table 4, the values for PAA-13-3 may be confirmed, where 23.0 % of carbon corresponds to 19.2 mmol $g^{-1}$ of the sample, while 11.2 % of nitrogen corresponds to 8.00 mmol $g^{-1}$ of the sample PAA-13-3. These results were compared with the calculated ones, which are 27.41 % for carbon and 13.70 % for nitrogen. The calculated mmol $g^{-1}$ of carbon and nitrogen from these percentages are 22.9 and 9.78, respectively.

## 5.2. Infrared Spectroscopy (FTIR):

Keeping in view the importance of the vibrational spectroscopy reported for compounds of this group, all the synthesized compounds were subjected to the IR-spectroscopic analysis. The IR-spectra for all synthesized compounds were taken using KBr discs, which were prepared with KBr:sample (10:1) mass ratio. All the IR-spectra were recorded in a Bomen FTIR MB series spectrometer, with 32 scans, and from 4000 $cm^{-1}$ to 400 $cm^{-1}$ region.

***Figure 26:*** *FT-IR spectrum of PAA-12*

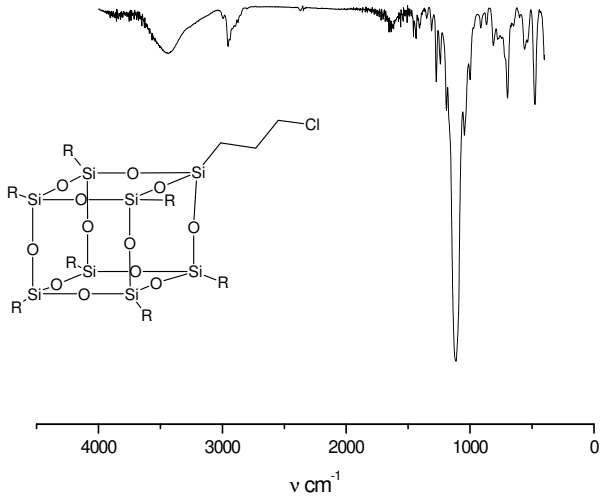

The infrared spectrum of the sample PAA-12 is shown in Figure 26. A well-formed band in the region of 2950 $cm^{-1}$ is attributed to asymmetric C-H vibration, while band at 2880 $cm^{-1}$ is assigned to the symmetric vibration of the same bond. The vibration of the Si-C bond leads to the formation of the band in the region of 1269 $cm^{-1}$. The narrow and intense bands observed at 1035 and 1115 $cm^{-1}$ are attributed to asymmetric stretching Si-O-Si siloxane group of the structure cage. Another band at about 1640 $cm^{-1}$ is attributed to angular vibration of water molecules bound to the inorganic framework. For these organosilicates, the presence of oxygen bonded to the metal atoms of the inorganic structure leads to a well-defined band δ Si-O at 695 $cm^{-1}$and 890 $cm^{-1}$.[153, 154]

***Figure 27:*** *FTIR spectra for the hybrids PAA-13, PAA-13-2 and PAA-13-3*

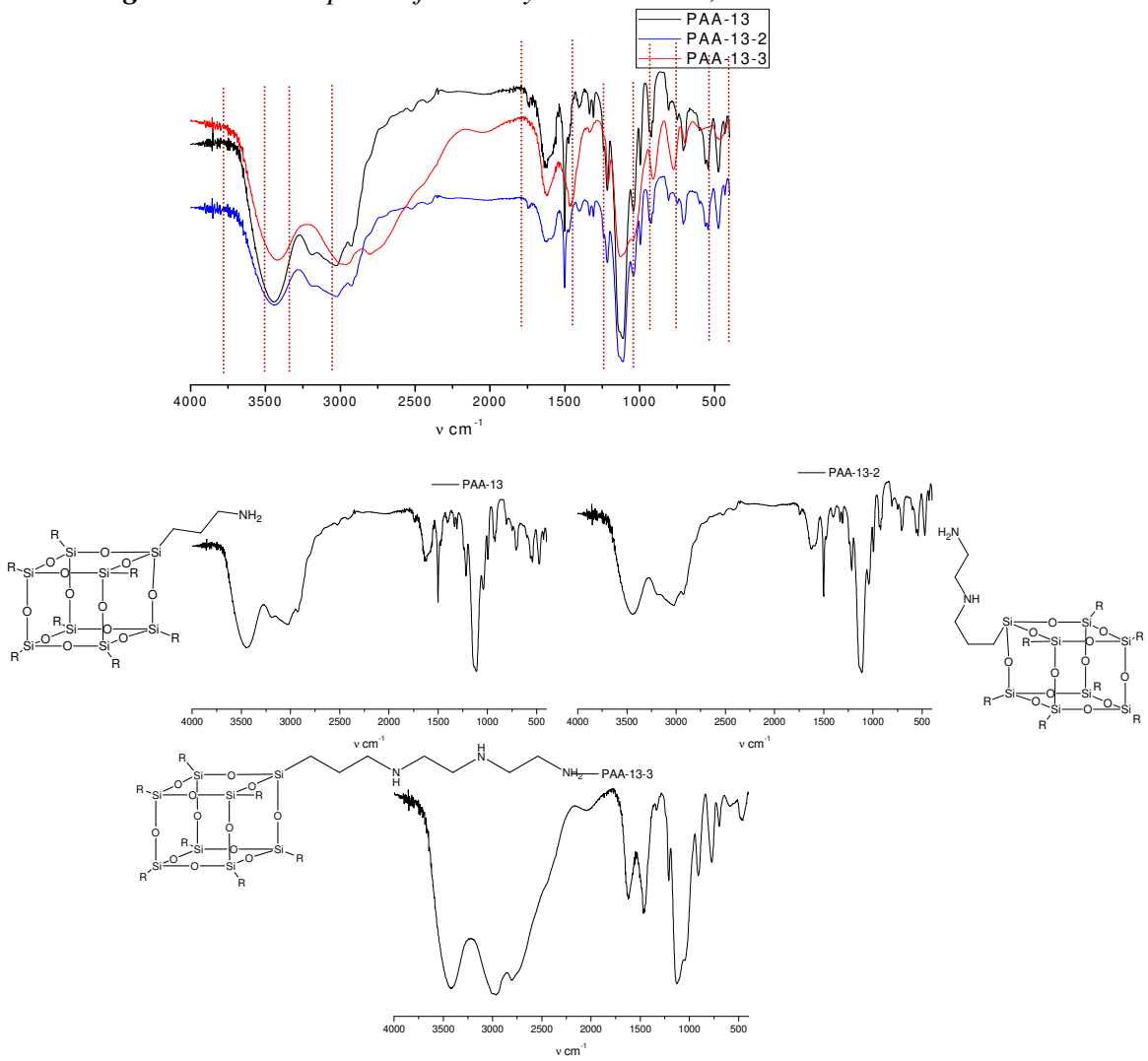

The FTIR spectrum of the hybrid materials PAA-13, PAA-13-2 and PAA-13-3 presents typical bands associated with the inorganic backbone, such as a large band between 3600 and 3250 $cm^{-1}$ assigned to the N-H stretching frequency of the amine groups bonded to the structure, which, in case of PAA-13, gives a band at 3441$cm^{-1}$, for PAA-13-2 it appears at 3449 $cm^{-1}$ and for PAA-13-3 appears at 3426 $cm^{-1}$.[157]

Two weak well-defined bands at the region between 3050 and 2800 $cm^{-1}$ are the characteristic bands for C-H stretching vibrations of the organic molecule bonded to the inorganic silica structure.[156] The C-H bond in PAA-13 leads to the formation of bands at 3022 and 2922 $cm^{-1}$, in case of PAA-13-2 the same band is observed at 3022 and 2914$cm^{-1}$, while in case of PAA-13-3 the respective bands may be confirmed at 2952 and 2806 $cm^{-1}$.The occurrence of the well defined bands in the region from 1050–1100 $cm^{-1}$ are typical characteristics for silica backbone material as previously observed in case of synthesized silsesquioxanes[61] as well as in other mesoporous silica materials.[155] Another set of absorption bands at 916 and 702 $cm^{-1}$ may be attributed to Si-O vibrations.[154]

The infrared spectrum of the sample PAA-GDP is shown in the Figure 28(a). A well-defined band at 1090 $cm^{-1}$ together with two less pronounced bands at 790 and 460 $cm^{-1}$and a weak band at 550 $cm^{-1}$, corresponding to the vibration absorption of Si—O—Si group, indicating that the sample is mainly composed of silica network. A weak band at 1661 $cm^{-1}$ is assigned to C—O vibration of γ-glycidoxypropyl group.[158]

PAA-MTC was also treated using FTIR for its structure elucidation. The infrared spectrum of the sample PAA-MTC is given in figure 28(b). From the spectrum it may be observed that the presence of a well defined band at 1139 $cm^{-1}$

indicates the presence of C—O—C group, while the band present at 1648 $cm^{-1}$ may be attributed to the presence of C=C whereas the band present at 1790 $cm^{-1}$ may be attributed to the C=O of methacrylate group.[169]

Here it is to note that some intense bands present in the region between 1500-1550 $cm^{-1}$ in infrared spectrum for PAA-MTC, which are the characteristic region for the –OH group, indicates that some of the methacrylate groups in the presence of higher acid concentration are cleaved producing some propanol pendant chains.

***Figure 28:*** *FTIR spectrum for the hybrid PAA-GDP(a), PAA-MTC(b).*

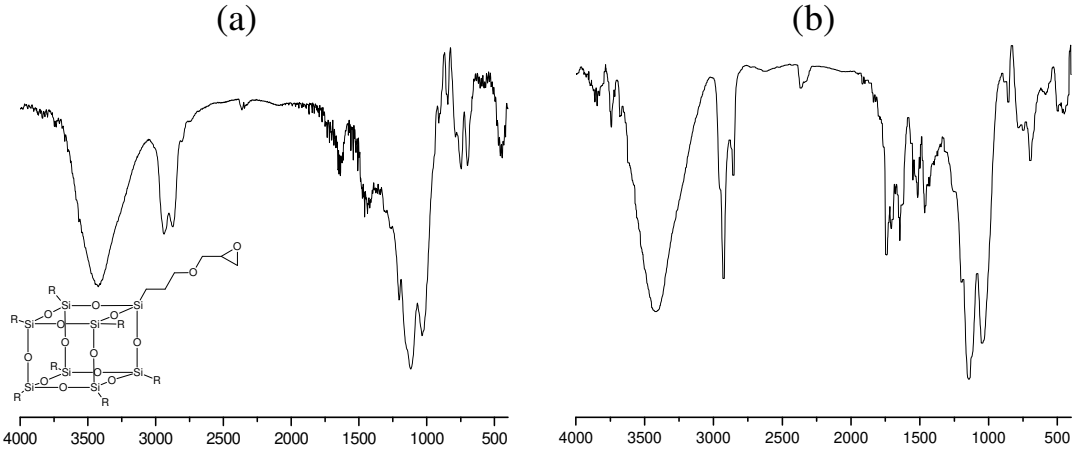


The IR spectrum given in figure 29 is the vibrational spectroscopic results for the sample PAA-Ph. Two well-defined bands at 3052 and 3074 $cm^{-1}$ are attributed to C—H, while bands at 1480 and 1590 $cm^{-1}$ indicates the presence of benzene ring.[159] A vibration of the bond Si-C gives the formation of band at 996 $cm^{-1}$. Some intense bands observed at 1041 and 1113 $cm^{-1}$ are attributed to asymmetric stretching of Si-O-Si group of the siloxane cage structure.[160] For these organosilicates, the presence of oxygen bonded to silicon, δ Si-O, gives a well-defined band at 702 $cm^{-1}$.[161] Other observed bands at 916 $cm^{-1}$ may be attributed to the δ Si-O.[162]

***Figure 29:*** *FTIR spectrum for the hybrid PAA-Ph.*

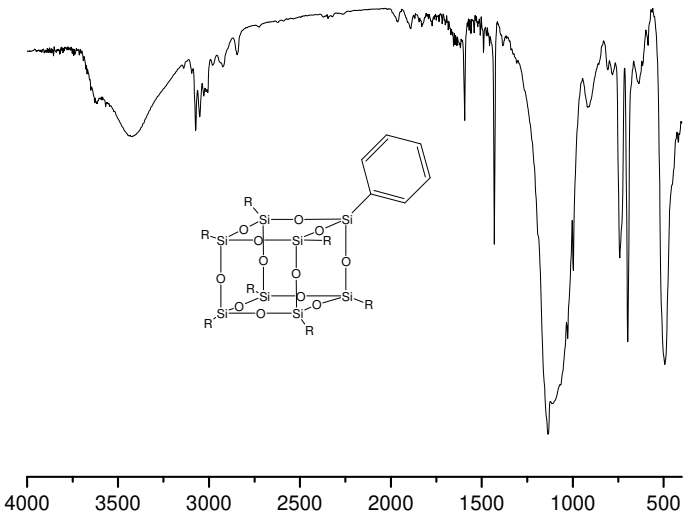


## 5.3. Solid state $^{13}$C-NMR:

The $^{13}$C-NMR spectrum in solid state with cross polarization and magic angle spinning was taken for the sample PAA-12, through Bruker 300 at 75 MHz, using the following experimental conditions: acquisition time of 0.05 s, pulse sequence with 4000 μs time of contact, pulse interval of 3 s and 256 accumulations.

***Figure 30:*** *Solid state $^{13}$C-NMR spectrum for the hybrid PAA-12.*

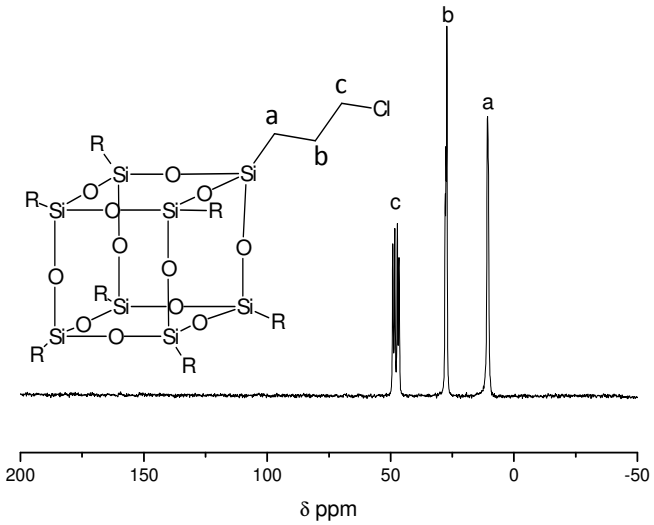

The pendant chain in PAA-12 has three carbon types, C-Si, $CH_2$ and C-Cl, therefore three peaks are to be expected in the $^{13}C$ NMR spectrum of the molecule. From the figure 30, three $^{13}C$ NMR singlets at 9.88 ppm for $SiCH_2$- (a), at 26.38 ppm -$CH_2$- (b), and at 47.06 ppm -$CH_2Cl$ (c), are observed, which is an evidence that the expected product was obtained successfully.[21]

The $^{13}C$-NMR/CPMAS in solid state for the sample PAA-13 was taken through Bruker 400 at 100 MHz, using the following experimental conditions: acquisition time of 0.05 s, pulse sequence with time of contact 4000μs, 3 s pulse interval and 531 accumulations.

***Figure 31:*** *Solid state $^{13}C$-NMR spectrum for the hybrid PAA-13*

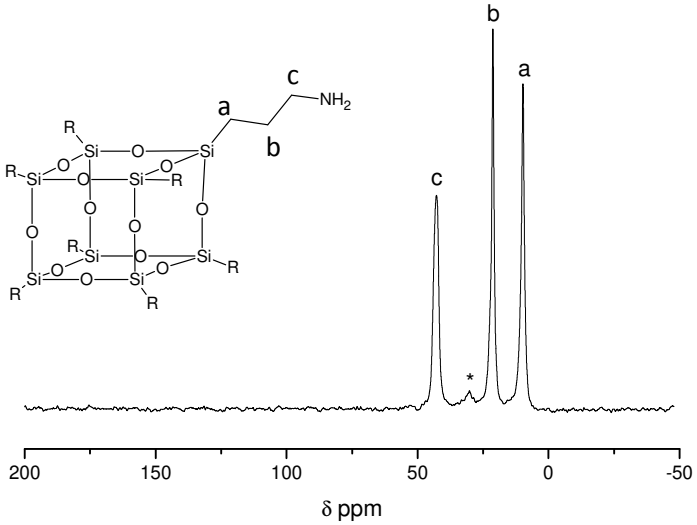


The $^{13}C$ NMR spectrum for octakis (3-aminopropyl) silsesquioxane, PAA-13, is given in Figure 31. The assignments were made based on reported $^{13}C$ NMR spectra of similar solid state compounds and with that of the precursor molecule. The chemical shifts at 9.76 ppm $SiCH_2$- (a), 21.25 ppm -$CH_2$- (b) and 42.76 ppm -$CH_2NH_2$(c) is observed. The chemical shift marked with "*" shown in spectrum is attributed to carbon atoms from residual aminopropyl groups that did not react.[164] The $^{13}C$ NMR spectrum confirms that the desired material was obtained.

***Figure 32:*** *Solid state $^{13}$C-NMR spectrum for the hybrid PAA-13-2.*

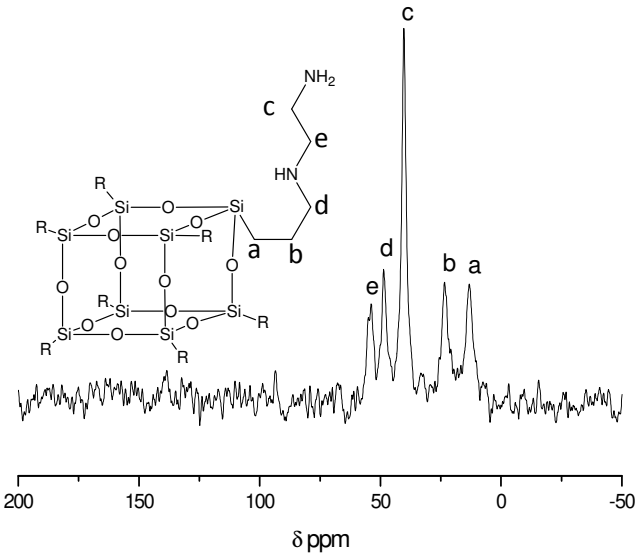


For the sample PAA-13-2 the $^{13}$C-NMR/CPMAS solid state spectra was recorded in a Bruker 300 at 75 MHz, with acquisition time of 0.05 s, pulse sequence with time of contact 4000 μs, pulse interval 3 s and 256 accumulations. The $^{13}$C-NMR/CPMAS spectra for the sample PAA-13-2 is given in Figure 32. In this spectrum five signals may be observed: a singlet at 13.14 ppm is attributed to the group $SiCH_2$- (a), singlet at 23,39 ppm to -$CH_2$- (b), at 40,21 ppm to -$CH_2$-$NH_2$(c); at 48,61 ppm to -NH-$CH_2$- (d) and at 54,94 ppm to -$CH_2$-NH- (e).[165] From the data it could be observed that all five non-equivalent carbons, according to the expectations, in the molecule were detected by the $^{13}$C-NMR. This is evidence that the expected pedant chain was anchored to the POSS structure.

The $^{13}$C solid state spectra with cross polarization and magic angle spinning for the sample PAA-13-3 was taken using a Bruker 300 at 75MHz, following the experimental conditions: acquisition time of 0.05 s, pulse sequence with time of contact 4000 μs, pulse interval 3 s and 260 accumulations.

***Figure 33:*** *Solid state $^{13}$C-NMR spectrum for the hybrid PAA-13-3.*

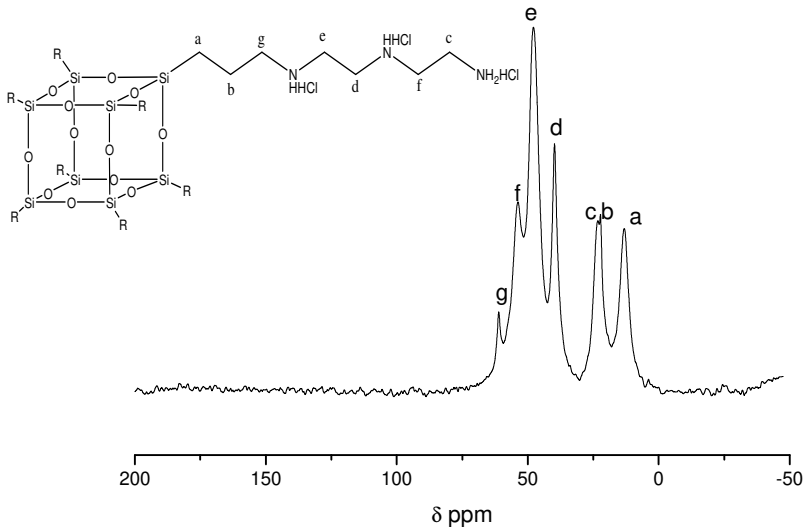


The $^{13}$C NMR spectrum of the hybrid material PAA13-3, presented in Figure 33, gives important information regarding attachment of the pendant groups in the inorganic structure of the hybrid.[7,155,166] The hybrid material showed well resolved peaks positioned at 10 ppm $SiCH_2$- (a), 17 ppm -$CH_2$- (b), and 22 ppm -$CH_2NH_2$- (c) for the spacer propyl chain carbon atoms attached to silica. Other carbon atoms were observed at 37 ppm -$CH_2NH_2$- (d), 47 ppm -$NHCH_2$- (e), 58 ppm -$NHCH_2$- (f) and 62 ppm -$CH_2NH$- (g), which reinforces the presence of the pendant chain. All the assignments were in good agreement with previously studied systems.[167] Thus, the sequence of peaks presented in the spectrum for the hybrid material confirms the sequence of carbons of the pendant groups obtained by the synthesis method employed in the obtaining these materials.[166, 167]

The $^{13}$C -NMR spectrum in solid state for the sample PAA-GDP, using CP/MAS technique was taken through Bruker 400 at 100MHz.

Figure 34 shows the $^{13}$C NMR spectrum for PAA-GDP. The spectrum shows six signals at 9.79, 23.52, 46.96, 61.20, 70.64, and 74.39 ppm. These signals confirm the presence of six types of carbon atoms in the POSS-GDP framework. The signal at 9.79 ppm may be attributed to the carbon of Si—$CH_2$ (a), at 23.52 ppm to Si—

$CH_2$—$CH_2$ (b), at 46.96 ppm to the $CH_2$—O (c), the band present at 61.20 ppm may be attributed to the $CH_2$—O (d) and the band present at 70.39 ppm may be attributed to the $CH_2$—O (e) and the band present at 74.39 may be attributed to $CH_2$—O (f).[168]

***Figure 34:*** *Solid state $^{13}$C-NMR spectrum for the hybrid PAA-GDP.*

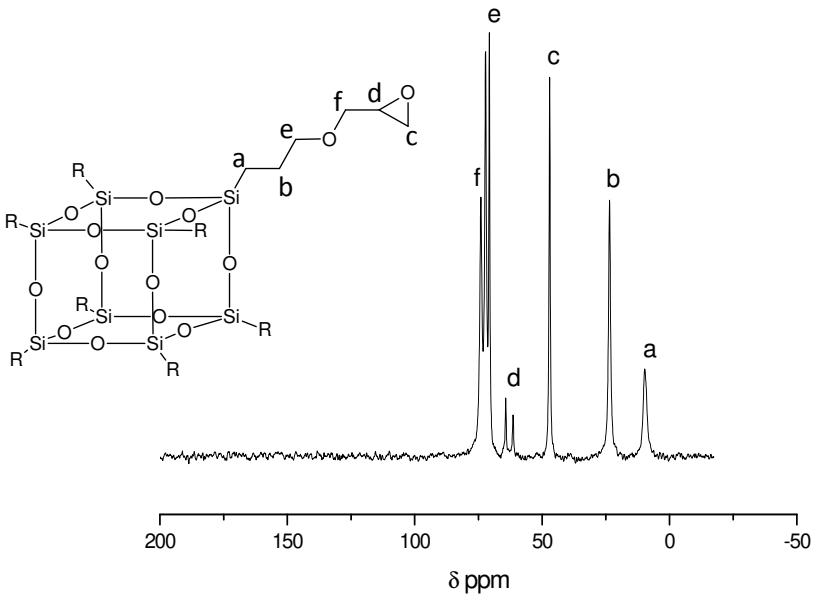


In Figure 35, the 13C-NMR spectra for the sample PAA-MTC is given. The NMR spectrum given in this figure represents the organic pendant chain anchored to the silsesquioxane cube. From the spectrum it may be observed that peak at 11 ppm represents the Si-CH- (a), peak at 25 ppm is for $–CH_3$ (b), while peak at 65 ppm represents $–CH_2$-O- (c). [169] Other carbons present in the spectrum are, 125 ppm $=CH_2$ (d), 129 ppm –C= (e) and at 166 ppm –C=O (f), these peaks were of lower intensity, which are magnified and shown in the insert graph.

***Figure 35:*** *Solid state $^{13}$C-NMR spectrum for the hybrid PAA-MTC.*

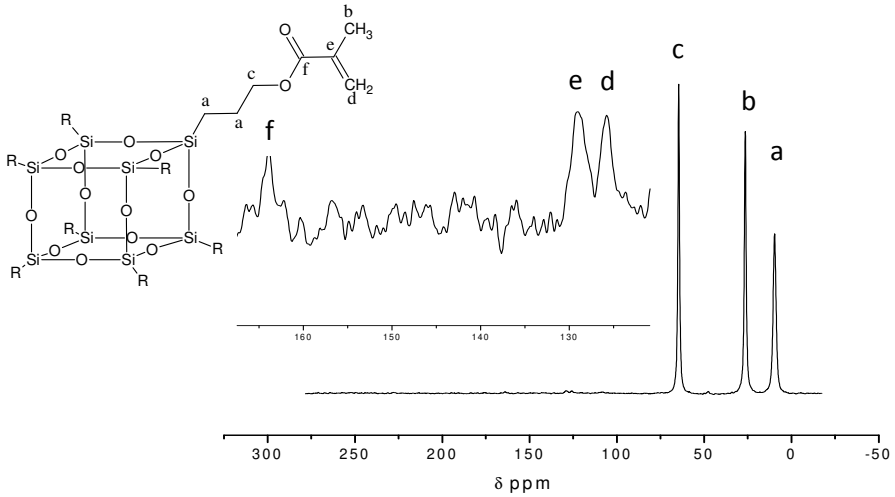


The $^{13}$C-NMR/CPMAS in solid state for the sample PAA-Ph was taken using Bruker 300 at 75 MHz.

***Figure 36:*** *Solid state $^{13}$C-NMR spectrum for the hybrid PAA-Ph.*

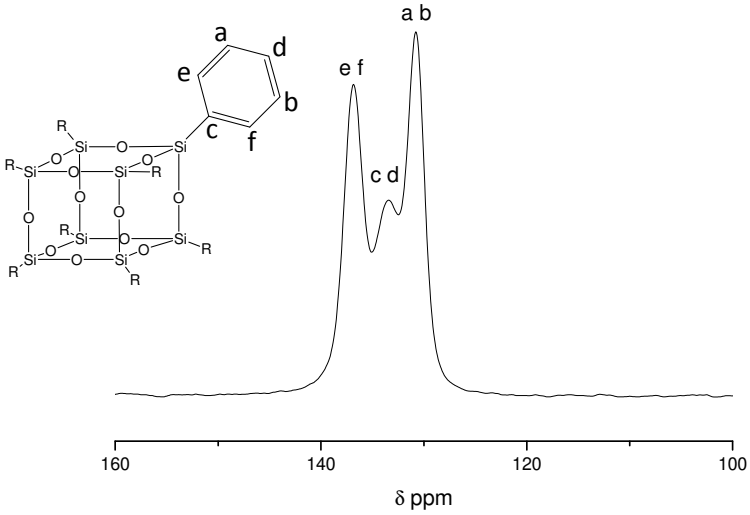


The $^{13}$C NMR spectrum of the compound PAA-Ph is shown in the Figure 36. In this spectrum three peaks appear: one singlet at 136.14 ppm (for carbons e, f), one broad signal that is composed of two peaks, one at 132.32 ppm (for carbon c), one at 131.7 ppm (for carbon d). The fourth one at 130.4 ppm representing a and b carbons of the benzene ring.[154]

## 5.4. Solid State $^{29}$Si-NMR:

The $^{29}$Si-NMR solid state spectrum of PAA-12 is given in Figure 37. There is only one peak in the spectrum, in the chemical shift of -66.5 ppm, indicating that there is only one structural conformation of the silicon atom in the compound. It also indicates that the product is an uniform structure of high purity. Moreover, the value of the chemical shift is near to that of the silicon atom in the cage structure of $(RSiO_{1.5})_8$.[171]

Similarly, the $^{29}$Si-NMR spectrum of PAA-13(Figure 38) in solid state have the chemical shift δ -64 ppm,[72] from which it can be confirmed that the synthetic compound POSS-$NH_2$ have the cage structure, and its structural formula should be $(H_2NCH_2CH_2)_8Si_8O_{12}$.

***Figure 37:*** *Solid state $^{23}$Si-NMR spectrum for the hybrid PAA-12.*

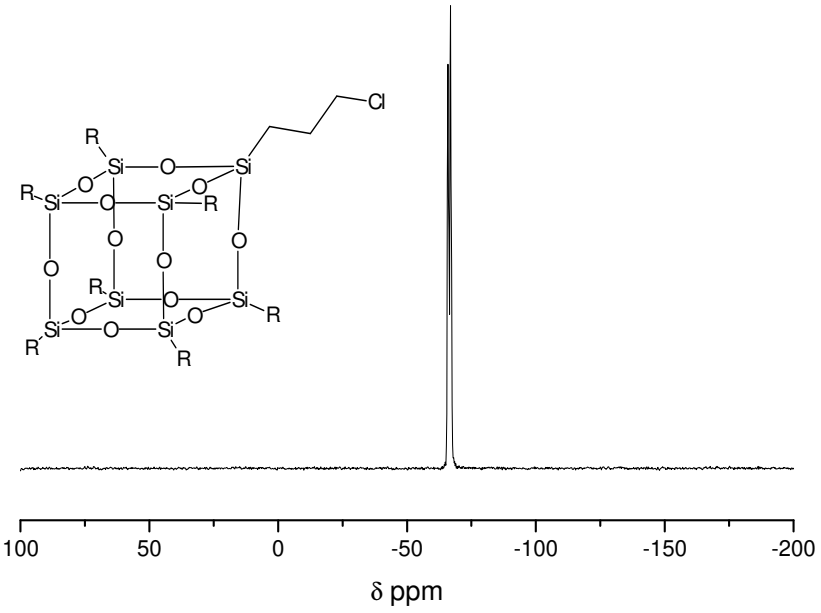

***Figure 38:*** *Solid state $^{23}$Si-NMR spectrum for the hybrid PAA-13.*

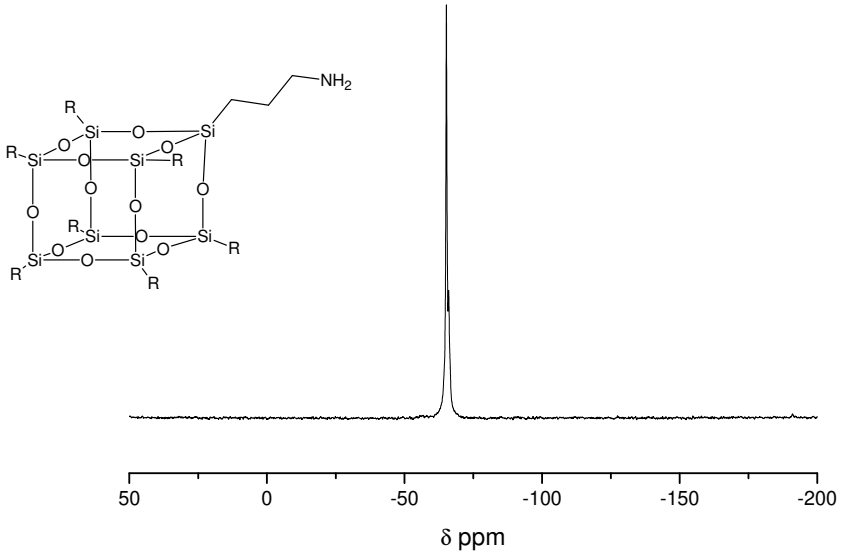


From the $^{29}$Si-NMR spectra of PAA-13-2 (Figure 39) and PAA-13-3 (Figure 40), the presence of only one conformational Si may be confirmed. The peaks at -64.64 ppm and -64.33 ppm, respectively, is the evidence of the presence of only one conformational Si atoms in the structures of the synthesized compounds.

***Figure 39:*** *Solid state $^{29}$Si-NMR spectrum for the hybrid PAA-13-2.*

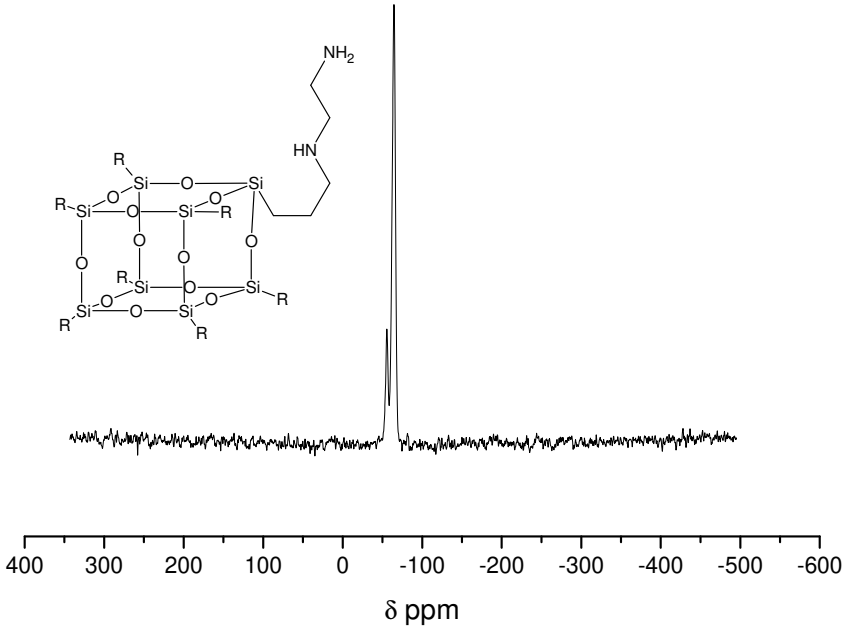

***Figure 40:*** *Solid state $^{23}$Si-NMR spectrum for the hybrid PAA-13-3.*

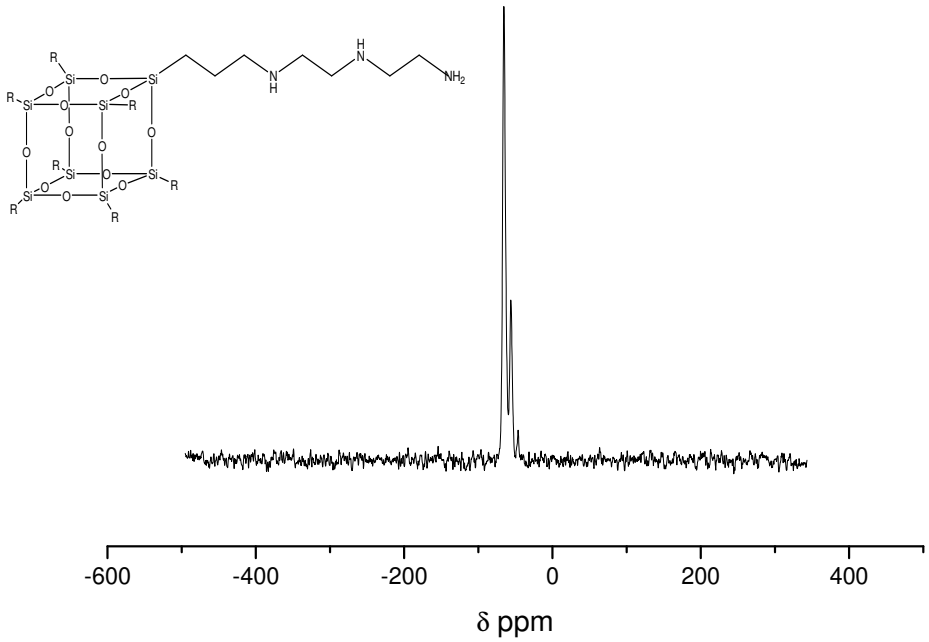


The $^{29}$Si NMR spectrum of the PAA-GDP is given in Figure 41. The spectrum shows a peak at -66.04ppm, that confirms the presence of Si in the PAA-GDP framework. The peak shows between -66.04 and -65.23, which may be attributed to the flexibility of the POSS cage. A small signal present at -55.07 is the signal that confirms the attachment of the glycidoxypropyl to the Si atom of the silsesquioxane cage.[168]

***Figure 41:*** *Solid state $^{23}$Si-NMR spectrum for the hybrid PAA-GDP.*

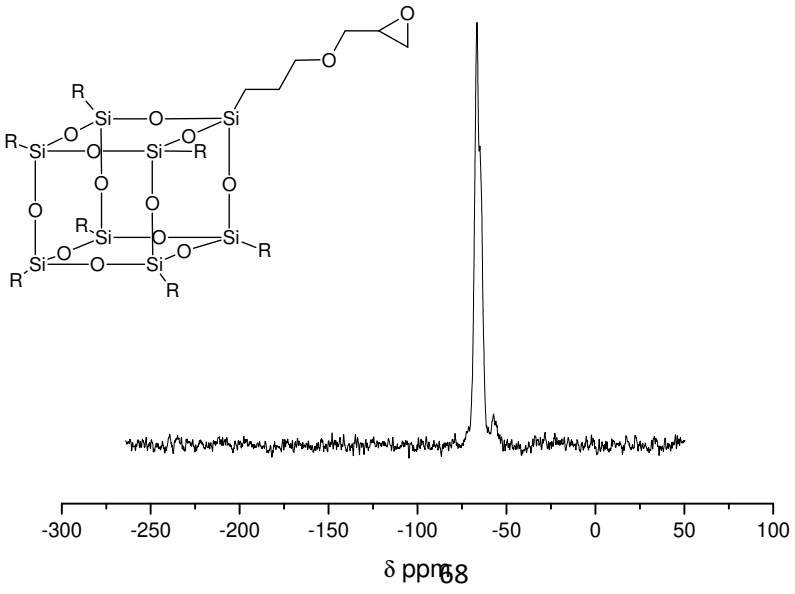

***Figure 42:*** *Solid state $^{23}$Si-NMR spectrum for the hybrid PAA-MTC.*

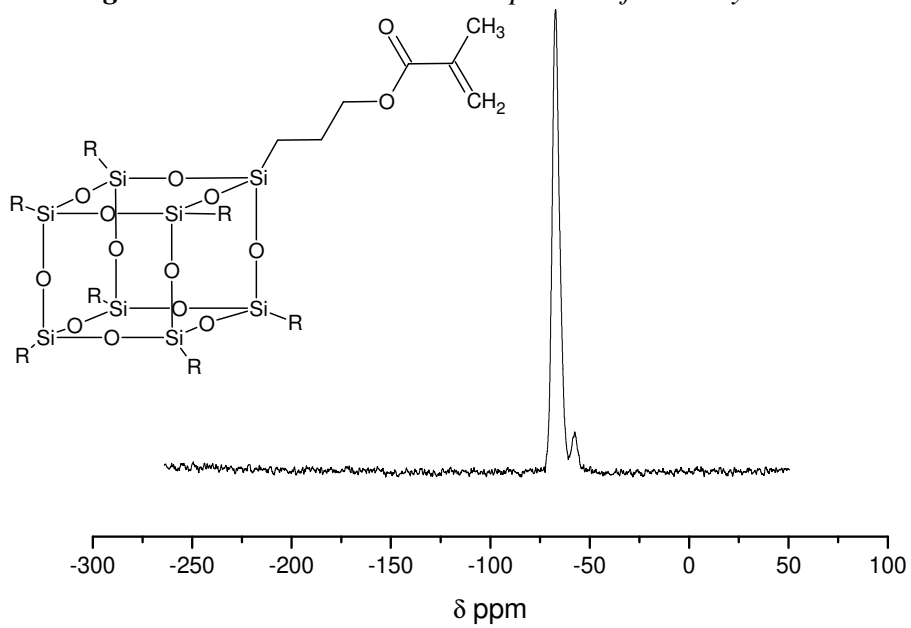


The $^{29}$Si RMN in solid state of was used to confirm the structure of the compound PAA-Ph. Two singlets for T-type silicon atom appears at -66.64 and -74.58 ppm (Figure 43). These signals may be attributed to the presence of the silicon atom bonded to oxygen in the cage structure as well as to the phenyl group of the synthesized compound. These peaks are similar to the reported results for such types of compounds.[153]

***Figure 43:*** *Solid state $^{23}$Si-NMR spectrum for the hybrid PAA-Ph.*

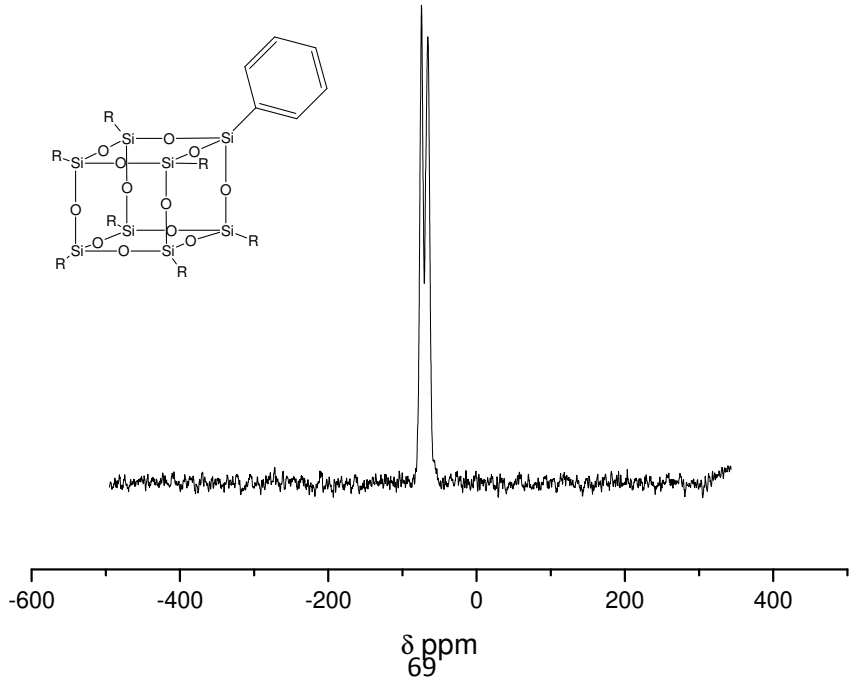

## 5.5. Thermogravimetric Analysis TGA:

There have been numerous studies on the thermal stability and decomposition pathways for $T_8R_8$ compounds by TGA. For $T_8Ph_8$, the thermal stability is greater, giving a high ceramic residue of silica containing carbon,[107,172] however, TGA of $T_8Me_8$ and $T_8Et_8$ in $N_2$ has also been reported to show almost 100 % of evaporation at ca. 250-260 °C.[108] The TGA of $T_8H_8$ shows rapid, near complete mass loss at temperatures over circa of 200 °C attributed to its sublimation.[173] The TGA curve for $T_8Me_8$ has been reported to show decomposition under nitrogen starting at ca. 230 °C, but in the light of other studies described above, the mass loss observed was actually likely to be due to sublimation. When blended with isotactic polypropylene $T_8Me_8$ forms a nanocomposite having a decomposition onset at 320-348 °C.[174]

In light of the above discussions, all the synthesized samples were analyzed for their respective thermal behaviors. The analyses have been done using the instrument TGA 2050 model of TA instruments.

The thermograms and the respective derivatives of the synthesized silsesquioxanes are given in Figure 44 to 49. From these thermograms the mass losses for all the synthesized compounds were calculated.

***Figure 44:*** *Thermogram for the hybrid PAA-12.*

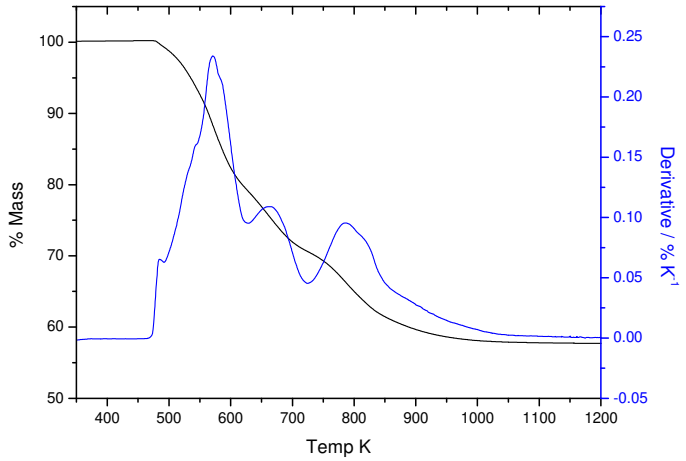

The thermogram given in Figure 44 shows the thermogravimetric behavior of the hybrid PAA-12. In this figure it may be observed that almost 40 % of the total mass is lost. The decomposition process is very slow and extends up to 970 K. In the beginning, the compound losses are very small amount, which could be attributed to the loss of physically sorbed water on the surface. The compound losses 17.2, 10.3 and 14.2 % mass in coming steps, which shows a gradual loss of the pendent organic chain. A total of 40 % mass is decomposed, which is quite close the CHN results.

The silsesquioxane hybrid molecules, PAA-13, PAA-13-2 and PAA-13-3 exhibited distinct decompositions during heating, as shown in Figures 45 (a) and (b). In the first step of all three hybrids, the physically adsorbed water on the surface was lost at a low temperature. The functionalised hybrids showed a loss in mass of physically adsorbed water in the first step, in almost the same range as is observed from the figures. An abrupt loss in mass was detected in the next step, which is 31.5 % in case of PAA-13, 42.9 % for PAA-13-2 and 47.0 % for PAA-13-3. These losses in mass are probably due to the decomposition of the anchored organic chains. The three hybrids after complete decomposition left the residue, which in case of PAA-13 is 43.4 %, for PAA-13-2 is 39.4 % and 30.9 % is for PAA-13-3. These residue percentages are quite compatible with the results obtained for CHN analysis of these compounds.

***Figure 45:*** *Thermogram for the hybrids PAA-13, PAA-13-2 and PAA13-3.*

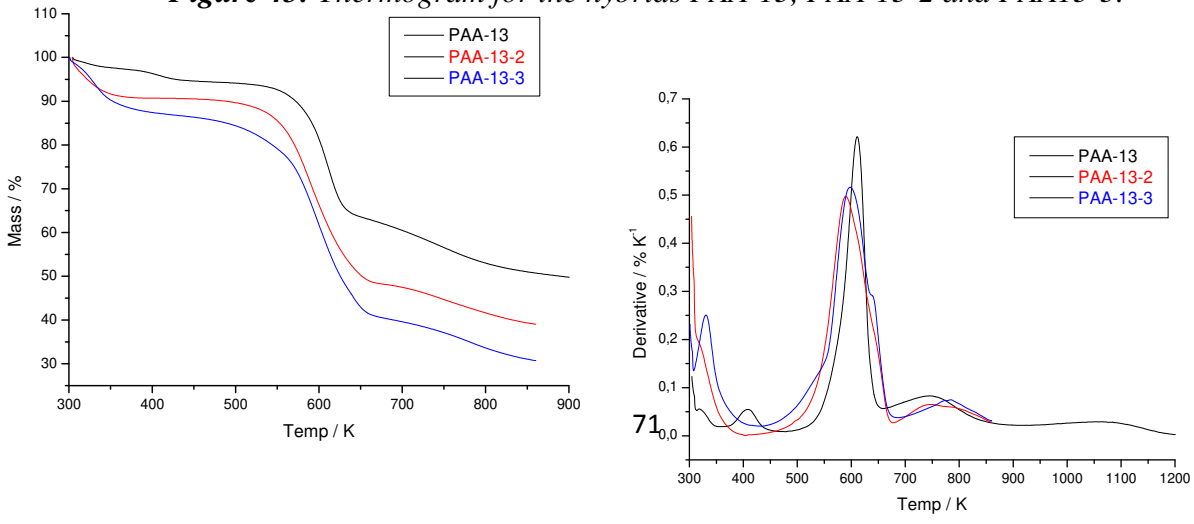

The thermogram of PAA-GDP (Figure 46.) shows a degradation that starts at 309 K which extends up to 852 K, with a total of 56 % mass loss. The first of this series 2.4 % mass loss is observed at 318 K, which may be attributed to the loss of volatile impurities. The mass loss of 38.4 % may be attributed to the organic pendant chain, which can be observed at 620 K, whereas a mass loss of 8.8 % at

***Figure 46.*** *Thermogram for the hybrid PAA-GDP.*

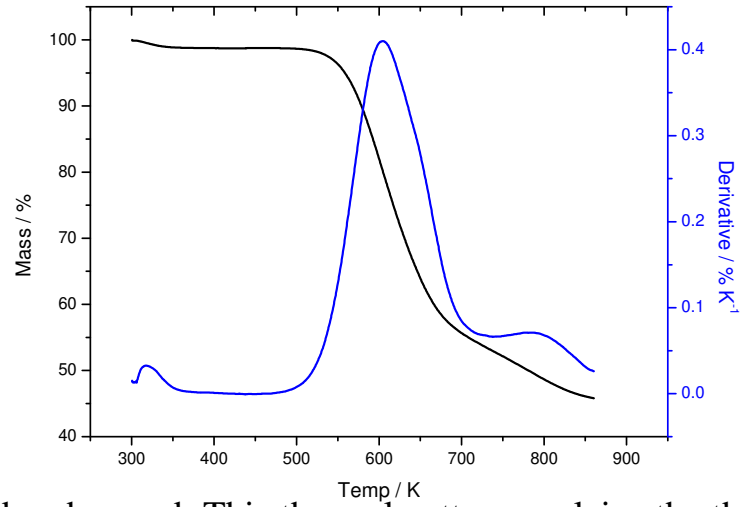


765 K may also be observed. This thermal pattern explains the thermal stability of the synthesized compound.

***Figure 47:*** *Thermogram for the hybrid PAA-MTC.*

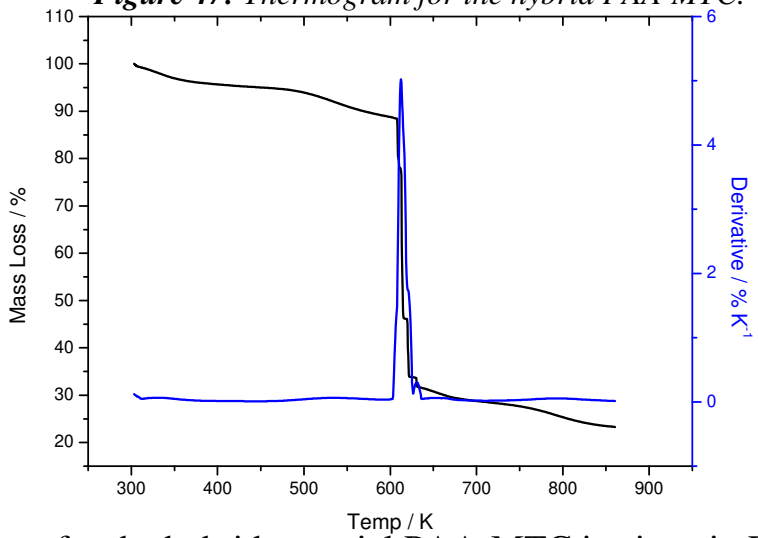


The thermogram for the hybrid material PAA-MTC is given in Figure 47, and their respective values are given in Table 5, where in three different mass losses may be observed. The first two mass losses, which are round about 11% of the total mass,

may be attributed to the desorption of water as well as volatile impurities. The next mass loss, which is very rapid and is equal to 58 % of the total mass, may be attributed to the typical decomposition of methacrylate esters. The abrupt mass loss at this stage may be justified through methacrylate decomposition mechanism (Figure 48.). Methacrylate esters upon heating, splits up and produces unsaturated alkenes along with the liberation of acetic acid. The liberation of acetic acid is a molecular chain reaction and is a rapid process.[175]

***Figure48:*** *Methacrylate decomposition patway*

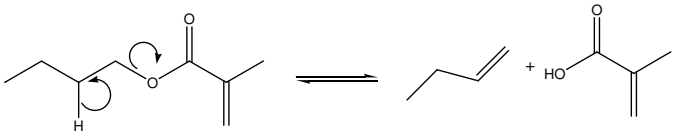


The TGA result for PAA-Ph is shown in Figure 49. The weight loss from 320 to 580 K for PAA-Ph is 6.6 %, this is mainly associated with the condensation reaction of residual silanols and ethoxy groups. The thermal degradation of siloxane network at 700–850 K, amounting to 12.2 % indicates the decomposition of phenyl groups in the sample. But 81 % residue of the PAA-Ph is very high, which was expected to be ± 40%. The literature[176] reveals that the combustion of the sample is incomplete and was needed to treat it for longer time and up to higher temperature.

***Figure 49:*** *Thermogram for the hybrid PAA-Ph.*

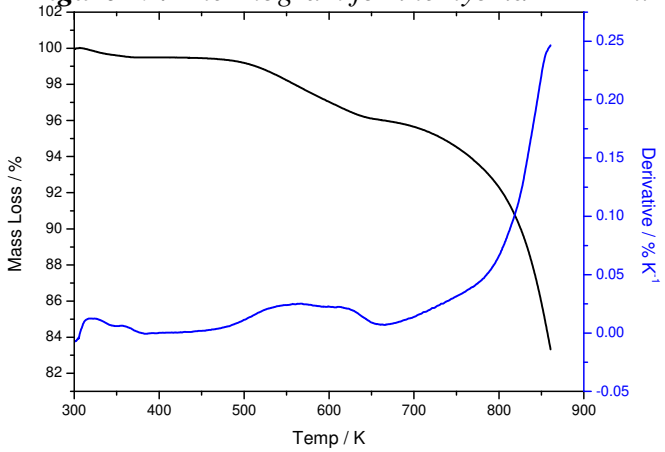

The mass losses as well as their respective temperatures for the synthesized hybrid materials are summarized in Table 5. From this table it can be observed that almost all synthesized silsesquioxane, except PAA-13, showed three step degradation leaving 30-60 % residues. The only exception in this series is the 81.2 % residue for the sample PAA-Ph. The literature reveals that this sample should be given more time and should be heated more for its complete degradation.

***Table 5. Thermogravimetric results obtained from the thermograms of the samples.***

| POSS | Mass Loss step | T onset/K | T offset/K | Mass loss / % | Mass char / (%) |
|---|---|---|---|---|---|
| PAA-12 | I | 478 | 597 | 17.2 | 58.3 |
| | II | 619 | 693 | 10.3 | |
| | III | 755 | 961 | 14.2 | |
| PAA-13 | I | 309 | 334 | 2.4 | 43.4 |
| | II | 390 | 428 | 3.0 | |
| | III | 581 | 611 | 31.5 | |
| | IV | 707 | 807 | 13.8 | |
| | V | 996 | 1143 | 5.9 | |
| PAA-13-2 | I | 314 | 344 | 8.6 | 39.4 |
| | II | 552 | 629 | 42.9 | |
| | III | 714 | 813 | 9.2 | |
| PAA-13-3 | I | 321 | 353 | 12.7 | 30.9 |
| | II | 557 | 637 | 47.0 | |
| | III | 741 | 818 | 9.4 | |
| PAA-GDP | I | 310 | 359 | 2.4 | 50.5 |
| | II | 532 | 670 | 38.4 | |
| | III | 726 | 839 | 8.8 | |
| PAA-MTC | I | 324 | 433 | 4.6 | 31.3 |
| | II | 497 | 606 | 6.1 | |
| | III | 606 | 636 | 58.1 | |
| PAA-Ph | I | 315 | 362 | 2.3 | 81.2 |
| | II | 496 | 636 | 4.3 | |
| | III | 716 | 861 | 12.2 | |

## 5.6. Wide angle Powder X-ray Diffraction WPXRD:

The X-ray diffraction spectra for the sample PAA-12 is given in figure 50, where well defined peaks can be observed. The X-ray diffraction reveals that the synthesized sample PAA-12 has some regular patterns, which may be due to the presence of POSS crystals. The spectral lines present in the PAA-12 are summarized in table 6. Values in table are generated in Origin® 8.0, whereas thickness of diffraction peaks are calculated using MS-Excel 2007. Lattice parameters were calculated using the software Chekcell.

***Figure 50:*** *X-Ray diffractogram for the hybrid PAA-12.*

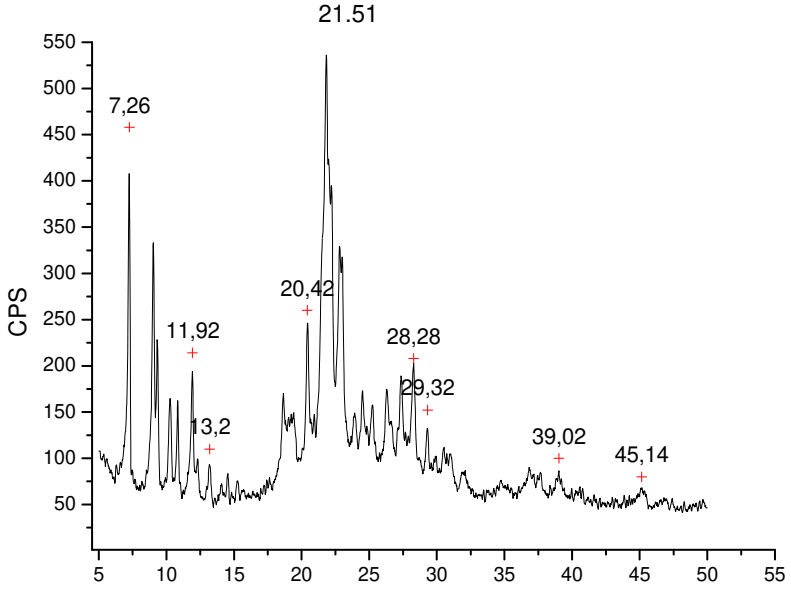


***Table 6. X-Ray Diffraction data for the hybrid PAA-12***

| | 2 Θ | Height (from base) | Width (at half height) | Area | Thickness Nm |
|---|---|---|---|---|---|
| **1** | 7.21 | 73.96 | 0.13 | 52.66 | 6 |
| **2** | 9.01 | 63.92 | 0.13 | 47.73 | 6 |
| **3** | 9.33 | 69.88 | 0.15 | 20.17 | 5 |
| **4** | 11.91 | 53.93 | 0.14 | 15.19 | 6 |
| **5** | 20.43 | 75.86 | 0.23 | 54.51 | 4 |
| **6** | 21.67 | 171.7 | 0.57 | 263.92 | 1 |
| **8** | 22.71 | 27.97 | 0.27 | 69.22 | 3 |
| **10** | 24.57 | 19.82 | 0.88 | 101.9 | 0.9 |
| **11** | 26.42 | 47.79 | 0.42 | 56.69 | 2 |
| **12** | 27.37 | 51.84 | 0.45 | 50.17 | 1.8 |
| **13** | 28.20 | 63.84 | 0.37 | 52.48 | 6 |

Here in table 6 the 2Θ, height of the peak from the base, width of the peak at half height, area of the peak and their respective thickness calculated by the Scherer's equation are given. From table one can easily observe that 2Θ values for major reflections ranges from 7.20$^{o}$ to 28.20$^{o}$. The last column of the table where, the thicknesses of the crystal lattice calculated by Scherer's equation demonstrate that crystal thickness ranges from 0.9 to 6 nm. Based on the experimental values, using the software Chekcell®, the reflection 010, 01-1, 011, 020, 021 etc identifies the crystal to be best fitted by the Rhombohedral lattice symmetry with space group R3M.

From figure 51 X-ray diffraction spectrum for the sample PAA-13 may be observed. Well defined peaks indicate the presence of some repeated units in the sample, which suggests that the sample PAA-13 is somehow crystalline in nature.

In table7. some well resolved reflection are summarized where 2Θ values ranges from 10.53$^{o}$ to 38.30$^{o}$. These experimental values on further calculations suggest the thickness of the crystals present in sample calculated through Scherer's equation, ranging from 0.63 nm to 3.20 nm.

***Figure 51:*** *X-Ray diffractogram for the hybrid PAA-13.*

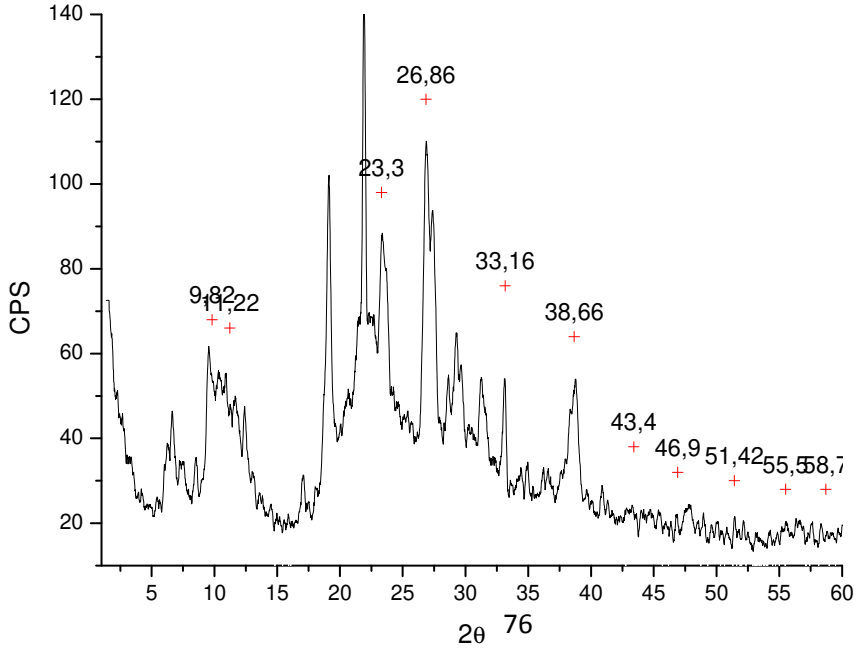

***Table 7. X-Ray Diffraction data for the hybrid PAA-13***

| | 2 Θ | Height (from base) | Width (at half height) | Area | Thickness nm |
|---|---|---|---|---|---|
| **1** | 10.53 | 14.78 | 1.30 | 48.82 | 0.63 |
| **2** | 19.14 | 30.32 | 0.37 | 37.36 | 2.25 |
| **3** | 20.62 | 2.75 | 1.21 | 21.60 | 0.69 |
| **4** | 21.94 | 60.54 | 0.26 | 45.13 | 3.24 |
| **5** | 23.48 | 26.58 | 0.94 | 49.89 | 0.89 |
| **6** | 26.76 | 30.87 | 0.56 | 51.33 | 1.50 |
| **7** | 28.52 | 12.37 | 0.43 | 12.48 | 1.95 |
| **8** | 31.56 | 13.47 | 0.75 | 23.02 | 1.14 |
| **9** | 33.03 | 12.72 | 0.27 | 10.52 | 3.20 |
| **10** | 38.30 | 1.40 | 0.54 | 18.45 | 1.59 |

The data obtained from the experiment was further treated using the software Chekcell®, where the reflection such as -100, 0-10, 001, 010 etc may easily be observed. These values in comparison with the database provided by the software Chekcell® suggest to be best fitted by the triclinic symmetry, having the space group P1.

The synthesized PAA-13-3 sample was subjected to powder X-ray technique to evaluate its crystalline or amorphous nature. Spectrum obtained for the compound may be observed in figure 52, where instead of expected well defined peaks, a shoulder type diffractogram is present.

The first impression about the synthesized compound was its amorphous form. But after thorough analysis of the nature of compound and comparing it with other, previously synthesized compounds, the results were seemed to be suspicious. After thorough analysis of the molecule it was believed that the long organic pendent chain attached to the cage may cover the cage and hence may disperse the normal reflections, resulting in a shoulder type diffractogram rather than well defined peaks. Compound was subjected to further powdered X-ray analysis but this time,

the temperature increased protocol was adopted. Spectra were recorded with an increase in temperature ranging from room temperature to 600 $^{o}$C, with an increase rate of 10 $^{o}$C min$^{-1}$. The results obtain through this experiment are shown in figure.

***Figure 52:*** *X-Ray diffractogram for the hybrid PAA-13-3.*

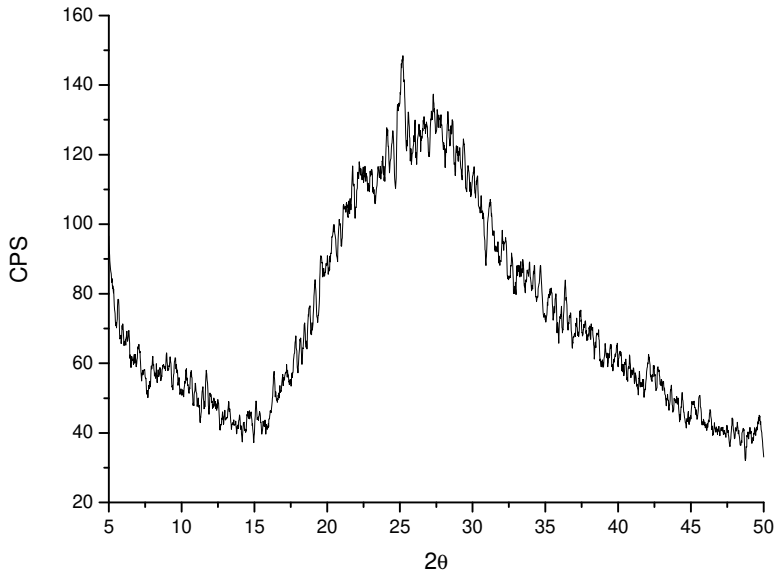


Analyzing the spectra from figure 53, upon heating the appearance of new peaks and the gradual disappearance of the shoulder supported to understand that the hypothesis regarding the organic pendent chain covering the POSS cage is to be true. The compound showed some crystalline nature while heating, which may probably be due to the decomposition of the organic pendant chain and hence it's consequential regularization of the X-ray dispersions.

***Figure 53:*** *X-Ray diffractogram for the hybrid PAA-13-3 with heating from room temperature to 600 $^{o}$C.*

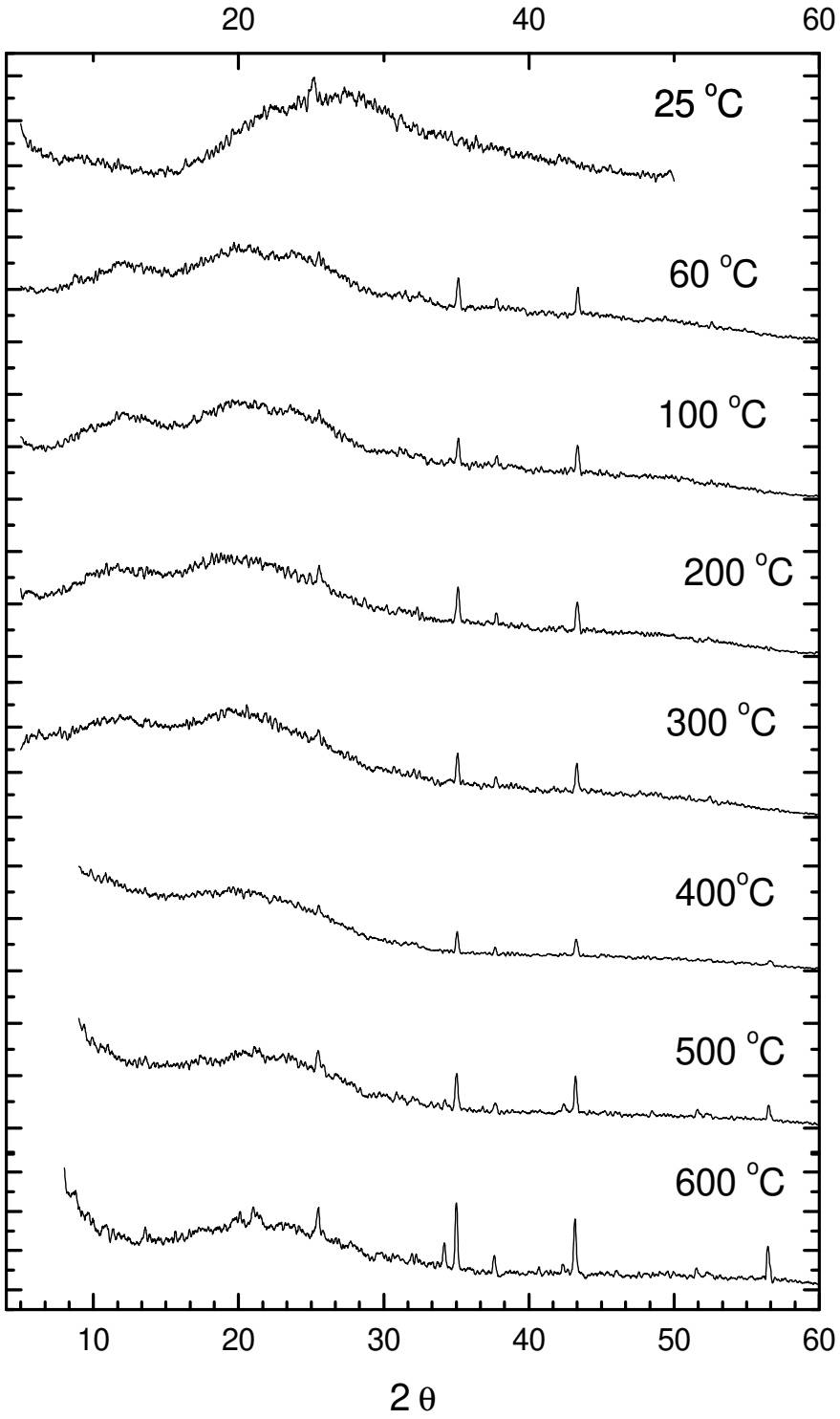

Figure 54. is the graphical representation of results obtained, while analyzing the synthesized PAA-13-3 by XRD technique, operating at 600 $^{o}$C. From the spectrum as well as from the inset table, some well defined peaks at 21.3, 25.36, 34.98, 43.18and 56.44 may be observed. These values correspond to the d-spacing 4.2, 3.5, 2.6, 2.1 and 1.6 Å calculated using Bragg's equation respectively. The diffractogram shows that the hybrid PAA-13-3 is somehow crystalline in nature, although the degree of crystallinity is not very high.

***Figure 54:*** *X-Ray diffractogram for the hybrid PAA-13-3 at 600 $^{o}$C.*

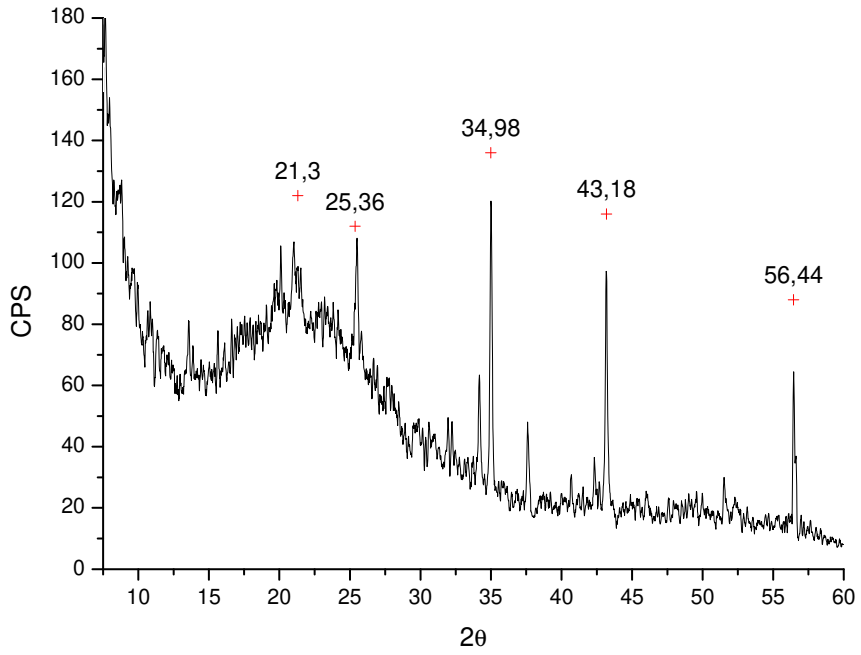


Difractograms for the hybrids PAA-GDP, PAA-MTC and PAA-Ph are given in figure 55. From the figure it is obvious that the degree of crytallinaty is low for all three compounds but still the data shows the presence of some crystalline forms.

These spectra have two types of peaks; one is comparatively narrow peak region and is bellow 10$^{o}$, while on other hand these spectra also have some broadened shoulders that extend from almost 15$^{o}$ to 25$^{o}$.

Observing the data summarized in table 8. as well as from the X-ray spectra, two peaks at 2Θ = 05.54° and 16.71° for the hybrid PAA-GDP corresponds to a cell thickness of 1.38 and 1.02 nm respectively. Similarly, for hybrid PAA-MTC the presence of peaks at 6.89°, 19.31° and 20.05° corresponds to a total thickness of 1.53, 1.84 and 1.44 nm respectively. In case of hybrid PAA-Ph these values are 7.00, 7.53 and 16.60 corresponding a thickness ranging from 0.88 to 2.70 nm.

***Figure 55:*** *X-Ray diffractograms for the hybrid PAA-GDP, PAA-MTC and PAA-Ph.*

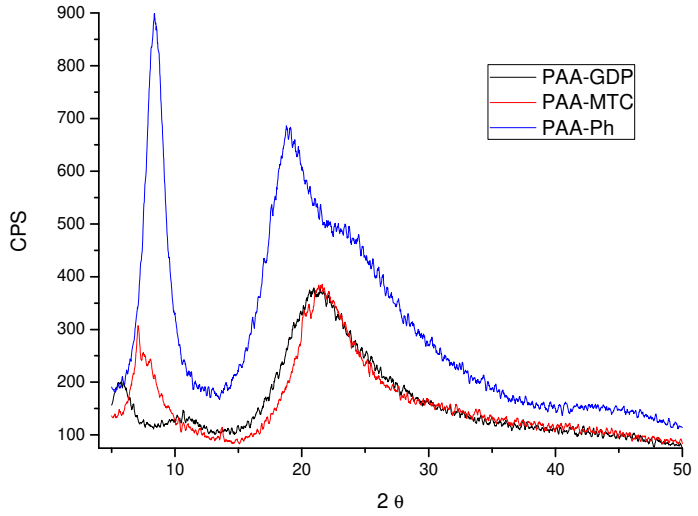


***Table 8. X-Ray Diffraction data for the Hybrids PAA-GDP, PAA-MTC and PAA-Ph***

| | | 2 Θ | Height (from base) | Width (at half height) | Area | Thickness Nm |
|---|---|---|---|---|---|---|
| **PAA-GDP** | 1 | 05.54 | 7.11 | 0.59 | 29.64 | 1.38 |
| | 2 | 16.71 | 4.60 | 0.81 | 44.27 | 1.02 |
| **PAA-MTC** | 1 | 6.89 | 64.88 | 0.54 | 106.98 | 1.53 |
| | 2 | 19.31 | 2.73 | 0.45 | 24.12 | 1.84 |
| | 3 | 20.05 | 10.13 | 0.58 | 65.67 | 1.44 |
| **PPA-Ph** | 1 | 07.00 | - | 0.34 | 74.57 | 2.38 |
| | 2 | 07.53 | - | 0.30 | 130.33 | 2.70 |
| | 3 | 16.60 | 47.73 | 0.94 | 131.41 | 0.88 |

## 5.7. Scanning Electron Microscopy SEM:

All synthesized POSS hybrids have been analyzed through Scanning Electron Microscopy. The samples were prepared without any grinding. Micrographs of the synthesized compounds may be observed in the Figure 56.

From the Figure 56(a) the micrograph for PAA-12 shows some cubic blocks. The size of the cubic blocks range from a few hundred nanometers to a few microns, and most of the products have sharp edges. These results further confirms that the expected product was obtained successfully.[108] But it is believed that these blocks are formed as a result of the aggregation of the POSS cages, forming some bulk like cubic structures.

Similarly in Figure 56(b) micrograph for PAA-13-2 shows some repeated units, and some plate like structures may be observed. These plates like structures have a thickness starting from a few hundred nanometers to 10 μm, but still they are in compacted form and are believed to be formed by the aggregation of the individual POSS hybrid molecules.

Micrograph given in Figure 56(c) is for PAA-13-3, which, at first glance, is a bulky bunch, but a thorough analysis reveals some repeating units having thickness of a few micrometers. Some cracks may also be observed in the micrograph, which exposes the inner surface of the product. As this material have a long pendent chain containing amine groups, which may probably form bulky groups by establishing hydrogen bonding in between them.

Almost identical behavior may be observed from the micrographs for the hybrids, PAA-GDP, PAA-MTC and PAA-Ph. They are also present in bulk forms having some sharp edges.

***Figure 56:*** *SEM micrographs for the hybrids PAA-12(a), PAA-13-2(b), PAA-13-3(c), PAA-GDP(d), PAA-MTC(e) and PAA-Ph(f).*

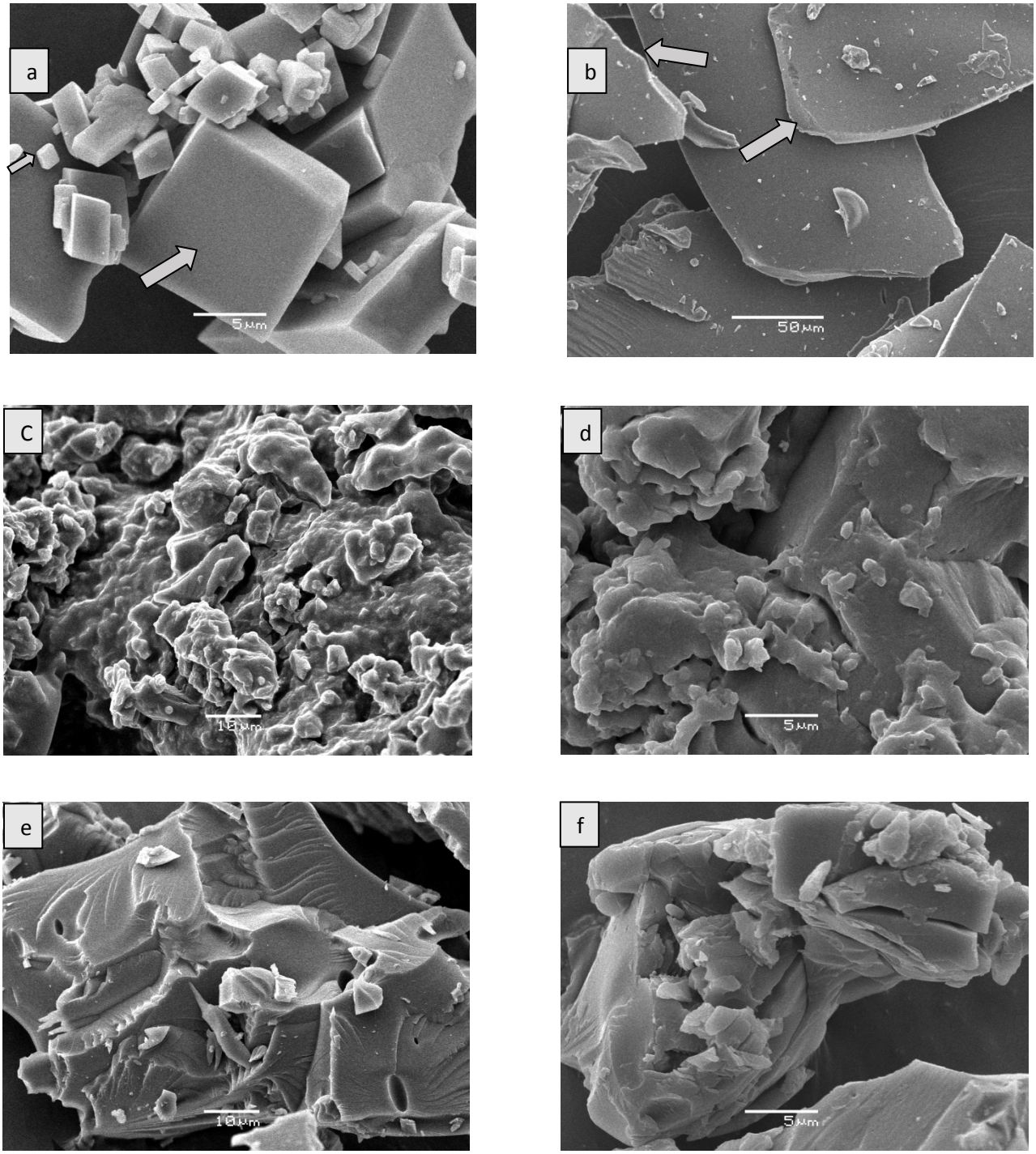

## 5.8. Sorption Studies of the synthesized POSS hybrids:

### 5.8.1. $CO_2$ Sorption:

There is a growing concern that anthropogenic $CO_2$ emissions into the atmosphere are contributing to global climate change. Several $CO_2$ capture and storage technologies have been explored to reduce $CO_2$ emissions during the post-, pre-, and oxy-combustion processes.

Several Carbon Dioxide Removal (CDR) methods such as Biochar, Direct Air Capture, Ocean Fertilization and Enhanced Weathering are tested, but as CDR reduces its emissions to the atmosphere only and cannot reduce the amount of carbon dioxide already present in the atmosphere. Therefore, $CO_2$ sequestration is expected to be the mid-term solution for the use of fossil fuel energy technologies against environmental calamities.

The $CO_2$ capture and separation technologies frequently involve metal oxides,[51] nickel complexes,[52] surface-modified silicas,[5,54] zeolites,[202] or metal-organic frameworks.[8,203] Recently, fabrication of amines on porous supports such as silica and carbon, through grafting and impregnation, has proved to be a feasible and beneficial route[204-208] as it overcomes the disadvantages of using amines compounds directly in aqueous solution.[209] The amine-grafted and/or impregnated porous solid sorbents become the prototype owing to their good selectivity, high surface area and higher tolerance to water.

Analyzing the importance of $CO_2$ sequestration, an experiment was designed to synthesize amine containing polyhedral oligomeric silsesquioxane and to measure its $CO_2$ sequestration ability, using the new inlab developed solid-gas sorption analyzer (SGSA).

In the experiment the instrument was adjusted to apply 10 doses of $CO_2$ using 200 mg of PAA-13-3, starting from the initial pressure of 10 mmHg, increasing 10 mmHg in each adsorption cycle up to a maximum of 100 mmHg. Results from the first experiment are shown in Figure 57, where pressure/time and energy/time graphs are given.

Analyzing the pressure/time graph in Figure 57, the first dose, which is 10 mmHg initially, remains constant and does not decrease with the time. The same behavior is observed for the pressures 20, 30 and 40 mmHg, and so on. From these results it can be concluded that the compound was not able to sorb $CO_2$. The same conclusion can be confirmed from the energy/time graph as well, where no any significant changes were observed. The small energy variations were results of the heating up of valve A, as it remains open during the sorption process and due to the passage of the current, it heats up, which is recorded by the microcalorimeter.

***Figure 57:*** *Graphical representation of the first sorption Experiment, change in pressure (— ), change in Energy of the system(—).*

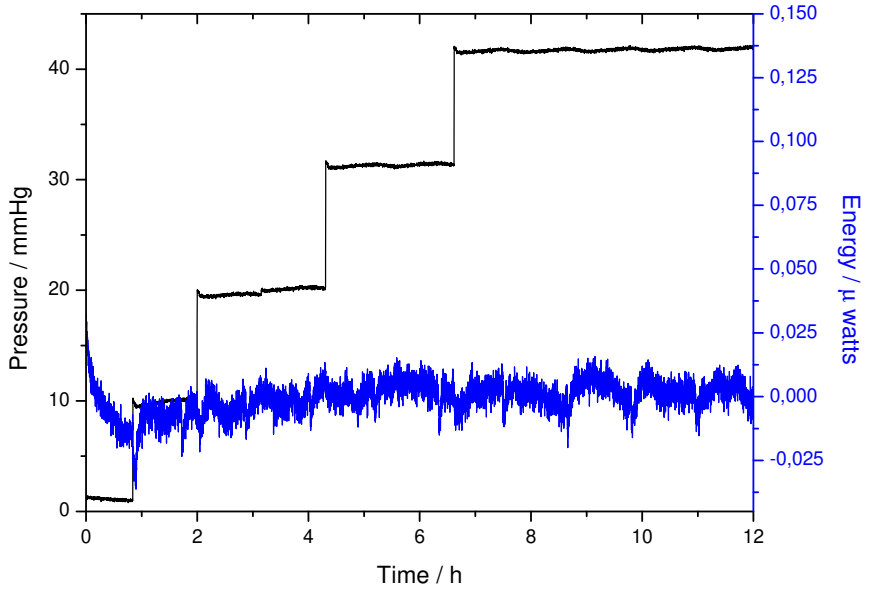


As the synthesis of the compound was done in the presence of the hydrochloric acid, so it was believed that $NH_2$ of the synthesized compound are protonated and may not be available for the sorption processes and the compound is unable to

capture $CO_2$. The proposed structure of the protonated compound is given as follows.

***Figure 58:*** *PAA-13-3 Structural formula showing protonated amin groups.*

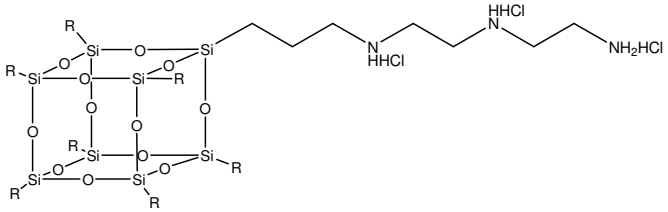


The compound was analyzed for the presence of Cl, using chlorine elemental analysis technique and the presence of 11% Cl was confirmed. The presence of Cl in the molecule confirmed the hypothesis of amine groups being protonated. The compound was treated for the removal of the acidic proton attached to the amine groups and once again was subjected to $CO_2$ sorption.

The calorimetric adsorption experiment was repeated using the same conditions and this time the results were totally different than the first one. Figure 59 (a) shows the pressure curve and Figure 59 (b) is the calorimetric signal recorded during the experiment. Both of them were recorded through SGSA, with duration of 7 h.

***Figure 59:*** *Graphical representation of the change in pressure(a),change in Energy of the system(b).*

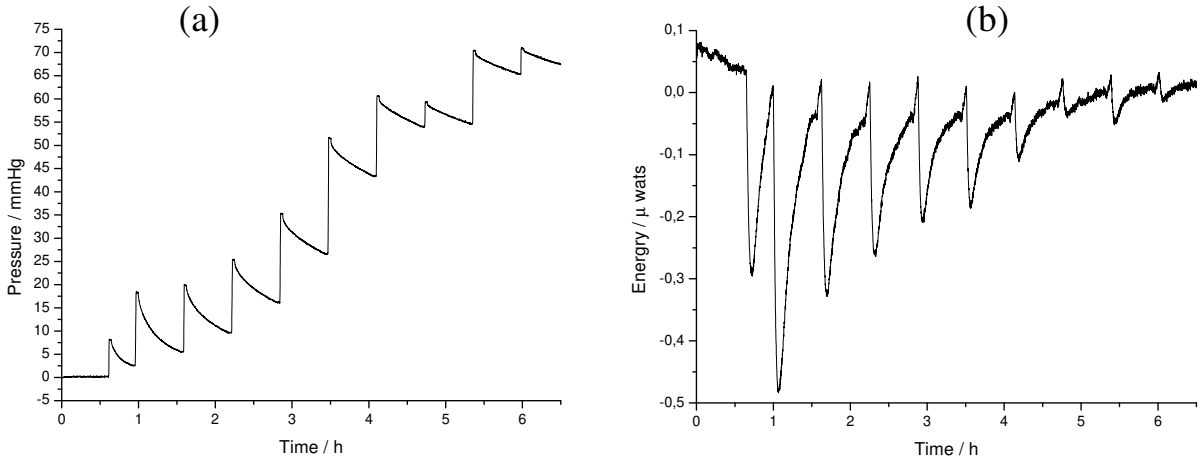

Although the results confirmed the success of $CO_2$ sorption, the experiment still needed some adjustments. For example, the pressure/time curve given in figure 59, shows some irregularity. In experimental procedure the program was set to increase the $CO_2$ pressure by 10 mmHg in each cycle. But from this figure it may be observed that the increases in pressure are irregular in each cycle, also it does not reach to the maximum pressure, 100 mmHg. Thorough analysis of the system revealed that the irregularity in the addition of $CO_2$ to the system was due to the improper functionality of the valve B, which is responsible to control the entrance of $CO_2$ to the system.

Valve B was replaced and the experiment was repeated with much care. With the replacement of the valve B the irregularity in the pressure was controlled. An exact amount of $CO_2$ was added to the system with regular intervals. The results obtained in this experiment are summarized in figure 60 and in table 9.

***Figure 60:*** *Graphical representation of the change in pressure(a),change in Energy of the system(b).*

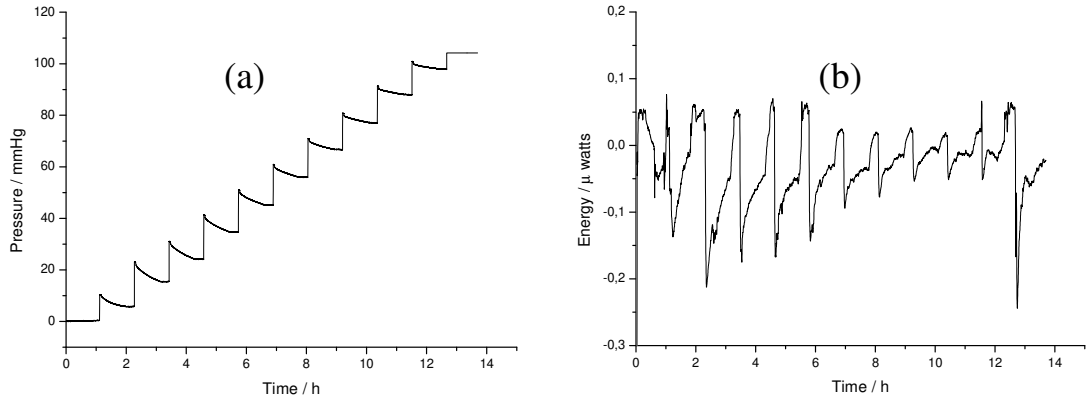


Table 9 shows the value of initial pressure, $P_i$, final pressure, $P_f$, adsorbed amounts, $n_{ads}$, and energies involved in the adsorption, $q_{diff}$ for the experiment. This table was automatically generated by the integrator program developed in Scilab and is presented taking in consideration uncertainties. The summation of the adsorbed

quantities in each dose $\Sigma n_{ads}$ is shown in the fourth column and indicates that the total adsorbed amount is 65.0 µmol of $CO_2$ adsorbed on an equilibrium pressure of 67.4 mmHg at the end of the experiment. The last two columns show the values of $Q_{diff}$ in kJ $mol^{-1}$ calculated from $Q_{int}$ raw and corrected respectively.

*Table 9. Calorimetric results for the adsorption of $CO_2$ in PAA-13-3, at 298,16 K*

| *Pi* / mmHg | *Pf* / mmHg | $n_{ads}$ / µmol | $\Sigma n_{ads}$ / µmol | *Qint* / mJ | *Qint* corrected / mJ | *Qdiff* / kJ $mol^{-1}$ | *Qdiff* corrected / kJ $mol^{-1}$ |
|---|---|---|---|---|---|---|---|
| 7.91 | 2.61 | 4.44 | 4.45 | -171 | -161 | -38.6 | -36.2 |
| 18.4 | 5.49 | 10.8 | 15.2 | -419 | -323 | -38.8 | -29.9 |
| 19.8 | 9.55 | 8.60 | 23.8 | -297 | -216 | -34.5 | -25.2 |
| 25.4 | 16.2 | 7.71 | 31.6 | -243 | -176 | -31.5 | -22.8 |
| 35.3 | 26.5 | 7.37 | 38.9 | -183 | -136 | -24.8 | -18.5 |
| 51.4 | 43.3 | 6.81 | 45.7 | -167 | -115 | -24.5 | -16.9 |
| 60.6 | 54.0 | 5.51 | 51.3 | -95.0 | -64.2 | -17.3 | -11.7 |
| 59.2 | 54.7 | 3.78 | 55.0 | -27.0 | -31.9 | -7.2 | -8.44 |
| 70.4 | 65.4 | 4.14 | 59.2 | -16.0 | -42.1 | -3.87 | -10.2 |
| 70.7 | 66.9 | 3.17 | 62.3 | -13.8 | -26.6 | -4.36 | -8.39 |
| 70.6 | 67.4 | 2.67 | 65.0 | -30.0 | -17.6 | -11.2 | -6.58 |

The graphical representation of the results obtained for the table 9 are as follows.

*Figure 61. Sorption isotherm(a), Calorimetric isotherm(b) for the sorption of $CO_2$ using PAA-13-3 sorbent.*

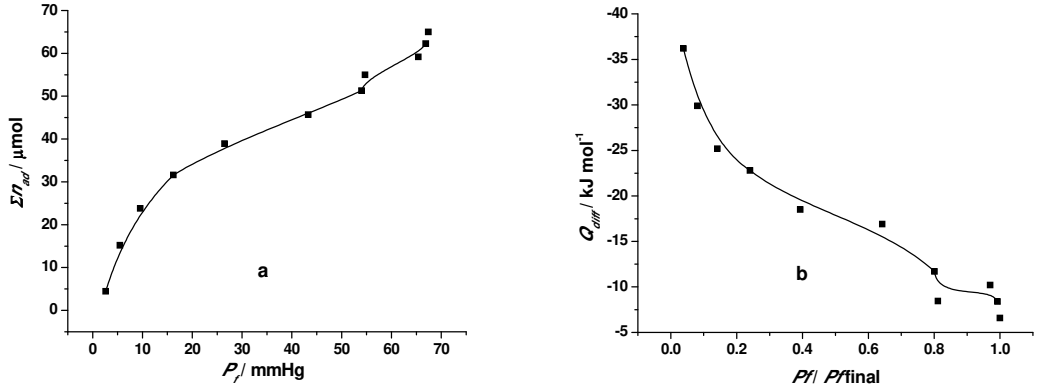

Figure 61a is a graphical representation of quantitative adsorption isotherm of $CO_2$ in PAA-13-3, while Figure 61b, which is also an isotherm, where the adsorption energy is represented in function of the covered fraction surface. From Figure 61a it is observed a maximum of 65 µmol adsorption of $CO_2$ that corresponds to 2.86 mg of $CO_2$ on 200 mg of material. This gives a percentage of adsorption (mass $CO_2$/mass material) of about 1.4%. This is a high value if it is considered that the final pressure was only 67 mmHg. The $CO_2$ adsorption devices usually operate at high pressures, which mean this material has attributes to be used as a $CO_2$ adsorbent. Referring to Figure 61b, it was expected that the differential energy values would be constant with the fraction of covered surface. However, this is not what was observed. The energy value at the beginning of the coverage is about -36 kJ $mol^{-1}$, a value compatible to the expected interaction energy between $CO_2$ and the amino group. This energy value decreases to about -7 kJ $mol^{-1}$, a very small value and not expected, as it would be speculated that the adsorption sites were all alike. This result, however, show that the adsorption process does not agree with the Langmuir isotherm model, where in the energy should be constant.

In the end of the experiment, PAA-13-3 was analyzed using CHN, FTIR and $^{13}$C-NMR techniques. The results obtained are shown in Table 10 and Figure 62. From the Table 10, it may be observed that the experimental values are very close to those of calculated ones. The presence of the C=O may also be confirmed from $^{13}$C-NMR. In Figure 62, a broad signal, which appeared at 132 ppm is an indication of the presence of the C=O functional group in the molecule.

*Table 10. CHN analysis for the hybrid PAA-13-3, before and after $CO_2$ sorption experiments*

| | **Experimental** | | | | | **Calculated** | | | | |
|---|---|---|---|---|---|---|---|---|---|---|
| | **C/%** | **N/%** | **C/ mmolg$^{-1}$** | **N/ mmolg$^{-1}$** | **C/N** | **C/%** | **N/%** | **C/ m.molg$^{-1}$** | **N/ m.molg$^{-1}$** | **C/N** |
| Before | 23.0 | 11.2 | 19.2 | 8.00 | 2.4 | 27.4 | 13.7 | 22.8 | 9.78 | 2.3 |
| After | 45.1 | 11.6 | 37.6 | 8.28 | 4.5 | 42.7 | 14.9 | 35.6 | 10.7 | 3.3 |

***Figure 62:*** *$^{13}$C-NMR spectrum for the hybrid PAA-13-3 Before $CO_2$ sorption (—) and after $CO_2$ sorption (—).*

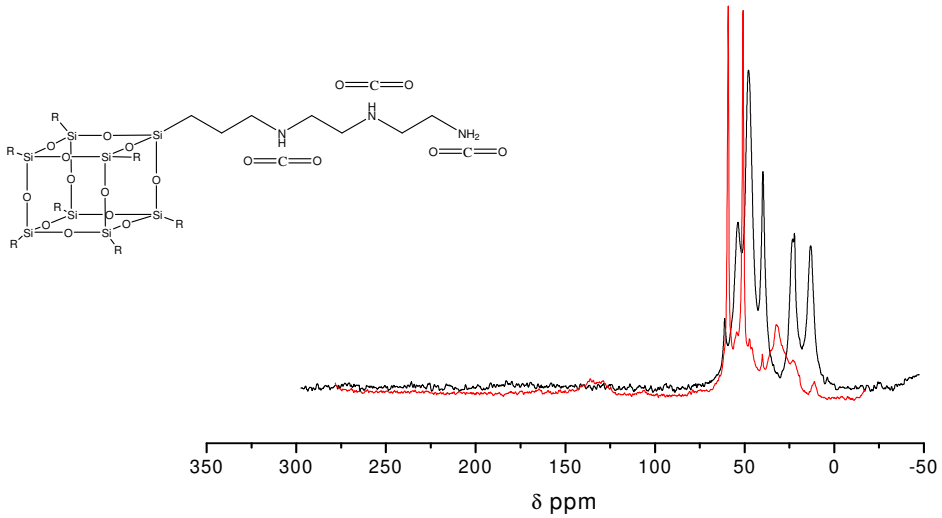


From figure 63 it may be observed that enlargement of the band in between 1199cm$^{-1}$ and 1449 cm$^{-1}$ as well as the decrease in the intensities of the bands in the range from 2800cm$^{-1}$ to 3000cm$^{-1}$, which is a characteristic region of NH functional group, confirm the presence of $CO_2$ in the PAA-13-3 molecule. Other remarkable bands present in the FTIR spectrum are 3416cm$^{-1}$ represents the presence NH streching, while the bands at 1627cm$^{-1}$ is due to $NH_3^+$ deformation, at 1541cm$^{-1}$ is C=O streching and at 1425cm$^{-1}$ represents the presence of $NCOO^-$ in the molecule.[210]

***Figure 63:*** *$^{13}$C-NMR spectrum for the hybrid PAA-13-3 Before $CO_2$ sorption (—) and after $CO_2$ sorption (—).*

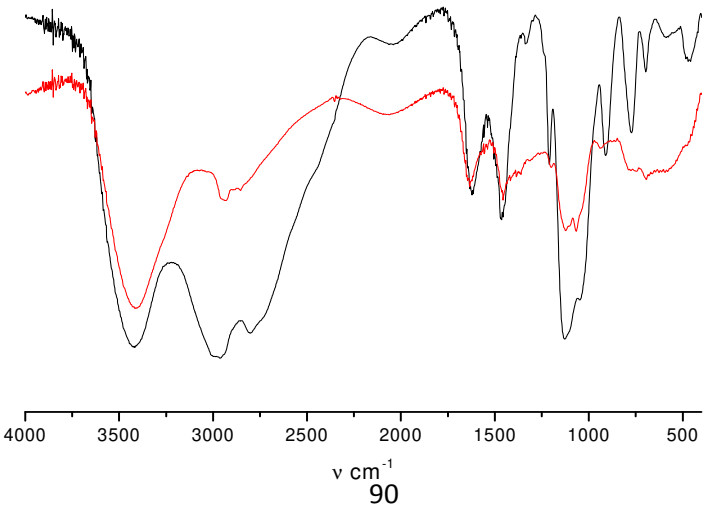

These results are similar to those reported by Sayari and Belmabkhout, on the $CO_2$ sorption mechanisms.

***Figure 64:*** *Mechanism for the sorption of $CO_2$ using PAA-13-3 as a sorbent.*

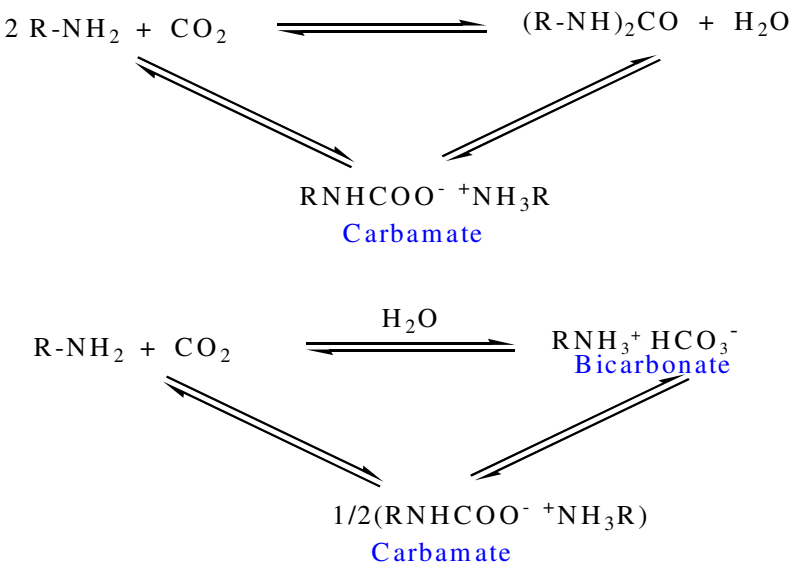


The formation of carbamate and bicarbonate under anhydrous and hydrous conditions, respectively are supposed to occur.[181]

In this experiment a total of 200 mg of PAA-13-3 was used, which is equal to $1.3x10^{-4}$ mol. From the table 9, the amount of sorbed $CO_2$ on PAA-13-3 was 65 µmol. The calculation reveals a total of 2.86mg of $CO_2$ sorbed per 200mg of the sample PAA-13-3, which is equal to 0.32 mmol $g^{-1}$. Further calculation showed that the amount sorbed on the surface of PAA-13-3 is only 2.08 % of the theoretically calculated amount, taking only in consideration stoichiometric arguments. The morphology of the sample PAA-13-3 given in Figure 56(c), shows that the sample is in bulk form, which is evidence, that only a few percent of the pendant chains are available for sorption of $CO_2$. Furthermore, Sayari et al., reported that the formation of bulk-like materials leads diffusion-limited process.[182] According to Heydari et al., at high temperature, the high $CO_2$ adsorption capacity

is possibly due to the high diffusion rate into bulk-like hybrid materials.[184] Similar findings are also reported by Qi et al.[183]

Another point of importance is related to the calorimeter baseline, which may be observed in Figure 65. While observing the pressure/time curve and its respective calorimetric curve for the first dose (first sorption cycle), it must be noted that energy cycle needs more time to complete and reach back to its baseline. But, in this case, the automatic program closed the valve A before the process to be completed. Hence, the program was adjusted to increase the time of the contact between $CO_2$ and the sample, by keeping valve A open for longer time than before. Valve A operates using the electromagnetic principle, and keeping it open for a long time means heating it up. This heating up of valve A provokes a transfer of heat to the system, which impede the calorimetric curve to get back to the base line.

***Figure 65:*** *Graphical representation of the first sorption cycle, change in pressure (— ), change in Energy of the system(—).*

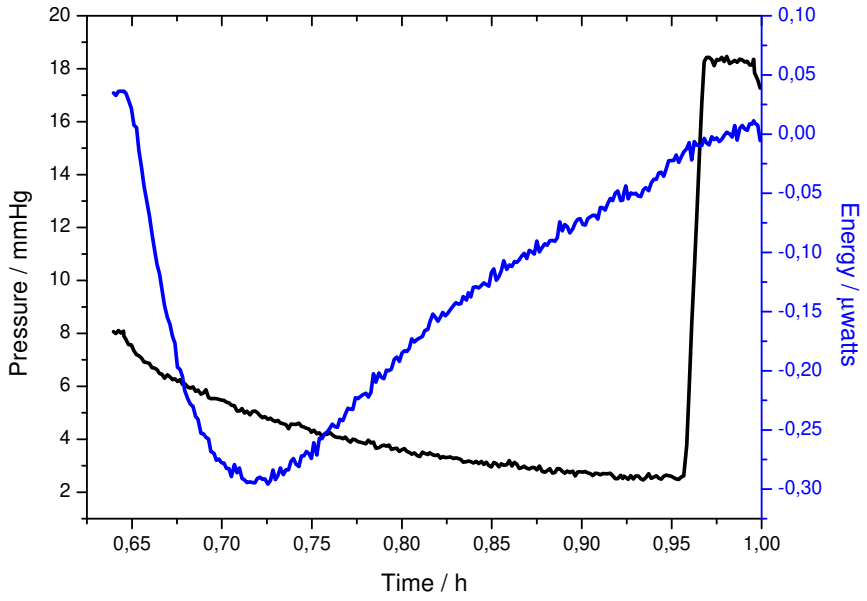


To solve the base line problem, a hybrid type protocol was performed. This time the operation was not allowed to be fully automatic, a manual-automatic protocol was adopted to overcome the base line problem. In this protocol, in first step,

sorption was performed at 10 mmHg of $CO_2$. The process was repeated till sorption saturation at this pressure. In next step pressure was increased to 20 mmHg and the sorption cycles were repeated till saturation reached. In the same way the experiment was repeated with pressures 30, 40 and so on. The results obtained from the experiment are as follows.

***Figure 66:*** *Graphical representation of the change in pressure(a),change in Energy of the system(b).*

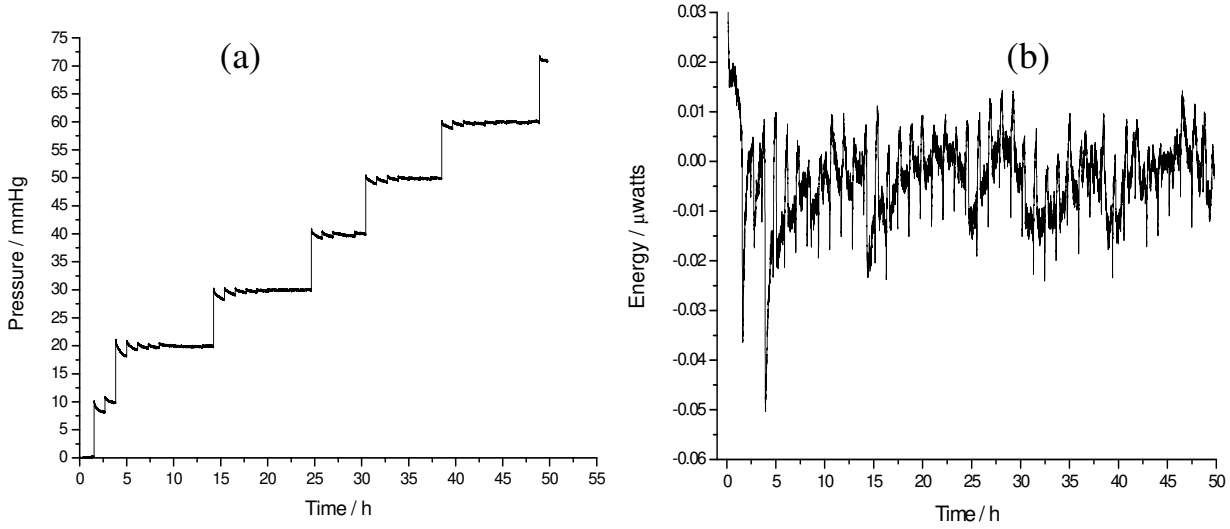


From the figure 66 it is worth mentioning that baseline problem seems to be solved up to some extent. The experiment was on test bases and needs some adjustments, before applying to other materials. The sorption curve obtained from this experiment is as follows.

***Figure 67:*** *Sorption isotherm for PAA-13-3 using it as a sorbent for $CO_2$.*

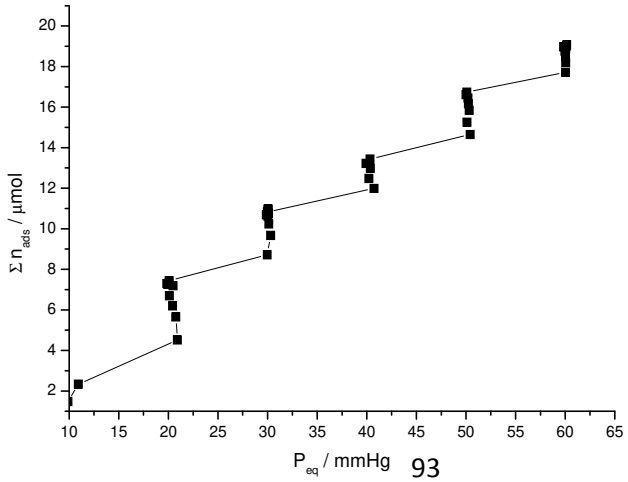

Sample PAA-13-3 has been tested for its sorption ability for $CO_2$ and was found to be a very useful sorbent for acidic gases like $CO_2$.

## 5.8.2.Sorption studies for divalent cations:

It is a well known fact that water is the most essential and precious natural resource. The concern about the fresh water condition around the globe is getting worse on daily bases. Among different factors affecting water quality, the heavy metal ion concentration in waste and drinking water and its potential health hazards on human, is the most wide spread. European Union Restriction of Hazardous Substances Directives and Priority List of Hazardous Substances by EPA have listed heavy metal ions as high priority contaminants.[185,186] Heavy metals like copper, zinc, lead, cadmium, and many more are among the high priority contaminants lists. They are mainly generated by the smelting and refining processes, electroplating and industrial waste.[187]

Removal of heavy metals from industrial wastes has been investigated by different researchers using conventional methods like oxidation, reduction, precipitation, pyrolysis, membrane filtration, ion exchange and adsorption. Of major interest, adsorption process, a surface phenomenon by which a multi-component fluid (gas or liquid) mixture is attracted to the surface of a solid adsorbent and forms attachments via physical or chemical bonds, is recognized as the most efficient, promising and widely used fundamental approach in waste water treatment processes,[211] mainly hinges on its simplicity, economically viable, technically feasible and socially acceptable.[212] However, low sorption capacities of adsorbents, in many cases have always been a challenge for the researchers. Therefore, new promising adsorbents have been investigated by different researchers. Among these, activated charcoal, SBA-15, MCM-41, MCM-48, are the most worked out

materials. New hybrid materials are being introduced to the hybrid material database from around the world.

The polyhedral oligomeric silsesquioxane (POSS) derivatives recently have been introduced as functional and reactive hybrid materials.[188] Dias Filho et al.[15] reported that polyhedral oligomer silsesquioxane adsorbs $Cu^{2+}$ from aqueous solution by forming surface copper complexes having similar structures to those found for immobilized molecules containing nitrogen on silica surfaces. The nanocage silsesquioxane cores showed to be an effective solid phase sorbent for copper. A similar work has been reported by Magosso et al.[189] They reported sorption equilibria of $ZnCl_2$, $CdCl_2$ and $HgCl_2$ from aqueous solutions using an ion exchange polymer.

In light of the above discussion, the experiments were planned to study the sorption properties of the synthesized polyhedral oligomeric silsesquioxanes. In the first experiment, PAA-13-3 was used for the sorption of divalent metals like $Cu^{2+}$, $Cd^{2+}$ and $Pb^{2+}$. While in next experiment PAA-MTC and PAA-GDP were used for the sorption of $Cu^{2+}$.

Results obtained from these experiments were treated statistically using "two parameter models" like Langmuir, Freundlich and Temkin as well as "three parameter models" like Sips and Redlich-Peterson.

### 5.8.2.1. Sorption capacity of PAA-13-3 for divalent metals:

The capacity of PAA-13-3 to extract divalent metals from aqueous solution was determined in duplicate runs, using a batch process with aqueous solutions of nitrates of the divalent copper, cadmium and lead, using a mass of approximately 20mg of PAA-13-3 suspended in 25.0 $cm^3$ of their solutions with concentrations ranging from 0.70 to 7.0 mmol $dm^{-3}$. The suspensions were shaken for 24 h in an

orbital bath at (298 ±1) K. At the end of this process, the solid was separated by filtration, aliquots of the supernatant were removed and the concentrations of the cations were determined by ICP-OES. The sorption quantities ($q_e$) were calculated by Eq.(9).

Where $N_f$ is the number of moles adsorbed, $n_i$ and $n_s$ are the number of moles of cation in the initial and the supernatant solutions after reaching equilibrium, respectively, and $m$ is the mass of the adsorbent used in each adsorption process.

The sorption data obtained from treatment of PAA-13-3 with divalent cations like $Cu^{2+}$, $Cd^{2+}$ and $Pb^{2+}$ are presented in Figure 68 and their statistical results are shown in Table 11. By comparing the sorption data it concluded that PAA-13-3 has shown a remarkable capacity towards $Cu^{2+}$ in comparison to $Cd^{2+}$ and $Pb^{2+}$.

***Figure 68:*** *Sorption isotherms for Cd (■), Cu (●) and Pb (▲) at 298 ± 1 K*

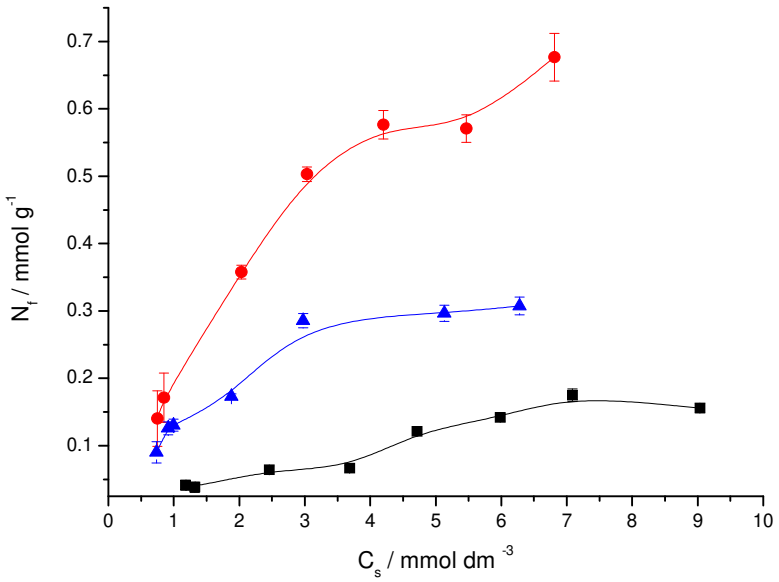


From the isotherms (Figure 68) and the data in Table 11, it is seen that PAA-13-3 has the following sorption quantity order for metal ions on its surface: $Cu^{2+}$ > $Pb^{2+}$ > $Cd^{2+}$. It is observed that the PAA-13-3, which contains nitrogen, had the high sorption capacity for copper compared to the other metals.

This can be explained by the presence of the amine group, and according to the concept of softness/hardness, the border element has a greater affinity for elements of the border region as copper.

This affinity order is also in agreement with the rule for the sequence of complex stability from the Irving-Williams concept based on ligand field theory. According to this rule, the stability of complexes of metal cations-oxygen donor groups decreases in the series: $Cu^{2+} > Cd^{2+}$. This general trend may also be explained by the fact that metal ions with smaller ionic radius diffuse faster in aqueous systems. Therefore, metal ion with a smaller ionic radius ($Cu^{2+}$ = 0.73Å) would easily react with adsorbent resulting in a greater surface coverage than those with large ionic size ($Cd^{2+}$ = 0.97 Å).

Data analysis of the isotherms can be adjusted to different isotherm models, which is important to find the suitable model that can be used, for example, to discuss the mechanism and the way of the adsorption process and determine some thermodynamic parameters like equilibrium constant, Gibbs free energy, enthalpy and entropy, these last one by applying the second law of the thermodynamics. In the present investigation, the equilibrium data were analyzed using the two parameter models like Langmuir, Freundlich and Temkin as well as three parameter models such as Sips and Redlich-Peterson.

From Table 11 it can be observed that maximum sorption value of $q_e$ was found to be in following order $Cu^{2+} > Pb^{2+} > Cd^{2+}$. Where the maximum value of $q_e$ is almost the double for $Cu^{2+}$ in comparison to $Pb^{2+}$, this one, in turn itself, is the double of $Cd^{2+}$. Analyzing the data from two parameter sorption models the coefficient of determination ($R^2$) demonstrate the following order Temkin > Langmuir > Freundlich for the divalent atom $Cu^{2+}$. Therefore it can be deduced that sorption

isotherm is better adjusted by Temkin isotherm model than other two models like Lnagmuir and Freundlich.

***Figure 69:*** *Sorption isotherm for $Cu^{2+}$ with PAA-13-3, $q_e$(■), Langmuir (●), Freundlich (▲) and Temkin (▼)*

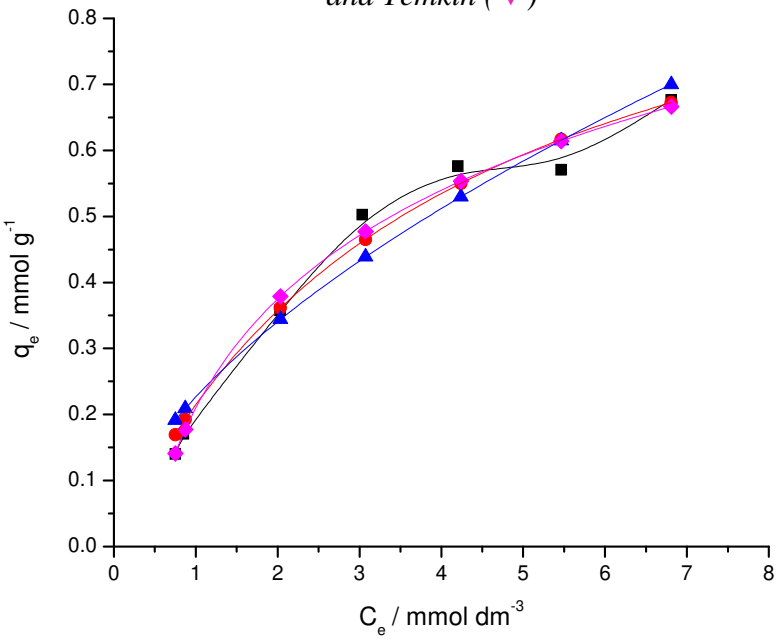


The linear form of Temkin adsorption isotherm is given as follow:

$$q_e = \frac{RT}{b_T} \ln A_t + \frac{RT}{b_T} \ln C_e \qquad \text{Equation 12}$$

Where T (K) is the absolute temperature, R (8.314 J/mol) is the universal gas constant, $A_T$ (L/mg) is the equilibrium binding constant and $b_T$ (J/mol) is related to the heat of adsorption. The isotherm constants $A_T$ and $b_T$ are calculated from the slope and intercept of the $q_e$ versus $\ln C_e$ plot. Applying the Temkin isotherm model in its linear form, the equilibrium binding energy was found to be 0.24 $dm^3$/mol, while the heat of adsorption was found to be 0.21 kJ/mol.

Analyzing the data in table 11, $R^2$ value for the Langmuir model (0.97) is greater than the $R^2$ value for the Freundlich model (0.94). Here form this data it can de deduced that the binding sites on the adsorbent are uniform and favors monolayer adsorption phenomenon. To further elaborate the Langmuir isotherm model for the

sorption of $Cu^{2+}$ on PAA-13-3 sorbent, the essential characteristics of the Langmuir isotherm can be expressed by a dimensionless constant called the equilibrium parameter, $R_L$:

$$R_L = \frac{1}{1 + K_L C_0} \qquad \text{Equation 13}$$

Where $K_L$ (mg/dm$^3$) is the Langmuir constant and $C_0$ (mg/dm$^3$) is the initial concentration. The $R_L$ value indicates the adsorption to be unfavorable ($R_L > 1$), linear ($R_L = 1$), favorable ($0 < R_L < 1$) or irreversible ($R_L = 0$). Here in this experiment the $R_L$ was found to be 0.68, which is between zero and one, indicating favorable adsorption.

On the other hand, in case of divalent $Pb^{2+}$ observing the $R^2$ values from Table 11, the value of 0.94 observed for the Langmuir isotherm model is greater than 0.93 calculated by Temkin, which in turn is greater than 0.89 calculated by Freundlich isotherm model. These finding may also be confirmed by the $\chi^2$ values. The data confirms that the binding sites are alike and an equilibrium is established in sorption and desorption phenomena and is indicative of the fact that sorption of $Pb^{2+}$ occurs in monolayer form than multilayer formation. The $R_L$ calculated for $Pb^{2+}$, using Langmuir adsorption isotherm, was found to be 0.27, conforming the sorption to be favorable.

Similarly in case of divalent $Cd^{2+}$ cation, observing the $R^2$ values, 0.91 > 0.90 > 0.87 gives us the order Langmuir > Freundlich > Temkin. These findings may also be verified from $\chi^2$. Here again the isotherm is best explained by the Langmuir sorption isotherm model. And the conditions are favorable for monolayer formation. The $R_L$ value calculated for the $Cd^{2+}$ was 0.56, hence confirming the sorption to be favorable.

***Figure 70:*** *Sorption isotherm for $Pb^{2+}$ with PAA-13-3, $q_e$ (■), Langmuir (●), Freundlich (▲) and Temkin (▼)*

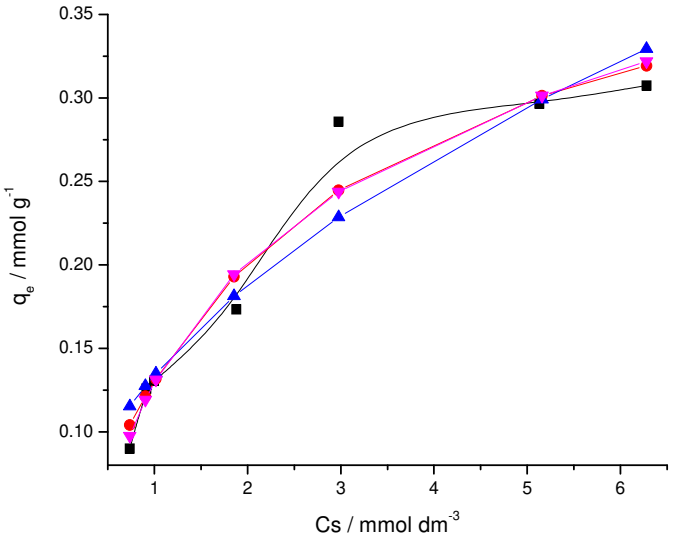


***Figure 71:*** *Sorption isotherm for $Cd^{2+}$ with PAA-13-3, $q_e$(■), Langmuir (●), Freundlich (▲) and Temkin (▼)*

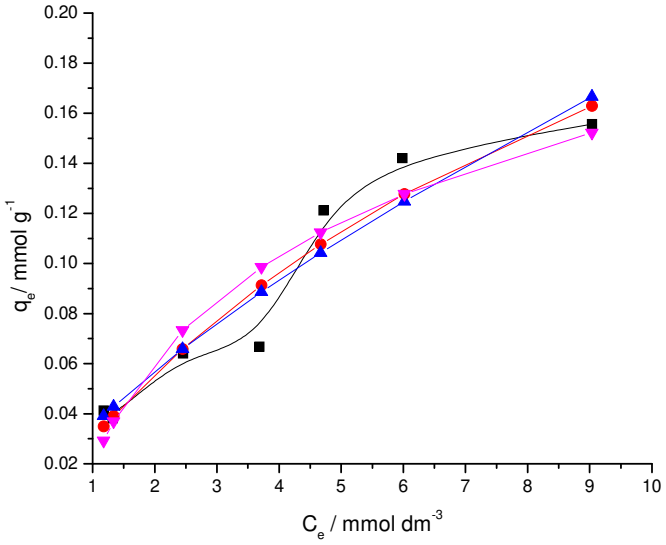


The data obtained from two parameter isotherm models are summarized in Table 11:

***Table 11. Some results from de application of the different models to the data come from the adsorption process of some divalente íons in PAA-13-3 at 298 K.***

| Model | Metal | $q_e$ / mmol $g^{-1}$ | $q_s$ /mmol $g^{-1}$ | b/ g mmol $^{-1}$ | $R^2$ | $\chi^2$ |
|---|---|---|---|---|---|---|
| Langmuir | $Cu^{2+}$ | 0.68 | 1.06 ± 0.12 | 0.25 ± 0.06 | 0.97 | 0.0010 |
| | $Pb^{2+}$ | 0.31 | 0.44 ± 0.05 | 0.42 ± 0.11 | 0.94 | 0.0005 |
| | $Cd^{2+}$ | 0.15 | 0.36 ± 0.13 | 0.09 ± 0.05 | 0.91 | 0.0002 |
| Freundlich | $Cu^{2+}$ | 0.68 | 0.23 ± 0.03 | 1.70 ± 0.23 | 0.94 | 0.0030 |
| | $Pb^{2+}$ | 0.31 | 0.13 ± 0.01 | 2.04 ± 0.32 | 0.89 | 0.0009 |
| | $Cd^{2+}$ | 0.15 | 0.03 ± 0.01 | 1.40 ± 0.22 | 0.90 | 0.0002 |
| Temkin | $Cu^{2+}$ | 0.68 | 0.24 ± 0.01 | 0.21 ± 0.02 | 0.98 | 0.0010 |
| | $Pb^{2+}$ | 0.31 | 0.10 ± 0.01 | 0.13 ± 0.01 | 0.93 | 0.0005 |
| | $Cd^{2+}$ | 0.15 | 0.06 ± 0.01 | 0.02 ± 0.01 | 0.87 | 0.0003 |

Where in $q_e$ is the experimental maximum sorption quantity, $q_s$ is the maximum sorption quantity provided by applying the non-linear models, $b$ Equations parameters ($K_L$, $K_F$, $n_F$, for Langmuir, Freundlich, and Temkin respectively) $R^2$ determination coefficient and $\chi^2$ chi-squared distribution.

For further confirmation of the results, the sorption data was also adjusted using three parameter models like Sips and Redlich-Peterson adsorption models. The results obtained from these adjustments are given in Table 12. Observing the obtained data for these models, in case of $Cu^{2+}$ the $R^2$ value for both models are the same but $\chi^2$ values demonstrate the $Cu^{2+}$ can be best fitted to the Sips model rather than the Redlich-Peterson one. From Table 12, the data for $Pb^{2+}$ confirms that Redlich-Peterson isotherm models seems to be a good fit rather than Sips. The $R^2$ value in case of Redlich-Peterson isotherm model is 0.95 which is greater than value of 0.94 calculated by Sips isotherm model. Similarly, in case of $Cd^{2+}$ the data can be best fitted by Redlich-Peterson model as compared to the Sips model. Where, the $R^2$ values demonstrate the following order 0.91 > 0.89 for Redlich-Peterson and Sips models, respectively. The same order is supported by the $\chi^2$ values as well.

***Figure 72.*** *Sorption isotherm for $Cu^{2+}$ with PAA-13-3, $q_e$ (■), Sips (●), Redlich-Peterson (▲).*

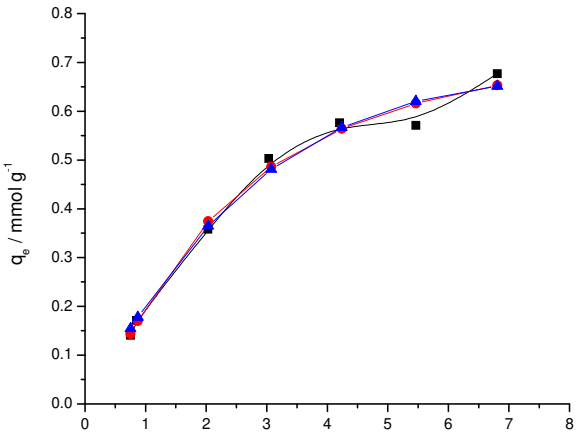


***Figure 73:*** *Sorption isotherm for $Pb^{2+}$ with PAA-13-3, $q_e$ (-■), Sips (●), Redlich-Peterson (▲).*

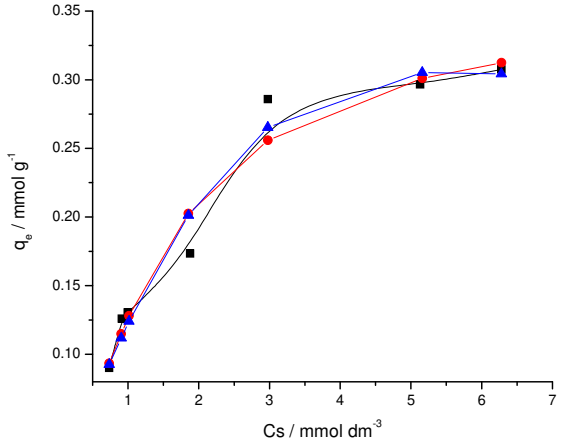


***Figure 74:*** *Sorption isotherm for $Cd^{2+}$ with PAA-13-3, $q_e$ (■), Sips (●), Redlich-Peterson (▲).*

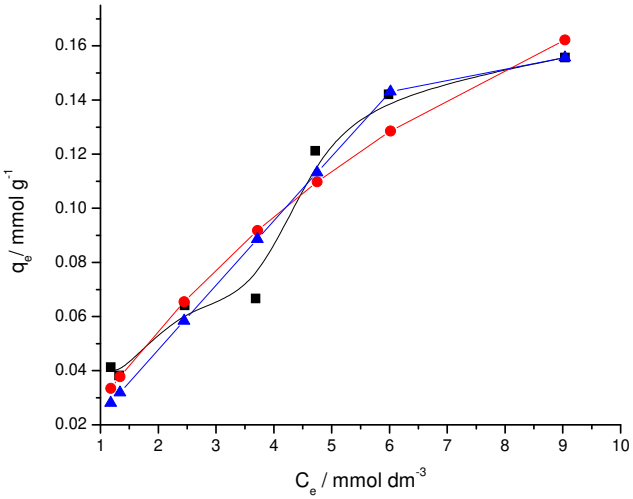


Analyzing the data in table 12,

***Table 12. Some results from de application of the different models to the data come from the adsorption process of some divalente íons in PAA-13-3 at 298 K.***

| Model | Metal | $q_e$ /mmol $g^{-1}$ | $q_s$ /mmol $g^{-1}$ | $K$ /mmol $g^{-1}$ | $b$ /g mmol $^{-1}$ | $R^2$ | $\chi^2$ |
|---|---|---|---|---|---|---|---|
| Sips | $Cu^{2+}$ | 0.68 | 0.78 ± 0.10 | 0.34 ± 0.06 | 1.41 ± 0.26 | 0.98 | 0.0009 |
| | $Pb^{2+}$ | 0.31 | 0.35 ± 0.06 | 0.56 ± 0.16 | 1.42 ± 0.47 | 0.94 | 0.0004 |
| | $Cd^{2+}$ | 0.15 | 0.31 ± 0.30 | 0.10 ± 0.09 | 1.09 ± 0.56 | 0.89 | 0.0002 |
| Redlich-Peterson | $Cu^{2+}$ | 0.68 | 3.16 ± 0.50 | 0.22 ± 0.04 | 1.52 ± 0.50 | 0.98 | 0.0030 |
| | $Pb^{2+}$ | 0.31 | 1.82 ± 0.24 | 0.13 ± 0.02 | 1.72 ± 0.53 | 0.95 | 0.0004 |
| | $Cd^{2+}$ | 0.15 | $11x10^9$ ± 20 | 0.02 ± 0.01 | 11.85 ± 05 | 0.91 | 0.0001 |

Where $q_e$ is the maximum experimental sorption, $q_s$ ($Q_s$ in case of Sips and $K_{RP}/a_{RP}$ in case of R-P) is the maximum sorption capacity, K ($K_s$ is for Sips and $K_{RP}$ is for R-P) the isotherm constant and b ($n_s$ for Sips and β for R-P) is the sorption parameters. If the value of $n_s$ is equal to 1, then Sips equation will become a Langmuir equation. Alternatively, as either $C_e$ or $K_S$ approaches 0, the isotherm reduces to the Freundlich isotherm. Similarly When the value of β is equal to 1, the Redlich-Peterson equation is reduced to the Langmuir isotherm, while it reduced to a Freundlich isotherm, in case the value of the parameter $a_R C_e^{\beta}$ is much bigger than 1.

Analyzing the data from table 12, three parameter models confirms the validity of Langmuir fitting for the divalent cations $Cu^{2+}$ and $Pb^{2+}$, as these models may be transformed to Langmuir adsorption isotherm using the above discussed parameters.

## Thermodynamic studies of the sorption systems:

Thermodynamic considerations of an adsorption process are necessary to conclude whether the process is spontaneous or not. Gibb's free energy change, ΔG°, is the fundamental criterion of spontaneity. Reactions occur spontaneously at a given temperature if ΔG° is a negative value. The thermodynamic parameter of Gibb's free energy change, was calculated using the following equations:

$$\Delta G^0 = -RT \ln K_L \qquad \text{Equation 14}$$

Where R is universal gas constant (8.314 J $mol^{-1}$ $K^{-1}$) and T is the absolute temperature in K and $K_L$ is the Langmuir adsorption isotherm constant. Using the above equation and data form table 11 the Gibb's free energy change, ΔG° calculated 3.15 kJ $mol^{-1}$ ($Cu^{2+}$), 1.97 kJ $mol^{-1}$ ($Pb^{2+}$), and 5.47 kJ $mol^{-1}$ ($Cd^{2+}$) are positive and indicates that sorption processes in all three cases are non-spontaneous.

### 5.8.2.2. Sorption capacity of PAA-13-3, PAA-MTC and PAA-Ph for $Cu^{2+}$:

The sorption experiment of $Cu^{2+}$ presented in the early section, showed good results in compared to other divalent atoms. Hence the next experiment was designed to test the sorption capacity of other synthesized POSS hybrids like PAA-MTC and PAA-Ph as well for $Cu^{2+}$. Procedure for the first experiment was reproduced in this case as well. The results obtained from this experiment are summarized in Figure 75 as well as in Table 13.

***Figure 75:*** *Sorption isotherms for $Cu^{2+}$ with PAA-13-3 (■), PAA-GDP (●) and PPA-Ph (▲) at 298 ± 1 K as sorbents.*

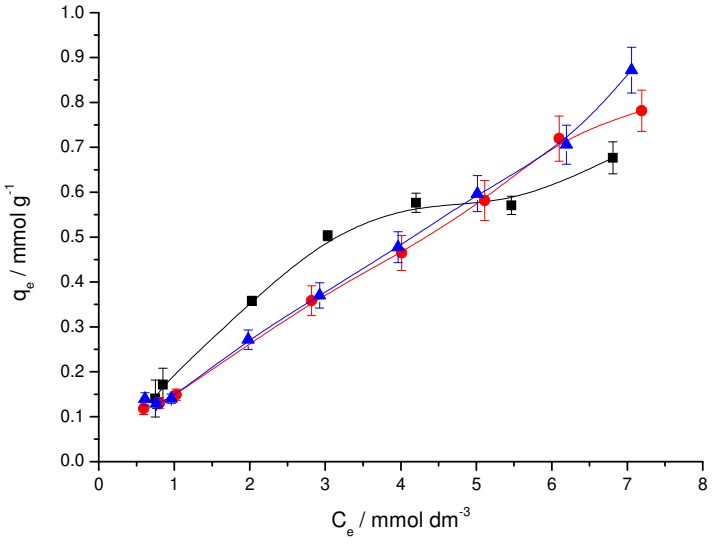

Observing the Table 13, from the $q_e$ value of 0.68 for PAA-13-3, 0.78 for PAA-MTC and 0.87 for PAA-Ph can be deduced that PAA-Ph shows more affinity towards sorption of $Cu^{2+}$ than PAA-MTC as well as PAA-13-3.

Data obtained from this experiment was treated statistically for their better adjustment, by using different sorption models. The data regarding sample PAA-MTC may be observed in Table 13, which demonstrate that sorption isotherm for $Cu^{2+}$ is best fitted by Freundlich isotherm model. While comparing the $R^2$ values one can easily observe that for both Langmuir and Freundlich models, the calculated value of 0.99, which is greater than the one calculated by Temkin model. However the $\chi^2$ value for Freundlich isotherm model is smaller than Langmuir. Consequently the isotherm models may be written in the order Freundlich > Langmuir > Temkin, in terms of adjustment.

***Figure 76:*** *Sorption isotherm for $Cu^{2+}$ with PAA-MTC, $q_e$(■), Langmuir (●), Freundlich (▲) and Temkin (▼).*

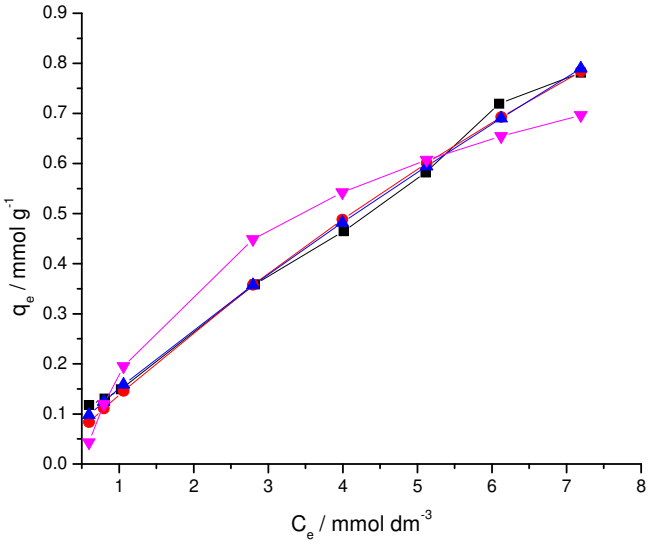


Similarly observing the data regarding the sorption of $Cu^{2+}$ for PAA-Ph from Table 13, $R^2$ calculated by Langmuir model is 0.98, by Freundlich is 0.99 and calculated by Temkin is 0.87. Hence it can be deduced that the isotherm is best fitted to the Freundlich model.

***Figure 77:*** *Sorption isotherm for $Cu^{2+}$ with PAA-Ph, $q_e$(■), Langmuir (●), Freundlich (▲) and Temkin (▼).*

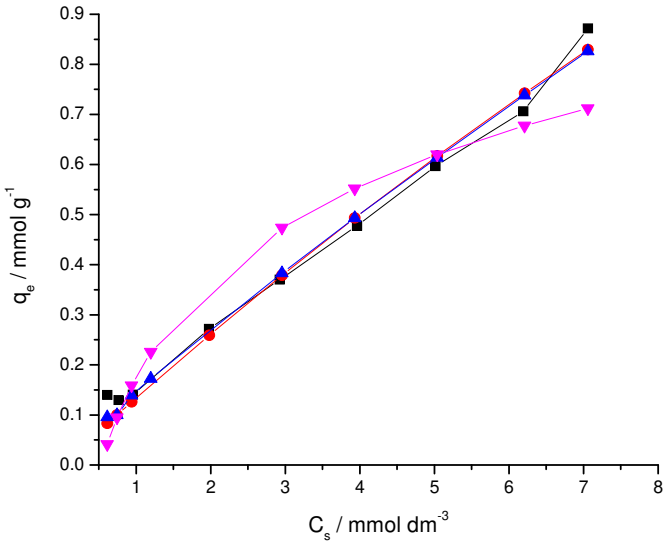


***Table 13. Some results from de application of the different models to the data come from the adsorption process of $Cu^{2+}$ in PAA-13-3, PAA-MTC and PAA-Ph, and applying the non-linear models.***

| Model | Material | $q_e$ / mmol $g^{-1}$ | $q_s$ /mmol $g^{-1}$ | b/ g mmol $^{-1}$ | $R^2$ | $\chi^2$ |
|---|---|---|---|---|---|---|
| Langmuir | PAA-13-3 | 0.68 | 1.06 ± 0.12 | 0.25 ± 0.06 | 0.97 | 0.0010 |
| | PAA-MTC | 0.78 | 3.22 ± 0.98 | 0.04 ± 0.02 | 0.99 | 0.0005 |
| | PAA-Ph | 0.87 | 5.88 ± 4.10 | 0.02 ± 0.02 | 0.98 | 0.0011 |
| Freundlich | PAA-13-3 | 0.68 | 0.23 ± 0.03 | 1.70 ± 0.23 | 0.94 | 0.0030 |
| | PAA-MTC | 0.78 | 0.15 ± 0.01 | 1.19 ± 0.05 | 0.99 | 0.0003 |
| | PAA-Ph | 0.87 | 0.15 ± 0.01 | 1.13 ± 0.06 | 0.99 | 0.0008 |
| Temkin | PAA-13-3 | 0.68 | 0.24 ± 0.01 | 0.21 ± 0.02 | 0.98 | 0.0010 |
| | PAA-MTC | 0.78 | 0.26 ± 0.03 | 0.18 ± 0.04 | 0.92 | 0.0060 |
| | PAA-Ph | 0.87 | 0.27 ± 0.04 | 0.18 ± 0.04 | 0.87 | 0.0088 |

Where in $q_e$ is the experimental maximum sorption quantity, $q_s$ is the maximum sorption quantity provided by applying the non-linear models, *b* Equations parameters ($K_L$, $K_F$, $n_F$, for Langmuir, Freundlich, and Temkin respectively) $R^2$ determination coefficient and $\chi^2$ chi-squared distribution.

The dimensionless constant from Langmuir adsorption isotherm $R_L$ (equilibrium constant) was calculated from the above data in table 13. The $R_L$ value is an

indicative of either the sorption isotherm is favorable, unfavorable, linear or irreversible.

The $R_L$ calculated (equation 13) for the sorption of $Cu^{2+}$ divalent ion using PAA-13-3 is 0.68 which is in between zero and one, indicative of the favorable sorption. Similarly in case of PAA-MTC the $R_L$ value was found to be 0.78 and in case of PAA-GDP is 0.88, confirming that sorption in both cases are favorable.

The data was also treated using three parameter sorption isotherm models like Sips and Redlich-Peterson. The results obtain by these treatments are summarized in Table 14.

Figure 78 is the graphical representation of the statistical treatment of the data obtained for the sorption of $Cu^{2+}$ by PAA-MTC. This graph demonstrates that the results can be best fitted by both Sips and Redlich-Peterson isotherm models. For both of them the $R^2$ value is 0.99 as well the $\chi^2$ for the both models are also identical.

From figure 79 and Table 14, the results for the three model treatment for the sample PAA-Ph may be confirmed. The values calculated by both Sips and Redlich-Peterson models are alike.

***Figure 78:*** *Sorption isotherm for $Cu^{2+}$ with PAA-MTC, $q_e$ (■), Sips (●), Redlich-Peterson (▲).*

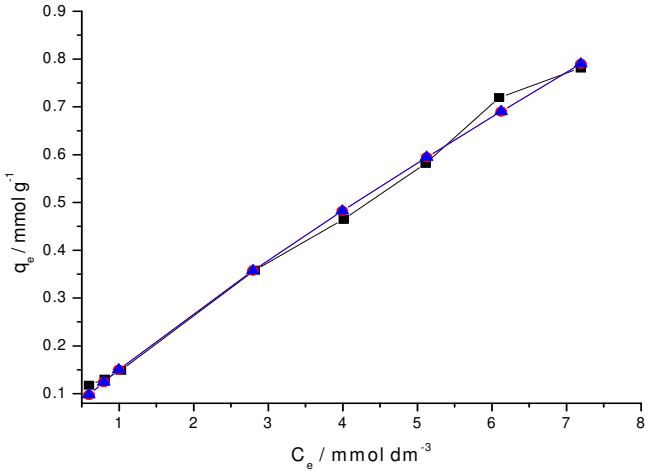

***Figure 79:*** *Sorption isotherm for $Cu^{2+}$ with PAA-Ph, $q_e$ (■), Sips (♦), Redlich-Peterson (▲).*

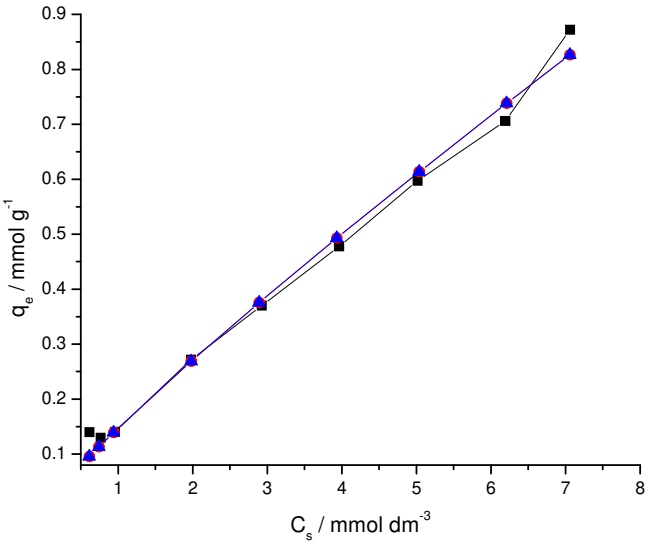


***Table 14. Some results from de application of the different models to the data come from the adsorption process of $Cu^{2+}$ with PAA-13-3, PAA-MTC and PAA-Ph, applying the non-linear models.***

| Model | Material | $q_e$/mmolg$^{-1}$ | $q_s$/mmolg$^{-1}$ | $K$/mmolg$^{-1}$ | $b$/gmmol$^{-1}$ | $R^2$ | $\chi^2$ |
|---|---|---|---|---|---|---|---|
| Sips | PAA-13-3 | 0.68 | 0.78 ± 0.10 | 0.34 ± 0.06 | 1.41 ± 0.26 | 0.98 | 0.0010 |
| | PAA-MTC | 0.78 | 798 ± 2E5 | 1.89E-4±0.05 | 0.84 ± 0.13 | 0.99 | 0.0004 |
| | PAA-Ph | 0.87 | 2251±2E6 | 6.53E-5± 0.06 | 0.88 ± 0.19 | 0.99 | 0.0010 |
| Redlich-Peterson | PAA-13-3 | 0.68 | 0.22 ± 0.04 | 0.07 ± 0.08 | 1.52 ± 0.50 | 0.98 | 0.0030 |
| | PAA-MTC | 0.78 | 0.15 ± 0.15 | 300 ± 2.4E6 | 0.16 ± 0.54 | 0.99 | 0.0004 |
| | PAA-Ph | 0.87 | 0.15 ± 0.14 | 445.51±1.5E7 | 0.12 ± 1.14 | 0.99 | 0.0010 |

Where $q_e$ is the maximum experimental sorption, $q_s$ ($Q_s$ in case of Sips and $K_{RP}/a_{RP}$ in case of R-P) is the maximum sorption capacity, K ($K_s$ is for Sips and $K_{RP}$ is for R-P) the isotherm constant and b ($n_s$ for Sips and β for R-P) is the sorption parameters.

Analyzing the data from the table 14, it can be observed that the $q_s$ and K values are very high in case of PAA-MTC and PAA-Ph for the sorption of divalent $Cu^{2+}$, hence these models may not be transformed to the monolayer Langmuir adsorption

isotherm and the idea that the sorption sites having same binding energies looks vanishing. The higher β values for Redlich-Peterson models suggest that Freundlich model could be the best fit for the sorption isotherm data. These findings from the three parameters models support the findings from the two parameter models in table 13.

Hence from the findings in table 13 from two parameter models and table 14 from three parameter models, it can be suggested that the sorption in case of PAA-MTC as well as in case of PAA-Ph could be of multilayer setup.

Using equation 12 and data form table 14 the Gibb's free energy change, $\Delta G^\circ$ calculated 3.15 kJ $mol^{-1}$ (PAA-13-3), 7.31 kJ $mol^{-1}$ (PAA-MTC), and 8.90 kJ $mol^{-1}$ (PAA-Ph) are positive and indicates that sorption processes in all three cases are non-spontaneous.

## 6. Conclusion:

POSS hybrids having cubic silsesquioxane cage to which the organic pendant chains are anchored were synthesized successfully. Reactions were worked out for reaction time reduction and % yield enhancement. PAA-13-3 was synthesized without using any catalyst, in a very short time and in a good % yield. The same procedure was adopted for the synthesis of PAA-GDP, PAA-MTC and PAA-Ph and the hybrids were synthesized successfully with reasonable yield as well as in a shorter time, without using any catalyst.

All the synthesized hybrids were then characterized for their structure elucidations using different physical techniques like FTIR, CHN, TGA, XRD, SEM, $^{13}$CNMR & $^{29}$SiNMR in solid state, where The Si—O cages of all compounds were elaborated through $^{29}$Si-NMR in solid state as well as through their respective FTIR patterns, followed by XRD analysis, while the pendant chains anchored to the POSS cages were being confirmed using $^{13}$C-NMR results along with their respective FTIR spectra. The synthesized compounds were then tested for their thermal stability using the TGA technique. SEM revealed the morphologies of the hybrids as bulk materials.

Hybrids were worked out for the sorption of divalent cations like $Cu^{2+}$, $Cd^{2+}$ and $Pb^{2+}$ from their aqueous solutions. These sorption systems were analyzed using the ICP-OES. Where the hybrid PAA-13-3 was worked out for the sorption of divalent cations like $Cu^{2+}$, $Cd^{2+}$ and $Pb^{2+}$ and the order $Cu^{2+}$> $Pb^{2+}$ > $Cd^{2+}$ was observed. Similarly the hybrids PAA-13-3, PAA-MTC and PAA-Ph were compared for their abilities of $Cu^{2+}$ sorptions and they were found to be in the order PAA-Ph > PAA-MTC > PAA-13-3.

To explain the sorption behaviour of these samples some statistical models like Langmuir, Fruendlich, Temkin, Redlich-Peterson and Sips were applied to the

sorption data. These analyses revealed that for PAA-13-3 the divalent sorption systems may be best fitted using Langmuir sorption isotherm model, where the $R_L$ calculated values reveal that sorption for $Cu^{2+}$, $Cd^{2+}$ and $Pb^{2+}$ are favorable using PAA-13-3 as a sorbent. On the other hand the sorption of $Cu^{2+}$ was best fitted by Fruendlich adsorption isotherm model, confirming their multilayer sorptions. $R_L$ values calculated for these hybrids revealed that the sorptions are favorable. The Gibb's free energies for all cations revealed that the processes are to be non-spontaneous in nature.

Hybrid material PAA-13-3 was also been used for the sorption of $CO_2$ at low pressure (max. 100 mmHg). The analysis was done using a new in-lab developed gas dosing system (GDS). A total of 65 µmol (2.86 mg) of $CO_2$ was sorbed on 200mg of the sample. The sorbed amount was found to be 1.4%, which is a reasonably higher amount considering the low $CO_2$ pressure sorption.

## Perspective:

1. The synthesized hybrid materials shall be modified and to be transformed to Janus particles. These Janus particle shall be work out for the sorption of $CO_2$.
2. Synthesized hybrids (POSS & Janus) shall be used as sorbent for the removal of cationic dyes like Remazol Yellow, Remazol Red, Remazol green.
3. These compounds shall also be tested for controlled drug delivery.
4. The hybrids shall be workout to use them as base for the formation of the Zn hollow balls, which could be used as photo catalysts.

## 7. References:


1. Sanchez, C.; Julian, B.; Belleville, P; Popall, M.: *J. Mater. Chem*., 2005, 15, 3559
2. Judeinstein, P.; Sanchez. C.: *J. Muter. Chem*., 1996, 6(4), 511.
3. Airoldi, C.: in Química de Coordenação Fundamentos e Atualidades, R.F. Farias, Ed., Ed. Átomo, p.123, Campinas, Brasil (2009).
4. Melo Jr, M.A.; Oliveira, F.J.V.E.; Sales, J.A.A.; Airoldi, C.: *New J. Chem.,* 2009, 33, 1038.
5. Hicks, J. C.; Drese, J. D.; Fauth, D. J.; Gray, M. L.; Qi, G.; Jones, C. W.: *J. Am. Chem. Soc.,* 2008, 130, 2902.
6. El-Nahhal, I.M.; El-Ashgar, N.M.: *J. Organometal. Chem.,* 2007, 692, 2861.
7. Jal, P.K.; Patel, S.; Mishra, B.K.: *Talanta,* 2004, 62, 1005.
8. Millward, A. R.; Yaghi, O. M.: *J. Am. Chem. Soc.,* 2005, 127, 17998.
9. Lazarin, A.M.; Airoldi, C.: *J. Chem. Thermodynamics*, 2009, 41, 21.
10. Dey, R.K.; Oliveira, F.J.V.E.; Airoldi, C.: *Colloids Surf. A*, 2008, 324, 41.
11. Dey, R.K.; Airoldi, C.: *J. Hazard. Mater*., 2008, 156, 95.
12. Airoldi, C.: *Quim. Nova.*, 2008, 31, 144.
13. Sales, J.A.A.; Petrucelli, G.C.; Oliveira, F.J. E.; Airoldi, C.: *J. Colloid Interface Sci.,* 2006, 297, 95.
14. Gnanasekaran, D.; Madhavan, K.; Reddley, B.S.R.: *J. Scient. Ind. Res*., 2009, 68, 437.
15. Dias Filho, N.L.; Costa, R.M.; Schultz, M.S.: *Inorg. Chim. Acta*, 2008, 361, 2314.
16. Dias Filho, N.L.; Costa, R.M.; Marangoni, F.; Pereira, D. S.: *J. Colloid Interface Sci*., 2007, 316, 250.
17. Ni, Y.; Zheng, S.; Nie, K.: *Polymer*, 2004, 45, 5557.
18. Zhang, C.; Laine, R.M.: *J. Organometal. Chem*., 1999, 521, 199.
19. Barney, R.H.; Itoh, M.; Sakakibara, A.; Suzuki, T.: *Chem. Rev.*, 1995, 95, 1409.
20. Li, G. Z.; Wang, L.; Ni, H.; Pittman Jr, C.U.: *Inorg. Organometal. Polym. Mater*., 2001, 11(3), 123.
21. Marciniec, B.; Dutkiewicz, M.; Maciejewski, H.; Kubicki, M.: *Organometallics*, 2008, 27, 793.
22. Liu, Y.; Yang, X.; Zhang, W.; Zheng, S.: *Polymer*, 2006, 47, 6814.
23. Chatterjee, S.; Chatterjee, B.P.; Guha, A.K.: *Colloids Surf. A*, 2007, 299, 146.
24. Sye, W.F.; Lu, L.C.; Tai, J. W.; Wang, C.I.: *Carbohydr. Polym*. 2008, 72, 550.
25. Zohra, B.; Aicha, K.; Fatima, S.; Nourredine, B.; Zoubir, D.: Chem. Eng. J., 2008, 136, 295.

26. Anderson, S. E.; Bodzin, D. J.; Haddad, T. S.; Boatz, J. A.; Mabry, J. M.; Mitchell, C.; Bowers, M. T.: *Chem. Mater*. 2008, 20, 4299.
27. Tamaki, R.; Tanaka, Y.; Asuncion, M.Z.; Choi, J.; Laine. R.M.: *J. Am. Chem. Soc*. 2001, 123, 12416.
28. Brick, C.M.; Tamaki, R.; Kim, S.G.; Asuncion, M.Z.; Roll, M.F.; Nemoto, T.; Ouchi, Y.; Chujo, Y.; Laine, R.M.: *Macromolecules* 2005, 38, 4655.
29. Roll, M.F.; Asuncion, M.Z.; Kampf, J.; Laine, R.M.: *ACS Nano* 2008, 2, 320.
30. Brown, J.F., Jr.: *J. Polym. Sci., Part C* 1963, 1, 83.
31. Frye, C.L.; Klosowski, J.M.: *J. Am. Chem. Soc*. 1971, 93, 4599.
32. Laine, R.M.; Youngdahl, K.A.; Babonneau, F.; Hoppe, M.L.; Zhang, Z.-F.; harrod, J.F.: *Chem. Mater*. 1990, 2, 464.
33. Tsumura, M.; Kiyoshi, A.; Kotani, J.; Hiraishi, M.; Iwahara, T.: *Macromolecules* 1998, 31, 2716.
34. Lee, E. C.; Kimura, Y.: *Polym J*. 1998, 30, 234.
35. Lee, E. C.; Kimura, Y.: *Polym. J*. 1998, 30, 730.
36. Pescarmona, P. P.; Maschmeyer, T.: *J. Aust. Chem.* 2001, 54, 583.
37. Buff, H.; Wohler, F.: *Ann. Chem.Phys.,* 1857**,** 104, 94.
38. Kipping, F. S.: *Journal of the Chemical Society, Transactions*, 1913, 103, 1871.
39. Friedel, C.; Ladenburg, A.: *Ann. Chem.Phys*., 1871**,** 23, 430.
40. Gatterman, L.: *Ber.,* 1889**,** 22, 186.
41. Stock, A.; Zeidler, F.: *Ber*., 1923, 56, 986.
42. Palmer, K. W.; Kipping, F. S.: *J. Chem. Soc.,* 1930, 1020.
43. Scott, D. W.: *J. am. Chem. Soc*., 1946, 68, 356.
44. Wahab, M. A.; Mya, K. Y.; He, C.: *J. Polym. Sci., Part A: Polym. Chem.,* 2008, 46, 5887.
45. Cheng, W. D.; Xiang, K.H.; Pandey, R.; Pernisz, U. C.: *J. Phys. Chem. B,* 2000, 104, 6737.
46. Iacono, T.; Vij, A.; Grabow, W.; Smith D. W. Jr.; Mabry, J. M.: *Chem. Commun.,* 2007, 4992.
47. Létant, S. E.; Herberg, J.; Dinh, L. N.; Maxwell, R. S.; Simpson, R. L.; Saab A. P.: *Catal. Commun*., 2007, 8, 2137.
48. Voronkov M. G.; Lavrent'yev V. I.: *Top. Curr. Chem*., 1982, 102, 199.
49. Brown, J. F.: *J. Am. Chem. Soc.,* 1965, 87, 4317.
50. Sprung, M.M.; Guenther, F.O.: *J. am. Chem. Soc*., 1955, 77, 6045.
51. Lee, K. B.; Beaver, M. G.; Caram, H. S.; Sircar, S.: *Ind. Eng. Chem. Res*. 2008, 47, 8048.
52. Huang, D.; Makhlynets, O. V.; Tan, L. L.; Lee, S. C.; Rabak- Akimova, E. V.; Holm, R. H.: *Proc. Natl. Acad. Sci. U.S.A*. 2011, 108, 1222.

53. Brown, J.F.: *Journal New Science*, 1963, 17, 304.
54. Chaffee, A. L.; Knowles, G. P.; Liang, Z.; Zhang, J.; Xiao, P.; Webley, P. A.: *Int. J. Greenhouse Gas Control* 2007, 1, 11.
55. Andrianov, K.A.; Izmailov, B.A. *Journal of Organometallic Chemistry*, 1967, 3, 435.
56. Voronkov, Mikhail G., and Vladimir I. Lavrent'yev. "Polyhedral oligosilsesquioxanes and their homo derivatives." *Inorganic Ring Systems*. Springer Berlin Heidelberg, 1982. 199.
57. Dittmar, U.; Hendan, B. J.; Florke, U.; Marsmann, H. C.: *J. Organomet. Chem.*, 1995, 489, 185.
58. Brown, J. F.; Vogt, L. H.: *J. Am. Chem. Soc*., 1965, 87, 4313.
59. Rościszewski, P.; Kazimierczuk, R.; Sołtysiak, J.: *Polimery*, 2006, 51,1.
60. Chojnowski, J.; Fortuniak, W.; Rosciszewski, P.; Werel, W.; Lukasiak, J.; Kamysz, W.; Halasa, R.: *J. Inorg. Organomet. Polym. Mater*, 2006, 16, 219.
61. Feher, F. J.; Newman, D. A.; Walzer, J. F.: *J. Am. Chem. Soc*. 1989, *111*, 1741.
62. Gießmann, S.; Fischer, A.; Edelmann, F. T.: *Z. Anorg. Allg. Chem.* 2004, *630*, 1982.
63. Kim, K.-M.; Ouchi, Y.; Chujo, Y.: *Polym. Bull. (Berlin)* 2003, *49*, 341.
64. Fu, B. X.; Lee, A.; Haddad, T. S.: *Macromolecules* 2004, *37*, 5211.
65. Anderson, S. E.; Mitchell, C.; Haddad, T. S.; Vij, A.; Schwab, J. J.; Bowers, M. T.: *Chem. Mater.* 2006, *18*, 1490.
66. Bassindale, A. R.; Parker, D. J.; Pourny, M.; Taylor, P. G.; Horton, P. N.; Hursthouse, M. B.: *Organometallics* 2004, *23*, 4400.
67. Bassindale, A. R.; Pourny, M.; Taylor, P. G.; Hursthouse, M. B.; Light, M. E.: *Angew. Chem., Int. Ed*. 2003, 42, 3488.
68. Okaue, Y.; Isobe, T.: *Kidorui* 2003, 42, 186.
69. Matsuda, Y.: *Appl. Magn. Reson.* 2003, 23, 469.
70. Takahashi, K.; Sulaiman, S.; Katzenstein, J. M.; Snoblen, S.; Laine, R. M.: *Aust. J. Chem.* 2006, 59, 564.
71. Liu, L.; Song, L.; Zhang, S.; Guo, H.; Hu, Y.; Fan, W.: *Mater. Lett.* **2006**, *60*, 1823.
72. Lee, L. H.; Chen, W.C.: *Polymer* 2005, 46, 2163.
73. Toepfer, O.; Neumann, D.; Choudhury, N. R.; Whittaker, A.; Matisons, J.: *Chem Mater* 2005, 17, 1027.
74. Huang, J.; He, C.; Liu, X.; Xu, J.; Tay, C. S. S.; Chow, S. Y.: *Polymer* 2005, 46, 7018.
75. Chan, S. C.; Kuo, S. W.; Chang, F. C.: *Macromolecules* 2005, 38, 3099.
76. Xu, H.; Kuo, S. W.; Huang, C. f.; Chang, F. C.: *J Appl Polym Sci* 2004, 91, 2208.

77. Bonhomme, C.; Coelho, C.; Azaïs, T.; Bonhomme, C. L.; Babonneau, F.; Maquet, J.; Thouvenot, R.; *C R Chim* 2006, 9, 466.
78. Croce, G.; Carniato, F.; Milanesio, M.; Boccaleri, E.; Paul, G.; Van, B. W.; Marchese, L.: *Phys Chem Chem Phys* 2009, 11, 10087.
79. Lickiss, P. D.; Rataboul, F.: (2008) Fully Condensed Polyhedral Oligosilsesquioxanes (POSS): From Synthesis to Application. In Hill AF, Fink MJ (eds) Advances in Organometallic Chemistry, Academic Press, Oxford, U.K., pp. 1-116.
80. Desmartin, C. A.; Dempsey, P.; Latournerie, J.; Hourlier, B. D.; Jayasooriya, U. A.: *Chem. Mater.* 2005, 17, 4468.
81. Liu, Y.; Zheng, S.; *J Polym Sci, Part A: Polym Chem* 2006, 44, 1168.
82. Mu, J.; Liu, Y.; Zheng, S.: *Polymer* 2007, 48, 1176.
83. Mu, J.; Zheng, S.: *J Colloid Interface* Sci 2007, 307, 377.
84. Liu, Y.; Meng, F.; Zheng, S.: *Macromol Rapid Commun* 2005, 26, 920.
85. Kim, Y.; Zhao, F.; Mitsuishi. M.; Watanabe, A.; Miyashita, T.: *J Am Chem Soc* 2008, 130, 11848.
86. Eon, D.; Raballand, V.; Cartry, G.; Cardinaud, C.; Vourdas, N.; Argitis, P.; Gogolides, E.: *J Vac Sci Technol*, B: 2006, 24, 2678.
87. Desmartin, C. A.; Jayasooriya, U. A.; Babonneau, F.: *Spectrochim Acta, Part A* 2004, 60, 1609.
88. Takamura, N.; Viculis, L.; Zhang, C.; Laine, R. M.: *Polym Int* 2007, 56, 1378.
89. Cordes, D. B.; Lickiss, P. D.; Rataboul, F.: *Chemical Reviews* 2010, 110, 2081.
90. Auner, N.; Ziemer, B.; Herrschaft, B.; Ziche, W.; John, P.; Weis, J.: *Eur J Inorg Chem*: 1999, 1087.
91. Luo, Q.; Tang, D.; Li, X.; Wang, Q.; Wang, Z.; Zhen, Z.; Liu, X.: *Chem Lett* 2006, 35, 278.
92. Handke, B.; Jastrzębski, W.; Mozgawa, W.; Kowalewska, A.: *J Mol Struct* 2008, 887(1), 159.
93. Vannier, A.; Duquesne, S.; Bourbigot, S.; Alongi, J.; Camino, G.; Delobel, R.: *Thermochim Acta* 2009, 495, 155.
94. Hato, M. J.; Ray, S. S.; Luyt, A. S.: *Macromol Mater Eng* 2008, 293, 752.
95. Kowalewska, A.; Rózga, W. K.; Handke, M.: (2008) e-Polymers. http:// www.e-polymers.org/journal/papers/akowalewska_101108.pdf. Acessed May 13, 2010.
96. Fina, A.; Tabuani, D.; Frache, A.; Camino, G.: *Polymer* 2005, 46, 7855.
97. Joshi, M.; Butola, B.S.; Simon, G.; Kukaleva, N.: *Macromolecules* 2006, 39, 1839.
98. Ma, J.; Li, Q.: *Adv. Mater. Res.,* 2006, 11-12, 323.

99. Markovic, E.: Matisons, J.; Hussain, M.; Simon, G. P.: *Macromolecules* 2007, 40, 4530.
100. Kim, K. M.; Chujo, Y.: *J Polym Sci, Part A: Polym Chem* 2003, 41, 1306.
101. Fina, A.; Tabuani, D.; Peijs, T.; Camino, G.: *Polymer* 2009, 50, 218.
102. Tanaka, K.; Adachi, S.; Chujo, Y.: *J Polym Sci, Part A: Polym Chem* 2009, 47, 5690.
103. Zhang, Z.; Liang, G.; Lu, T.: *J Appl Polym Sci* 2007, 103, 2608.
104. Seçkin, T.; Köytepe, S.; Adıgüzel, H. İ.: *Mater Chem Phys* 2008, 112, 1040.
105. Seçkın, T.; Gültek, A.; Köytepe, S.: *Turk J Chem* 2005, 29, 49.
106. Liu, L.; Hu, Y.; Song, L.; Chen, H.; Nazare, S.; Hull, T. R.: *Mater Lett* 2007, 61, 1077.
107. Pakjamsai, C.; Kawakami, Y.: *Des Monomers Polym* 2005, 8, 423.
108. Jung, C. Y.; Kim, H. S.; Hah, H. J.; Koo, S. M.: Chem Commun: 2009, 1219.
109. do Carmo, D. R.; Dias Filho, N. L.; Stradiotto, N. R.: *Mater Res* 2004, 7, 499.
110. Ricco, L.; Russo, S.; Monticelli, O.; Bordo, A.; Bellucci, F.: *Polymer* 2005, 46, 6810.
111. Perrin, F. X.; Chaoui, N.; Margaillan, A.: *Thermochim Acta* 2009, 491, 97.
112. do Carmo, D. R.; Paim, L. L.; Dias Filho, N. L.; Stradiotto, N. R.: *Appl Surf Sci* 2007, 253, 3683.
113. Schwab, J. J.; Lichtenhan, J. D.: *Applied Organometallic Chemistry* 1998, 12, 707.
114. Zhang, C.; Laine, R.M.: *J. Organomet. Chem.* 1996, 521, 199.
115. Bassindale, A. R.; Codina-Barrios, A.; Frascione, N.; Taylor, P. G.: *New J. Chem.*: 2008, 32, 240.
116. Qiu, L.G.; Xie, A.J.; Zhang, L.D.: *Adv. Mater.,* 2006, 17, 689.
117. Bordiga, S.; Lamberti, C.; Ricchiardi, G.; Regli, L.; Bonino, F.; Damin, A.; Lillerud, K. P.; Bjorgen, M.; Zecchina, A.: *Chemical communications* 2004, 2300.
118. Collins, D. J.; Zhou, H.: *J. mater. Chem..,* 2007, 17, 3154.
119. James, S. L.: *Chem. Soc. Rev*. 2003, 32, 276.
120. Eddaoudi, M.; Li, H.; Yaghi, O. M.: *J. Am. Chem. Soc.* 2000, 122, 1391.
121. Sun, D.; Cao, R.; Sun, Y.; Bi, W.; Li, X.; Wang, Y.; Shi, Q.; Li, X.: *Inorg. Chem.* 2003, 42, 7512.
122. Sing, K.S.W.; Everet, D.H.; Haul, R.A.W.; Moscou, L.; Pierotti, R. A.; Rouqueról, J.; Siemieniewska, T.: Pure Applied and Chemistry, Oxford, v.57, p.62, 1985.
123. O'Connella, D. W.; Birkinshawb, C.; O'Dwyera, T. F.: *Bioresource Technology* 2008, 99, 6709.

124. Cheremisinoff, P. N.: “Encyclopedia of Environmental Control Technology: Wastewater Treatment Technology”, Gulf Publishing Company, Houston, Texas, Vol. 3 (1989).
125. Patra, M.; Bhowmik, N.; Bandopadhyay, B. ; Sharma, A.: *Environ. Exp. Bot.*, 2004, 52, 199.
126. Grimalt, J. O.; Ferrer, M.; Macpherson, *E.: Sci. Total Environ*., 1999, 242, 3.
127. Kudo, A;. Fujikawa, Y.; Miyahara, S.; Zheng, J.; Takigami, H.; Sugahara, M.; Muramatsu, T.: *Water sci, technol*., 1998, 38, 187.
128. Smith, A. H.; Lingas, E. O.; Rahman, M.: *Bull. world health organ.* 2000, 78, 1093.
129. Ishaque, A. B.; Johnson, L.; Gerald, T.; Boucaud, D.; Okoh, J.; Tchounwou, P. B.: *Int. j. Environ. Res. Publ. health*, 2006, 3, 118.
130. Reinhold, J. G.: *Clin. Chem*. 1975, 21, 476.
131. Flora, S.J.S.; Mittal, M.; Mehta, A.: *Indian j. Med. Res*., 2008, 128, 501.
132. Lech, T.; Sadlik, J. K.: Biol. *Trace. Elem. Res*., 2007, 118, 10.
133. Kim, M.: *Food addit. Contam*. 2004, 8, 763.
134. Agbozu, I. E.; Ekweozor, I. K. E.; Opuene, k.: *int. j. environ. Sci. tech.*, 2007, 4, 93.
135. Needleman, H.: *Annu. Rev. Med*., 2004, 55, 209.
136. Hartinger, L.; “Hand book of effluent treatment and recycling for the metal finishing industry” Finishing publications Ltd., Stevenage, (1994).
137. Mcquarrie, D.A.; Simon, J.D.: Physical Chemistry: a molecular approach. Sausalito: University Science Books, 1997.
138. Tóth, J.: Adsorption Isotherms. In: ENCYCLOPEDIA of surface and colloid science. New York: Taylor & Francis, 2002. p. 212.
139. Dias, N. L.; do Carmo, D. R.: (2nd ed.). ENCYCLOPEDIA of surface and colloid science. New York: vol. 1, Taylor & Francis, New York (2006), pp. 209–228.
140. Ge, Z.; Wang, D.; Zhou, Y.; Liu, H.; Liu, S.: *Macromolecules* 2009, 42, 2903.
141. Dutkiewicz, M.; Maciejewski, H.; Marciniec, B.: *Synthesis* 2009, 2019.
142. Dias Filho, N. L.; Marangoni, F.; Costa, R. M.: *J. Colloid Interface Sci*. 2007, 313, 34.
143. Ibrahim, G. M.; Ahmad, M. o. I.; El-Gammal, B.: *J. Appl. Polym. Sci*. 2009, 113, 3038.
144. do Carmo, D. R.; Paim, L. L.; Metzker, G.; Dias Filho, N. L.; Stradiotto, N. R.:*Materials Research Bulletin,* 2010, 45, 1263.
145. Gu¨ltek, A.; Sec¸kin, T.; Adigu¨zel, H. I ˙.: *Turk. J. Chem.* 2005, 29, 391.
146. Naka, K.; Fujita, M.; Tanaka, K.; Chujo, Y.: *Langmuir* 2007, 23, 9057.

147. Tanaka, K.; Inafuku, K.; Naka, K.; Chujo, Y.: *Org. Biomol. Chem*. 2008, 6, 3899.
148. Tanaka, K.; Inafuku, K.; Chujo, Y.: *Bioorg. Med. Chem*. 2008, 16, 10029.
149. Tanaka, K.; Kitamura, N.; Naka, K.; Chujo, Y.: *Chem. Commun*. 2008, 6176.
150. Tanaka, K.; Inafuku, K.; Adachi, S.; Chujo, Y.: *Macromolecules* 2009, 42, 3489.
151. Tanaka, K.; Kitamura, N.; Naka, K.; Morita, M.; Inubushi, T.; Chujo, M.; Nagao, M.; Chujo, Y.: *Polym. J.* 2009, 41, 287.
152. Goodgame, D. M. L.; Kealey, S.; Lickiss, P. D.; White, A. J. P.: *J. Mol. Struct.* 2008, 890, 232.
153. Fonseca, M.G.; Airoldi, C.: *Termochimica Acta*, 2001, 359, 1.
154. Bianchini, D.; Butler, I.S.; Barsan, M.M.; Martens, W.; Frost, R.L.; Galland G.B.; dos Santos, J.H.: *Spectrochimica Acta Part A*, 2008, 71, 45.
155. Sales, J.A.A.; Prado, A.G.; Airoldi, C.: *Surf. Sci*. 2005, 590, 51.
156. Arakaki, L.N.H.; Airoldi, C.: *Polyhedron* 2000, 19, 367.
157. Zhang, Z.; Liang, G.; Lu, T.: *Journal of Applied Polymer Science*, 2006, 2608.
158. Gravel, M. C.; Laine, R. M.: *Polym Prep (Am Chem Soc Div Polym Chem)* 1997, 38, 155.
159. Erba, I. E.; Fasce, D. P.; Williams, R. J.; Balsells, R. E.; Fukuyama, Y.; Nonami, H.: *J Organomet Chem* 2003, 686, 42.
160. Pescarmona, P. P.; van der Waal, J. C.; Maschmeyer, T.: *Eur J Inorg Chem* 2004, 5, 978.
161. Schönherr, P.; Seifert, A.; Lungwitz, R.; Simon, F.; Moszner, N.; Burtscher, P.; Spange, S.: *Progress in Organic Coatings* 2012, 75, 335.
162. Gao, J.; Zhang, X.; Wang, S.; Run, M.: *Chem. J. on Internet*, 2005, 7 (7), 48. Available from: http://www.chemistrymag.org/cji/2005/077048ne.htm (Accessed on 04/10/2014)
163. Unno, M.; Matsumoto, T.; Mochizuki, K.; Higuchi, K.; Goto, M.; Matsumoto, H.: *J. Organomet. Chem.*, 2003, 685, 156.
164. Gravel, M. C.; Zhang, C.; Dinderman, M.; Laine, R. M.: *Appl. Organometal. Chem*., 1999, 13, 329
165. Kim, K.; Adachi, K.; Chujo, Y.: *Polymer* 2002, 43, 1171.
166. Sales, J.A.A.; Prado, A.G.S.; Airoldi, C.: *Polyhedron,* 2002, 21, 2647.
167. Cestari, A.R.; Vieira, E.F.S.; Nascimento, A.J.P.; Oliveira, F.J.R.; Bruns, R.E.; Airoldi, C.: *J. Colloid Inteface Sci*., 2001, 241, 45.
168. Feher, F. J.; Wyndham, K. D.: *Chem Commun*., 1998, 102, 323.
169. Sellinger, A.; Laine, R. M.: *Macromolecules*, 1996, 29(6).
170. Clark, J. C.; Barnes, C. E.: *Chem. Mater*., 2007, 19, 3212.

171. Davidova, I.E.; Gribov, L. A.; Maslov, I. V.; Dufaud, V.; Niccolai, G. P.; Bayard, F.; Basset, J. M.: *J Mol Struct*., 1998, 443, 89.
172. Fina, A.; Tabuani, D.; Carniato, F.; Frache, A.; Boccaleri, E.; Camino, G.: *Thermochim. Acta*, 2006, 440, 36.
173. Nie, W. Y.; Li, G.; Li, Y.; Xu, H. Y.: *Chin. Chem. Lett*., 2009, 20, 738.
174. Chen, J.-H.; Chiou, Y.-D.: *J. Polym. Sci., Part B: Polym. Phys*., 2006, 44, 2122.
175. Grassie, N.: *Trans. Faraday Soc*. 1952, 48, 379.
176. Sulaiman, S.; Zhang, J.; Goodson, T.; Laine, R. M.: *J. Mater. Chem*., 2011, 21, 11177
177. Waddon, A. J.; Coughlin, E. B.: *Chem. Mater*. 2003, 15, 4555.
178. Feng Y,; Jia Y,; Xu H: *J Appl Polym Sci* 2009, 111, 2684.
179. Zhou, Z.; Cui, L.; Zhang, Y.; Zhang, Y.; Yin, N.: *Eur Polym J* 2008, 44, 3057.
180. Wang, R.; Wang, S.; Zhang, Y.: *J Appl Polym Sci* 2009, 113, 3095.
181. Sayari, A.; Belmabkhout, Y.: *J. Am. Chem. Soc.* 2010, 132, 6312.
182. Sayari, A.; Belmabkhout, Y.; Serna, G. R.: *Chem. Eng. J.* 2011, 171, 760.
183. Qi, G.; Wang, Y.; Estevez, L.; Duan, X.; Anako, N.; Park, A.H.A.; Li, W.; Jones, C.W.; Giannelis, E.P.: *Energy Environ. Sci.* 2011, 4, 444.
184. Heydari, G. A.; Sayari, A.: *Chem. Eng. J.* 2011, 173, 72.
185. ATSDR, CERCLA Priority List of Hazardous Substances, 2007.
186. The restriction of the use of certain hazardous substances in electrical and electronic equipment, O.J. L. 2003, 37, 19.
187. Lone, M. I.; He, Z. L.; Stoffella, P. J.; Yang, X. E.: J Zhejiang Univ Sci B. 2008, 9(3), 210.
188. Liu, H.; Kondo, S.; Tanaka, R.; Oku, H.; Unno, M.: *J. Organomet. Chem.*, 2008, 693, 1301.
189. Magosso, H. A.; Panteleimonov, A. V.; Kholin, Y. V.; Gushikem, Y.: *J. Colloid Interface Sci.,* 2006, 303, 18.
190. Donia, A.M.; Atia, A. A.; Al-Amrani, W. A.; Ei-Nahas, A. M.: (2009). *J. Hazard. Mater.*, 2009, 161, 1544.
191. Hou, A.; Chen, B.; Dai, J.; Zhang, K.: *Journal of Cleaner Production*, 2010, 18, 1009.
192. Hou, A.; Wang, X.; Yu, Y.: *Carbohydrate Polymers*, 2009, 77, 201.
193. Sang, L.; Hudson, S.M.: *Coloration Technology*, 2004, 120, 108113.
194. Wang, H.; Lewis, D. M.: *Coloration Technology*, 2002, 118, 159.
195. Husain, Q.: *Critical Review Biotechnology*, 2006, 26, 201.
196. Qada, E. N. E.; Allen, S. J.; Walker, G. M.: *Chemical Engineering*, 2008, 135, 174184.
197. Xie, K.; Zhao, W.; He, X.: *Carbohydrate Polymers* 2011, 83, 1516.

198. Gupta,V.K.; Suhas.: *Journal of Environmental Management*, 2009, 90, 2313.
199. Xue, Y.; Hou, H.; Zhu, S.: *Chemical Engineering Journal*, 2009, 147, 272.
200. Hou, A.; Sun, Y.: *Journal of Dispersion Science and Technology*, 2009, 30, 643.
201. Xie, K.; Gao, Y.; Gao, X.: *International Journal of Nonlinear Sciences and Numerical Simulation*, 2010, 11, 429.
202. Cavenati, S.; Grande, C. A.; Rodrigues, A. E.: *J. Chem. Eng*. Data 2004, 49, 1095.
203. Llewellyn, P. L.; Bourrelly, S.; Serre, C.; Filinchuk, Y. T.; Ferey, G.: *Angew. Chem., Int. Ed*. 2006, 45, 7751.
204. Kim, S.; Ida, J.; Guliants, V.V.; Lin, Y.S.: *J. Phys. Chem. B* 2005, 109, 6287.
205. Xu, X.; Song, C.; Andresen, J.M.; Miller, B.G.; Scaroni, A.W.: *Energy Fuels* 2002, 16, 1463.
206. Harlick, P.J.E.; Sayari, A.; *Ind. Eng. Chem. Res*. 2006, 45, 3248.
207. Harlick, P.J.E.; Tezel, F.H.; *Micropor. Mesopor. Mater*. 2004, 76, 71.
208. Satyapal, S.; Filburn, T.; Trela, J.; Strange, J.: *Energy Fuels* 2001, 15, 250.
209. Reddy, E.P.; Smirniotis, P.G.: *J. Phys. Chem. B* 2004, 108, 7794.
210. Hiyoshi, N.; Yogo, K.; Yashima, T.: *Microporous and Mesoporous Materials.* 2005, 84, 357.
211. Foo, K. Y.; Hameed, B. H.: *J. Hazard. Mater.* 2009, 171(1), 54.
212. Nouri, L.; Ghodbane, I.; Hamdaoui, O.; Chiha, M.: *J. Hazard. Mater.* 2007, 149, 115.
213. Oliveira Junior, N. G. (2012) Desenvolvimento de um Sistema de Dosagem de Gás (SDG) projetado para estudos termoquímicos de adsorção de gases em materiais sólidos. *doctoral dissertation*, 2012, University of Campinas, Campinas-SP, Brazil.

# Appendix A:

**Figure A 1. Sorption isotherm of hybrid PAA13-3 for, $Cu^{2+}$ (■), Langmuir (▲) at 298 ± 1 K.**

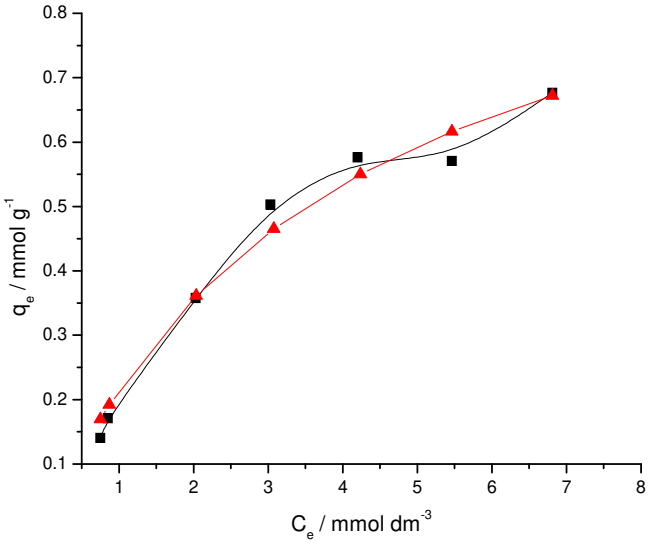


**Figure A 2. Sorption isotherm of hybrid PAA13-3 for, $Cu^{2+}$ (■), Fruendlich (▲) at 298 ± 1 K.**

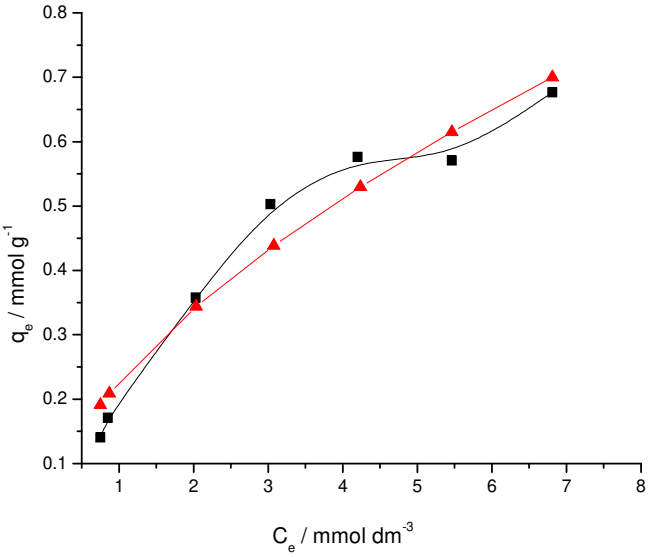

**Figure A 3. Sorption isotherm of hybrid PAA13-3 for, $Cu^{2+}$ (■), Temkin (▲) at 298 ± 1 K.**

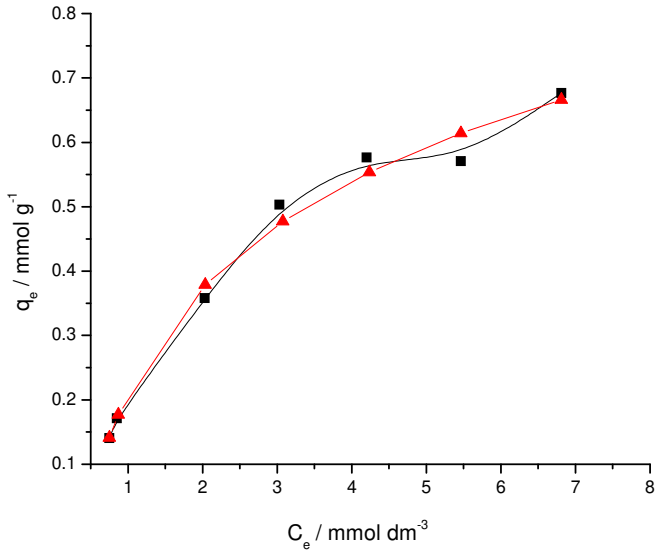


**Figure A 4. Sorption isotherm of hybrid PAA13-3 for, $Cu^{2+}$ (■), Langmuir (▲), Fruendlich (▼) at 298 ± 1 K.**

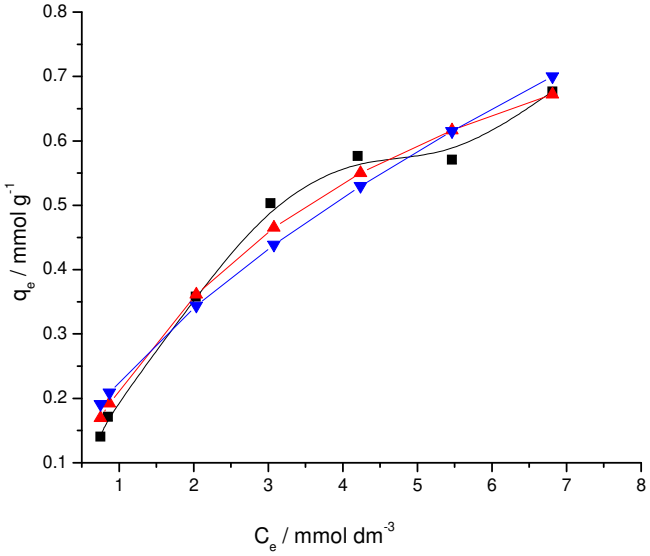

Figure A 5. Sorption isotherm of hybrid PAA13-3 for, $Cu^{2+}$ (■), Langmuir (▲), Temkin (▼) at 298 ± 1 K.

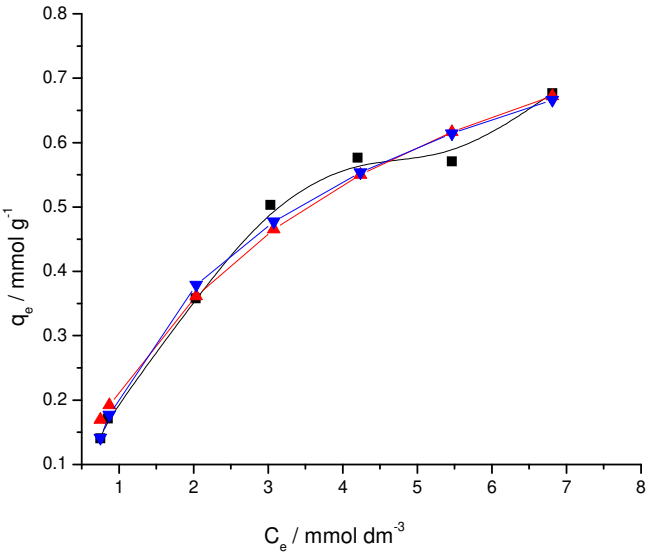


**Figure A 6. Sorption isotherm of hybrid PAA13-3 for, $Cu^{2+}$ (■), Fruendlich (▲), Temkin (▼) at 298 ± 1 K.**

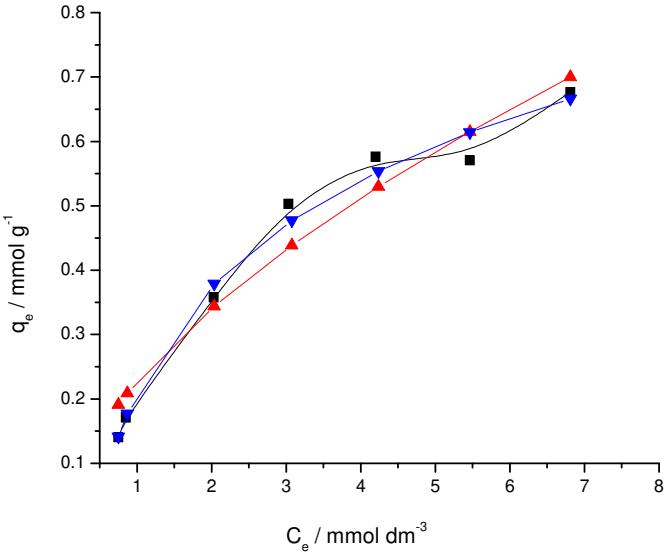

**Figure A 7. Sorption isotherm of hybrid PAA13-3 for, $Cu^{2+}$ (■), Sips (▲), at 298 ± 1 K.**

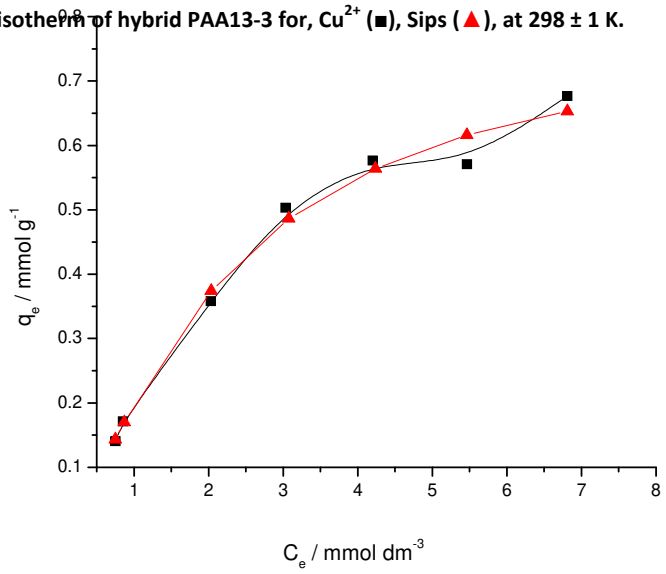


**Figure A 8. Sorption isotherm of hybrid PAA13-3 for, $Cu^{2+}$ (■), Redlich-Peterson (▲) at 298 ± 1 K.**

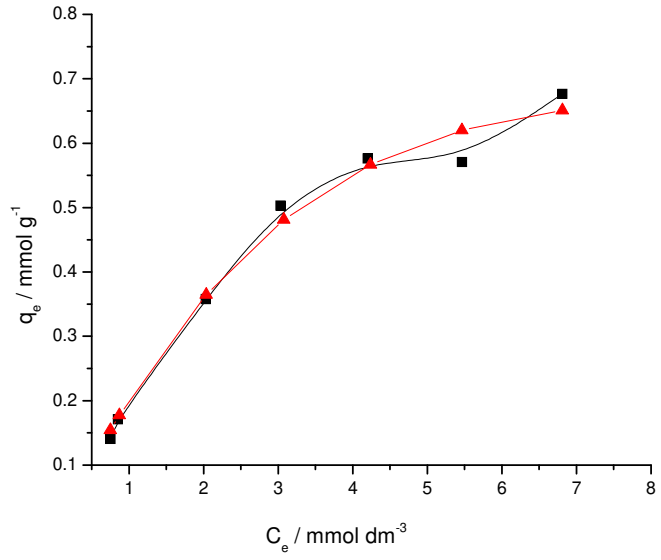

**Figure A 9. Sorption isotherm of hybrid PAA13-3 for, $Pb^{2+}$ (■), Langmuir (▲) at 298 ± 1 K.**

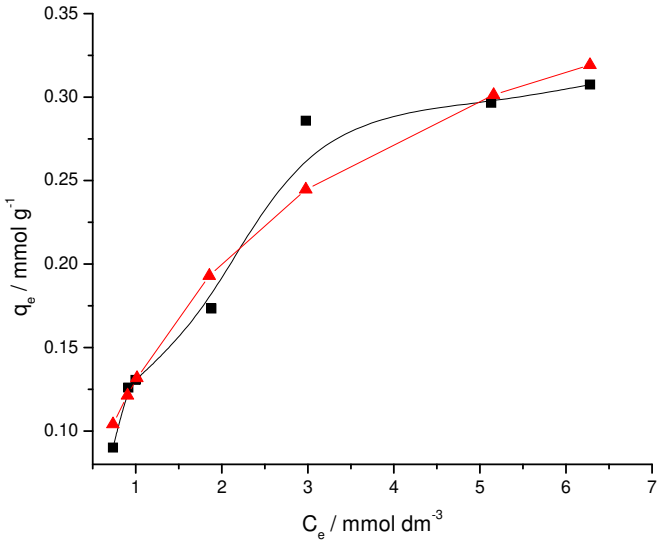


**Figure A 10. Sorption isotherm of hybrid PAA13-3 for, $Pb^{2+}$ (■), Fruendlich (▲) at 298 ± 1 K.**

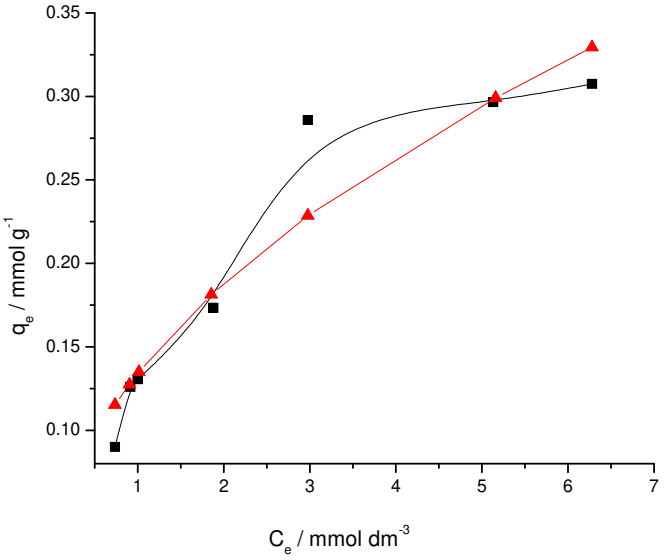

**Figure A 11. Sorption isotherm of hybrid PAA13-3 for, $Pb^{2+}$ (■), Temkin (▲) at 298 ± 1 K.**

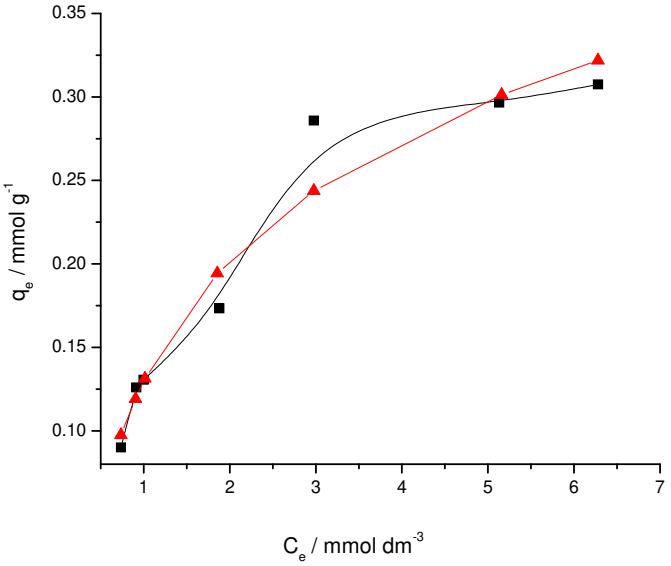


**Figure A 12. Sorption isotherm of hybrid PAA13-3 for, $Pb^{2+}$ (■), Langmuir (▲), Fruendlich (▼) at 298 ± 1 K.**

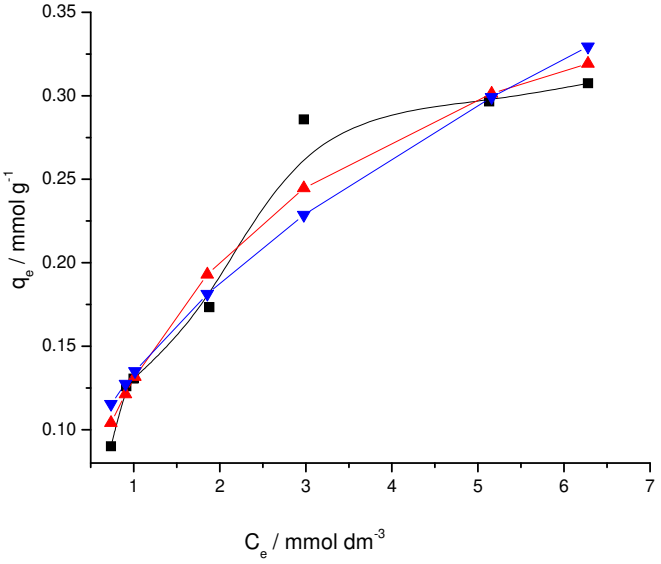

**Figure A 13. Sorption isotherm of hybrid PAA13-3 for, $Pb^{2+}$ (■), Langmuir (▲), Temkin (▼) at 298 ± 1 K.**

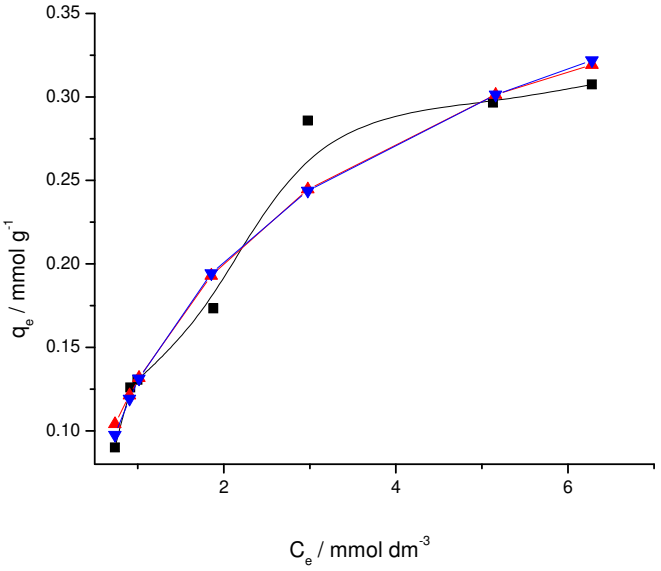


**Figure A 14. Sorption isotherm of hybrid PAA13-3 for, $Pb^{2+}$ (■), Fruendlich (▲), Temkin (▼) at 298 ± 1 K.**

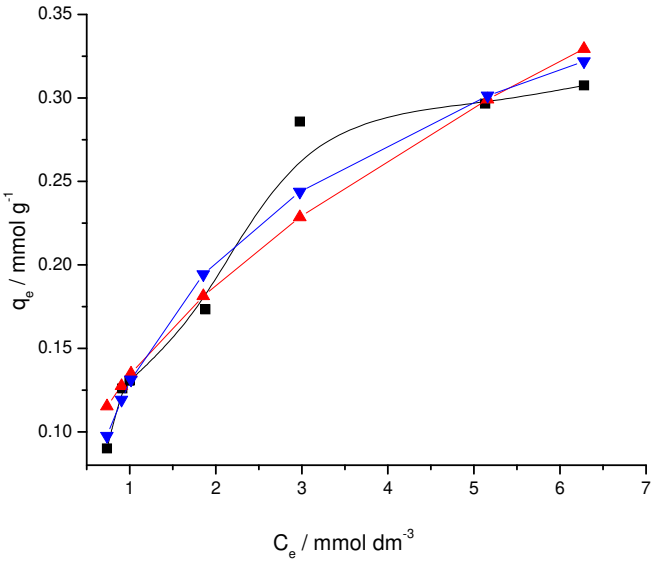

**Figure A 15. Sorption isotherm of hybrid PAA13-3 for, $Pb^{2+}$ (■), Sips (▲) at 298 ± 1 K.**

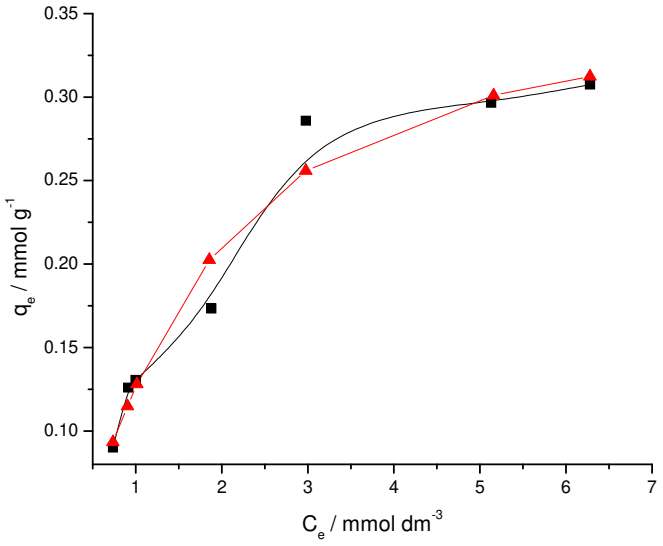


**Figure A 16. Sorption isotherm of hybrid PAA13-3 for, $Pb^{2+}$ (■), Redlich-Perterson (▲) at 298 ± 1 K.**

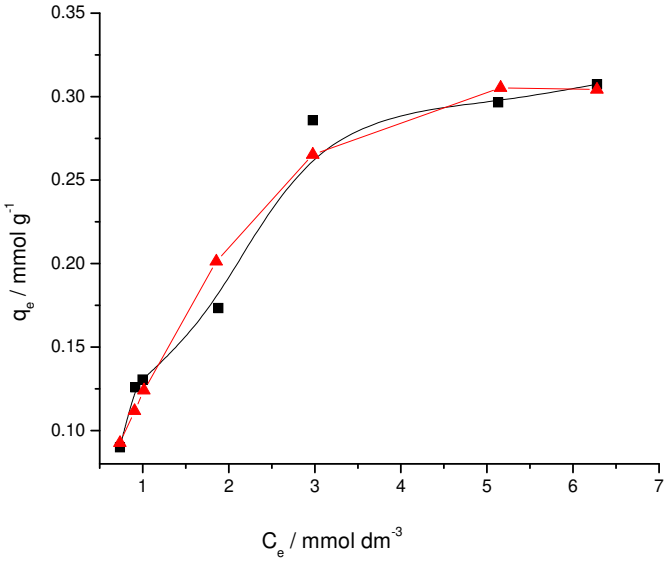

**Figure A 17. Sorption isotherm of hybrid PAA13-3 for, $Cd^{2+}$ (■), Langmuir (▲) at 298 ± 1 K.**

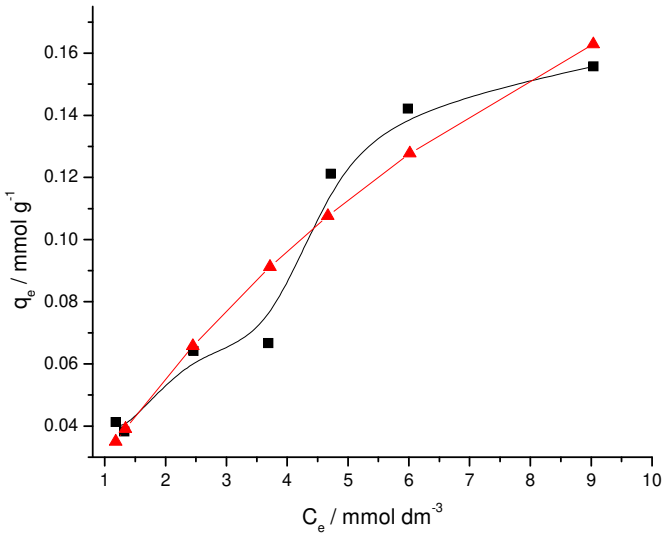


**Figure A 18. Sorption isotherm of hybrid PAA13-3 for, $Cd^{2+}$ (■), Fruendlich (▲) at 298 ± 1 K.**

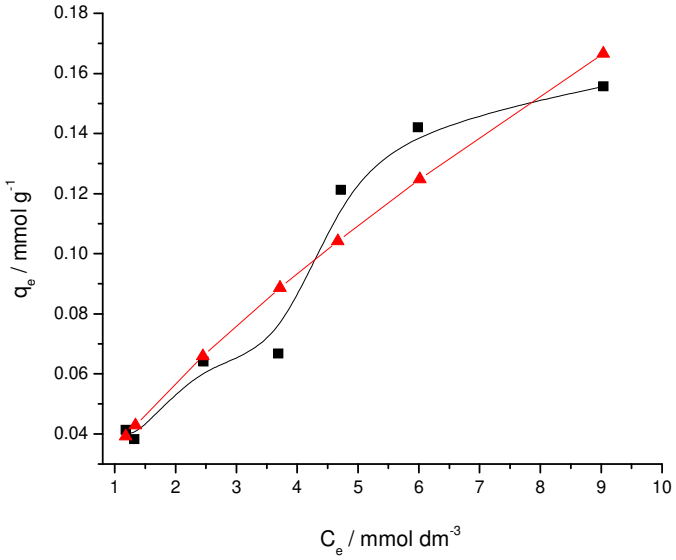

**Figure A 19. Sorption isotherm of hybrid PAA13-3 for, $Cd^{2+}$ (■), Temkin (▲) at 298 ± 1 K.**

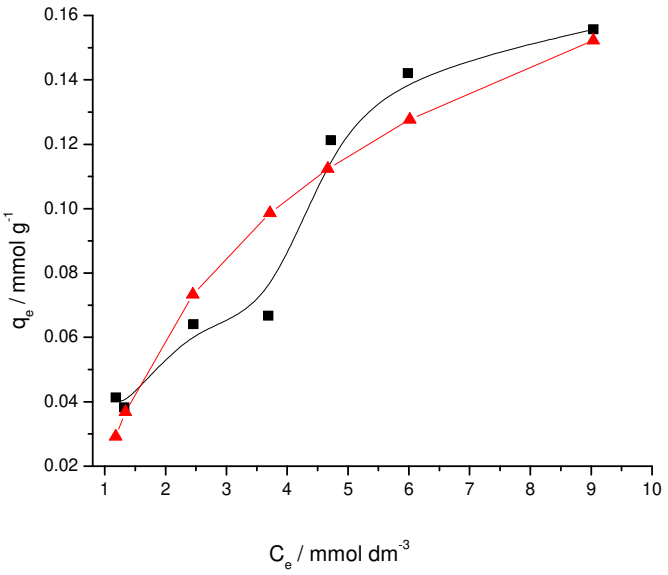


**Figure A 20. Sorption isotherm of hybrid PAA13-3 for, $Cd^{2+}$ (■), Langmuir (▲), Fruendlich (▼) at 298 ± 1 K.**

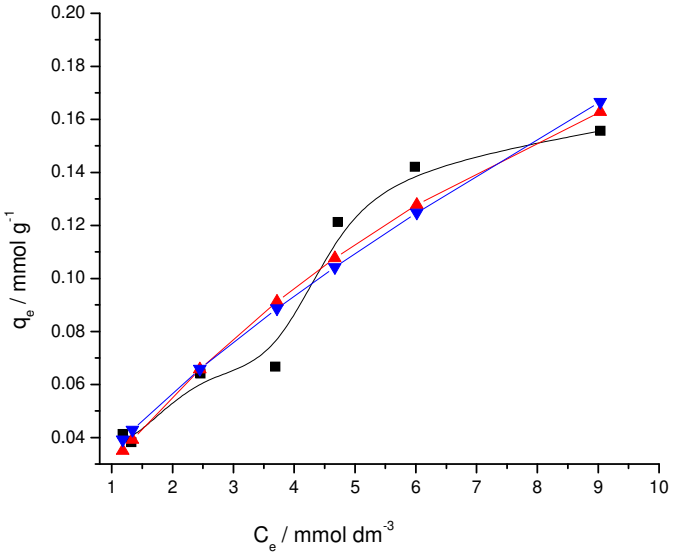

**Figure A 21. Sorption isotherm of hybrid PAA13-3 for, $Cd^{2+}$ (■), Langmuir (▲), Temkin (▼) at 298 ± 1 K.**

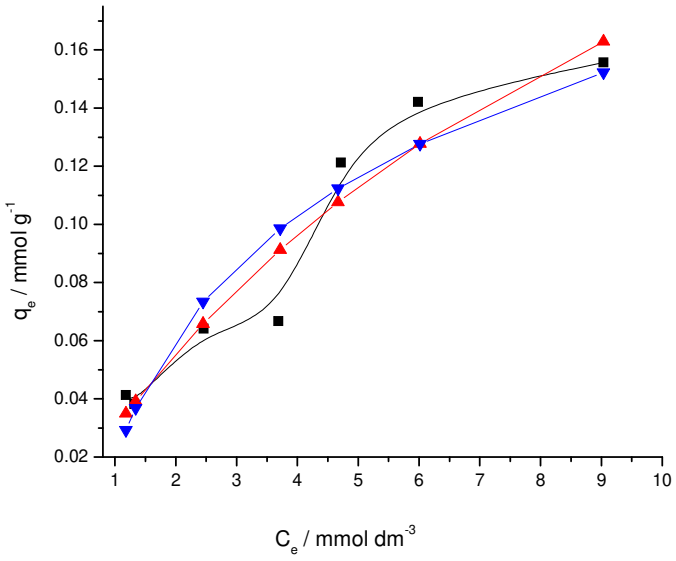


**Figure A 22. Sorption isotherm of hybrid PAA13-3 for, $Cd^{2+}$ (■), Fruendlich (▲), Temkin (▼) at 298 ± 1 K.**

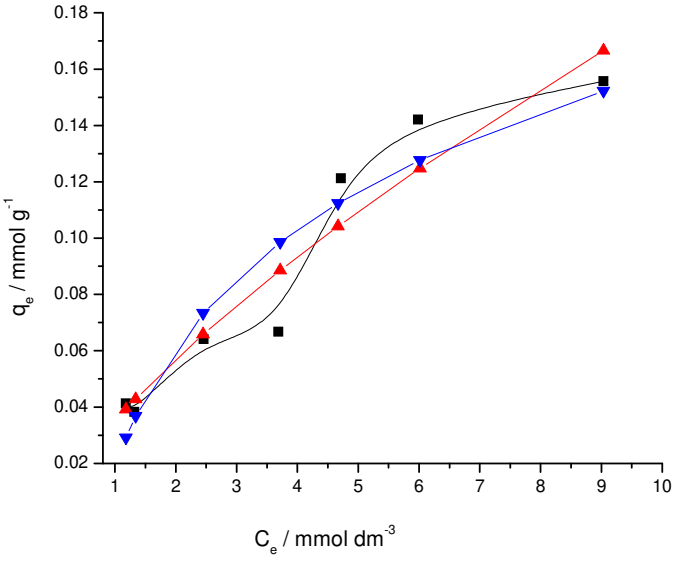

**Figure A 23. Sorption isotherm of hybrid PAA13-3 for, $Cd^{2+}$ (■), Sips (▲) at 298 ± 1 K.**

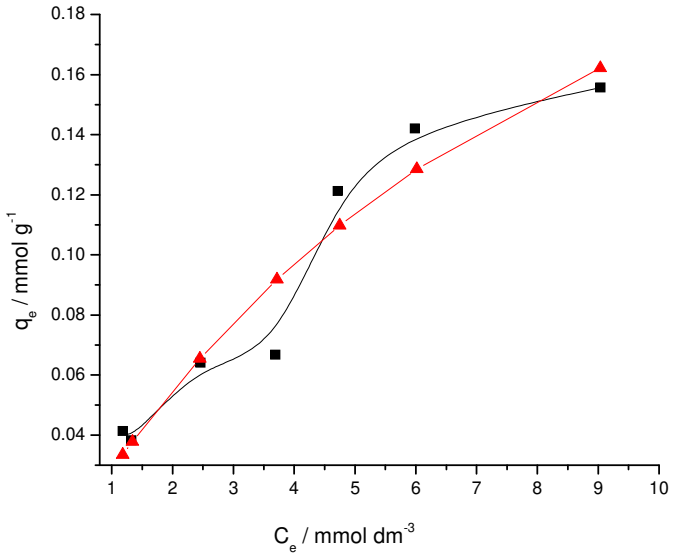


**Figure A 24. Sorption isotherm of hybrid PAA13-3 for, $Cd^{2+}$ (■), Redlich-Peterson (▲), Temkin (▼) at 298 ± 1 K.**

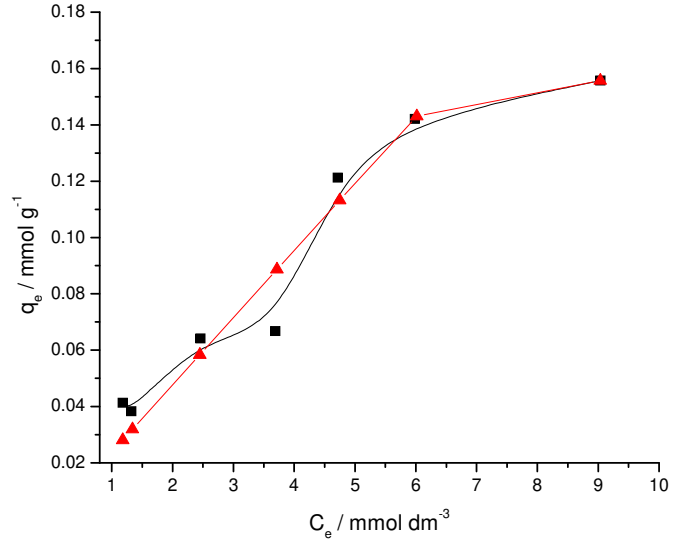

**Figure A 25. Comparison of the sorption isotherms of the hybrid PAA13-3 for, $Cu^{2+}$ (■), Langmuir for $Cu^{2+}$(□), $Pb^{2+}$ (●), Langmuir for $Pb^{2+}$ (○) at 298 ± 1 K.**

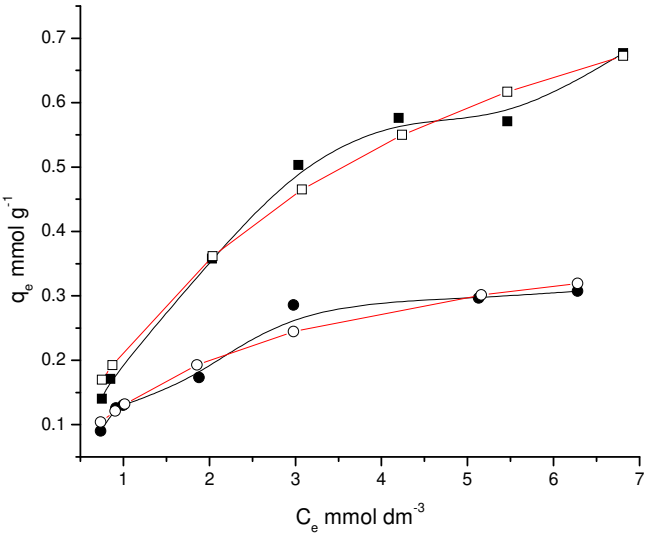


**Figure A 26. Comparison of the sorption isotherms of the hybrid PAA13-3 for, $Cu^{2+}$ (■), Langmuir for $Cu^{2+}$(□), $Cd^{2+}$ (●), Langmuir for $Cd^{2+}$ (○) at 298 ± 1 K.**

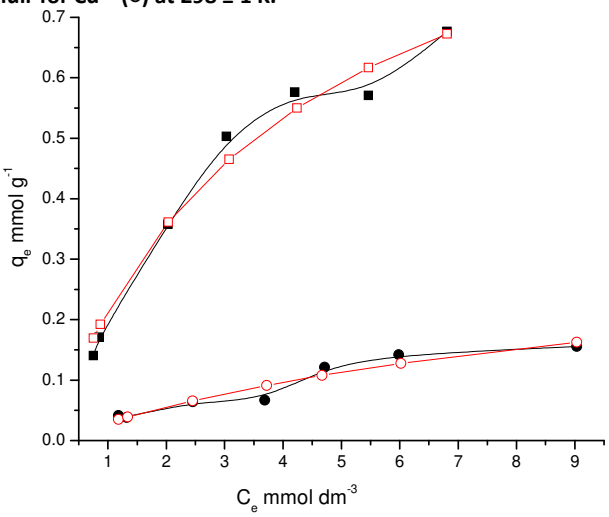

**Figure A 27. Comparison of the sorption isotherms of the hybrid PAA13-3 for, $Pb^{2+}$ (■), Langmuir for $Pb^{2+}$(□), $Cd^{2+}$ (●), Langmuir for $Cd^{2+}$ (○) at 298 ± 1 K.**

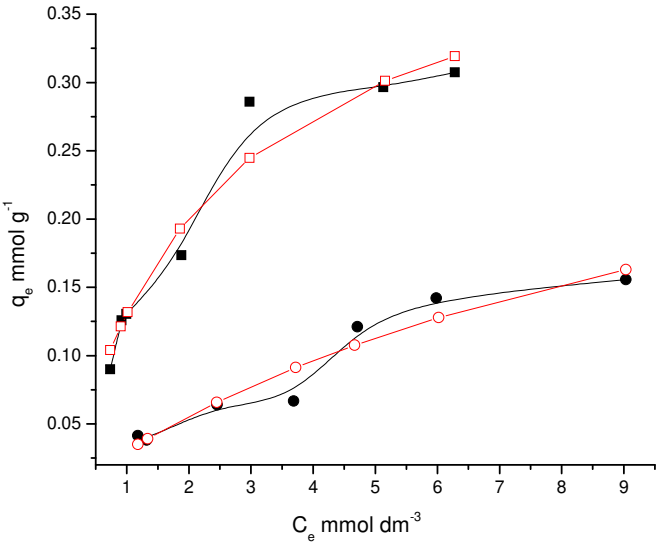


**Figure A 28. Comparison of the sorption isotherms of the hybrid PAA13-3 for, $Cu^{2+}$ (■), Fruendlich for $Cu^{2+}$(□), $Pb^{2+}$ (●), Fruendlich for $Pb^{2+}$ (○) at 298 ± 1 K.**

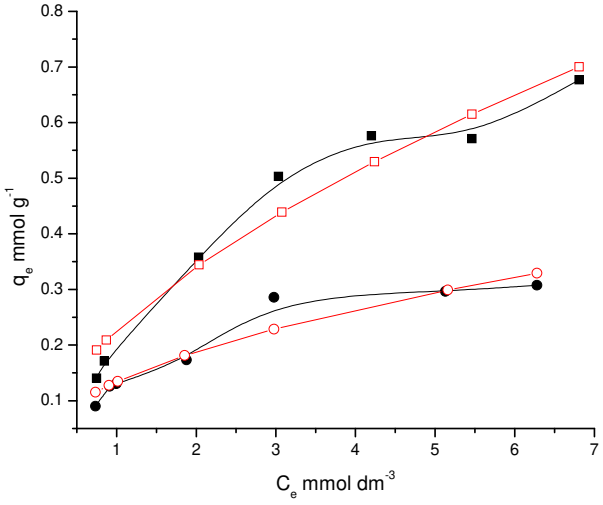

**Figure A 29. Comparison of the sorption isotherms of the hybrid PAA13-3 for, $Pb^{2+}$ (■), Fruendlich for $Pb^{2+}$(□), $Cd^{2+}$ (●), Fruendlich for $Cd^{2+}$ (○) at 298 ± 1 K.**

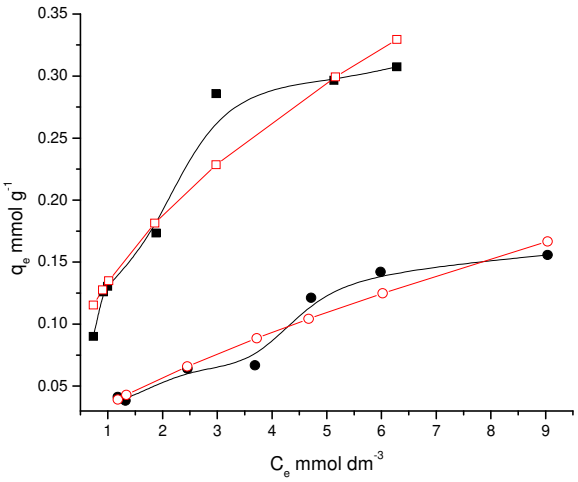


**Figure A 30. Comparison of the sorption isotherms of the hybrid PAA13-3 for, $Cu^{2+}$ (■), Fruendlich for $Cu^{2+}$(□), $Cd^{2+}$ (●), Fruendlich for $Cd^{2+}$ (○) at 298 ± 1 K.**

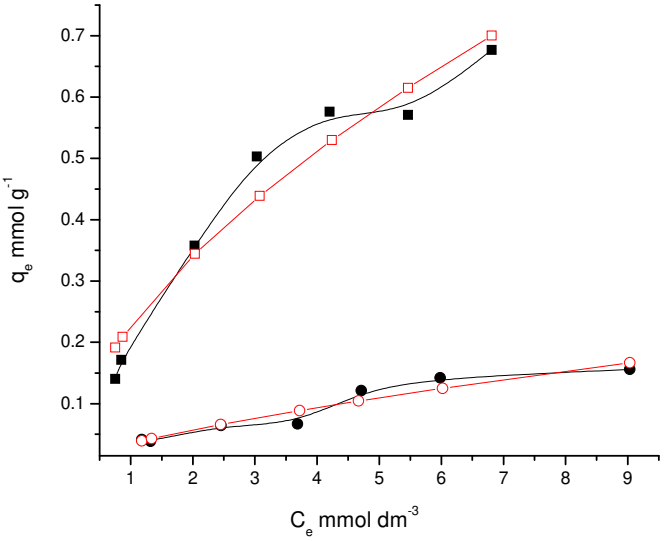

Figure A 31. Comparison of the sorption isotherms of the hybrid PAA13-3 for, $Cu^{2+}$ (■), Temkin for $Cu^{2+}$(□), $Pb^{2+}$ (●), Temkin for $Pb^{2+}$ (○) at 298 ± 1 K.

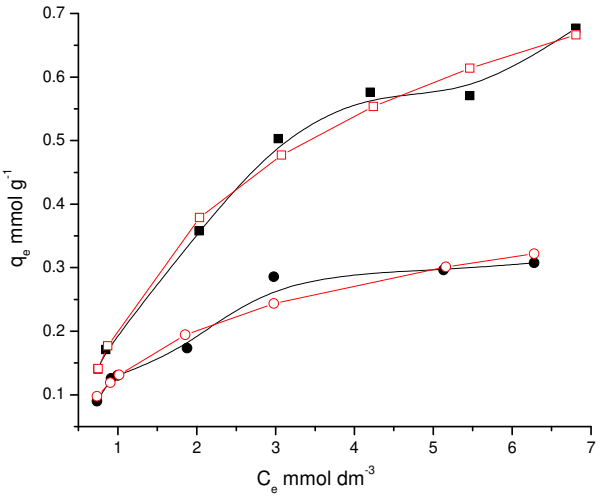


**Figure A 32. Comparison of the sorption isotherms of the hybrid PAA13-3 for, $Cu^{2+}$ (■), Temkin for $Cu^{2+}$(□), $Cd^{2+}$ (●), Temkin for $Cd^{2+}$ (○) at 298 ± 1 K.**

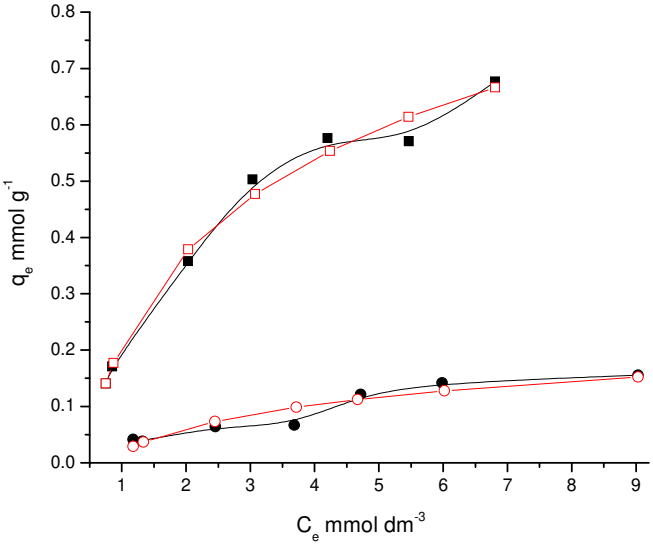

**Figure A 33. Comparison of the sorption isotherms of the hybrid PAA13-3 for, $Pb^{2+}$ (■), Temkin for $Pb^{2+}$(□), $Cd^{2+}$ (●), Temkin for $Cd^{2+}$ (○) at 298 ± 1 K.**

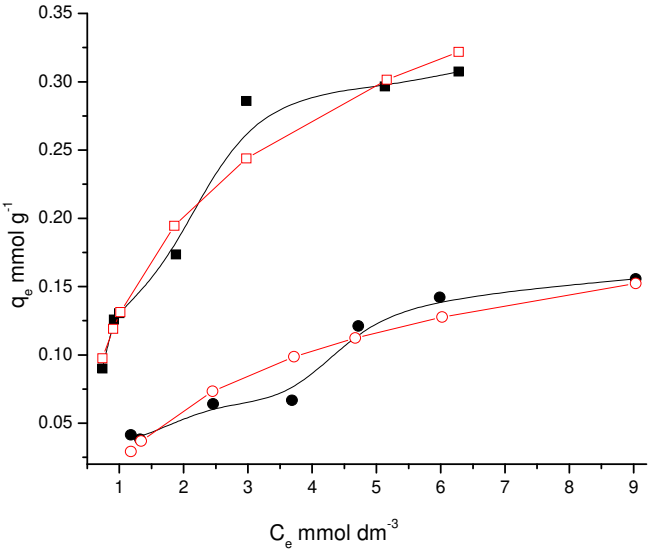

# Appendix B:

**Figure B 1. Langmuir's linearization of sorption isotherm for $Cu^{2+}$ with PAA-13-3:**

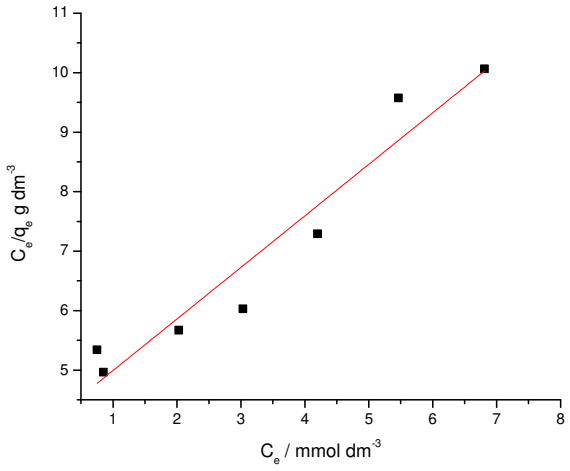


**Figure B 2. Fruendlich's linearization of sorption isotherm for $Cu^{2+}$ with PAA-13-3**

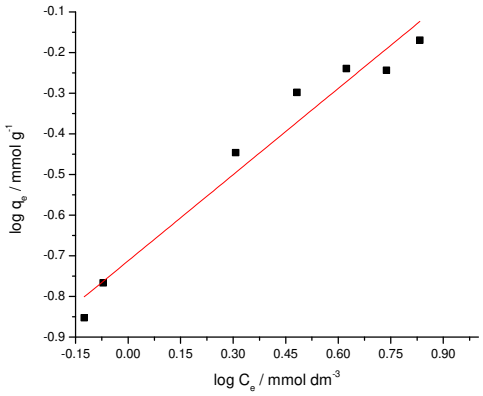


**Figure B 3. Temkin's linearization of sorption isotherm for $Cu^{2+}$ with PAA-13-3**

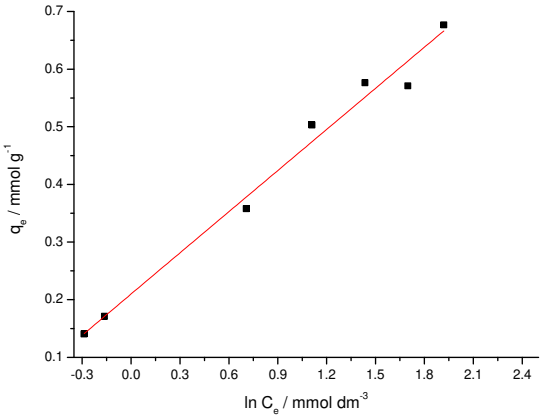

Figure B 4. Langmuir's linearization of sorption isotherm for $Pb^{2+}$ with PAA-13-3

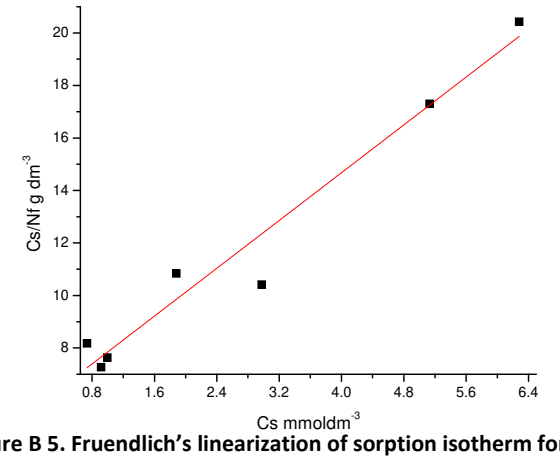


**Figure B 5. Fruendlich's linearization of sorption isotherm for $Pb^{2+}$ with PAA-13-3**

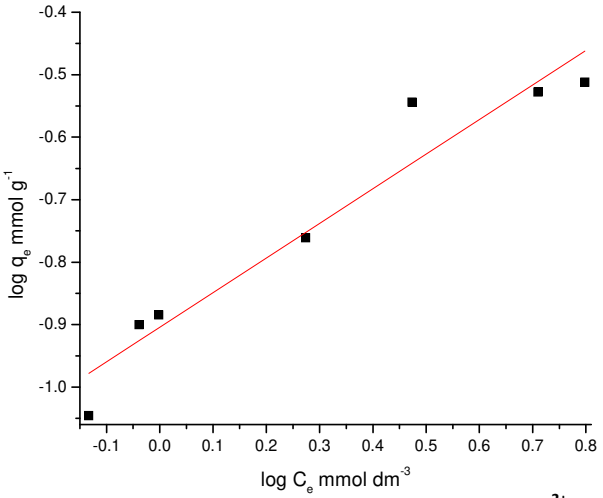


**Figure B 6. Temkin's linearization of sorption isotherm for $Pb^{2+}$ with PAA-13-3**

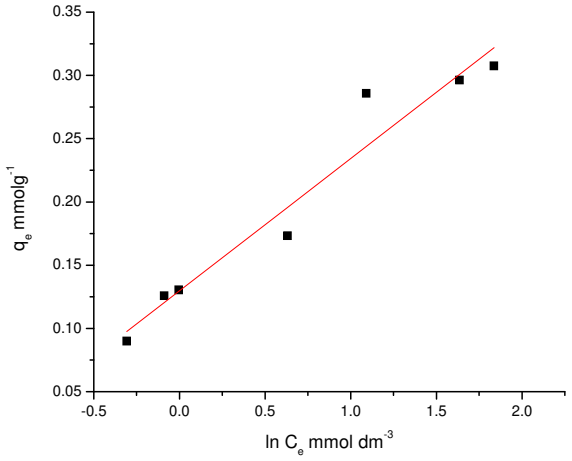

Figure B 7. Fruendlich's linearization of sorption isotherm for $Cd^{2+}$ with PAA-13-3

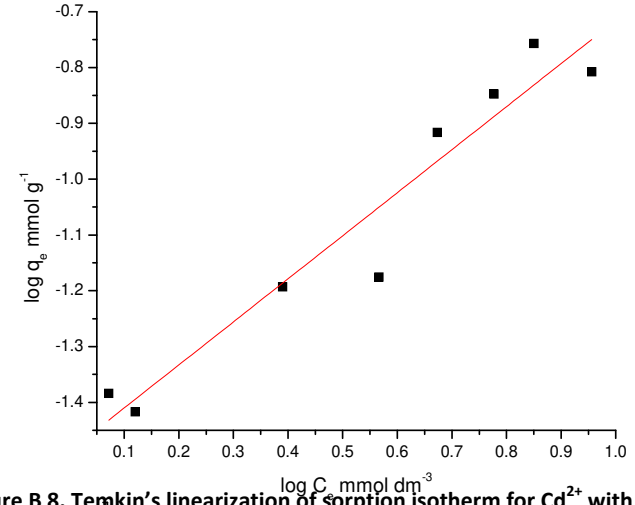


**Figure B 8. Temkin's linearization of sorption isotherm for $Cd^{2+}$ with PAA-13-3**

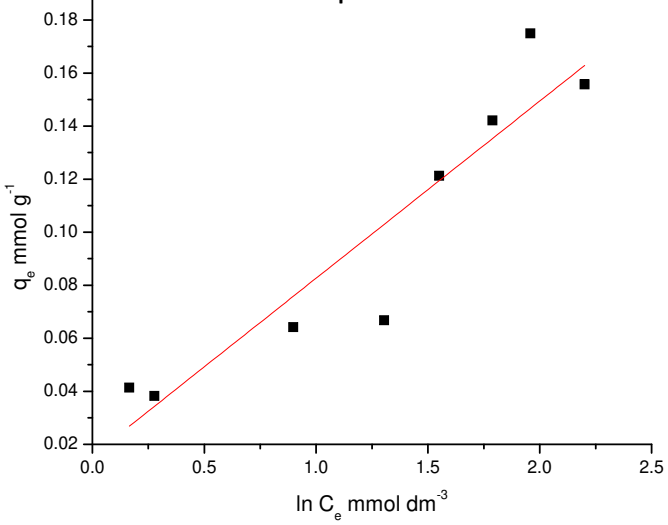


**Figure B 9. Langmuir's linearlization of sorption isotherm for $Cu^{2+}$(■), $Pb^{2+}$(●)**

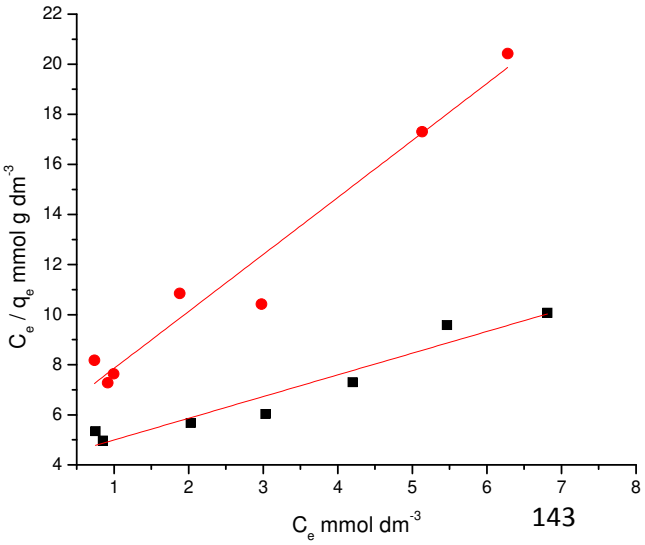

**Figure B 10. Fruendlich's linearlization of sorption isotherm for $Cu^{2+}$(■), $Pb^{2+}$(●), $Cd^{2+}$(▲)**

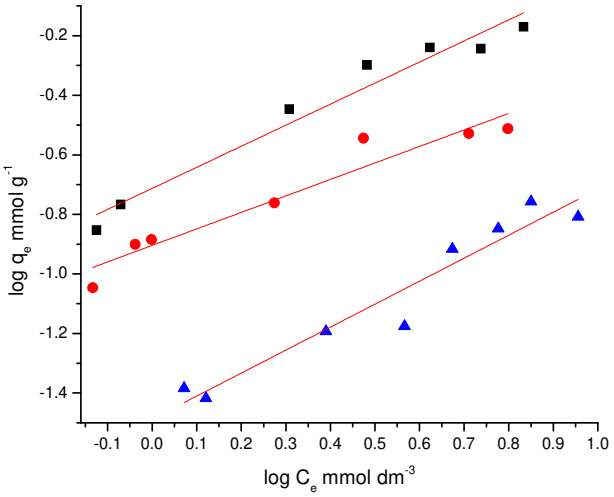


Figure B 11. Temkin's linearlization of sorption isotherm for $Cu^{2+}$(■), $Pb^{2+}$(●), $Cd^{2+}$(▲)

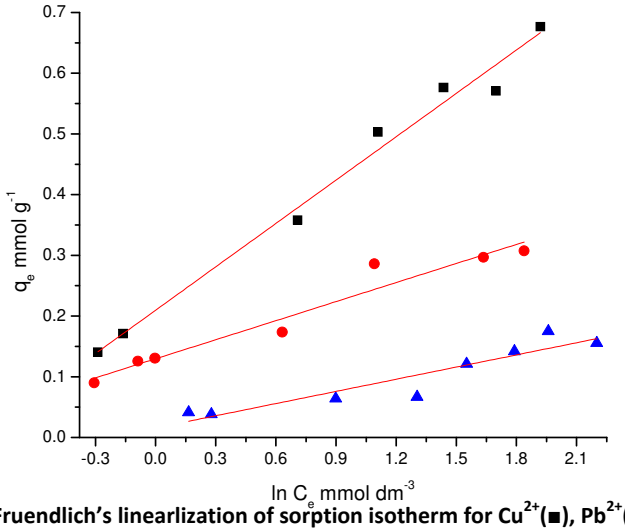


**Figure B 12. Fruendlich's linearlization of sorption isotherm for $Cu^{2+}$(■), $Pb^{2+}$(●),**

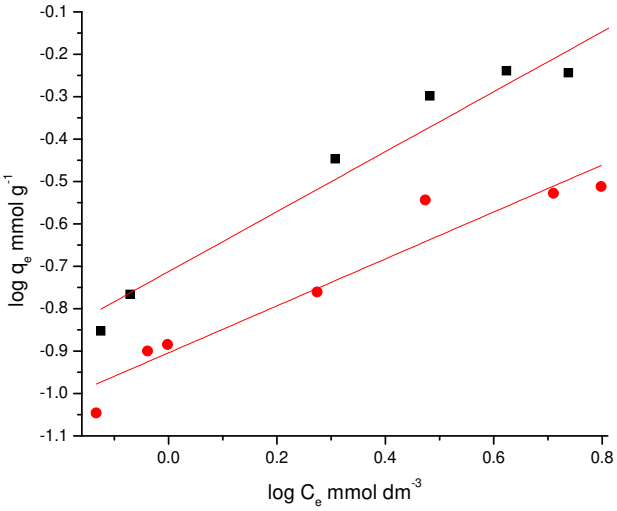

**Figure B 13. Fruendlich's linearlization of sorption isotherm for $Cu^{2+}$(■), $Cd^{2+}$(▲)**

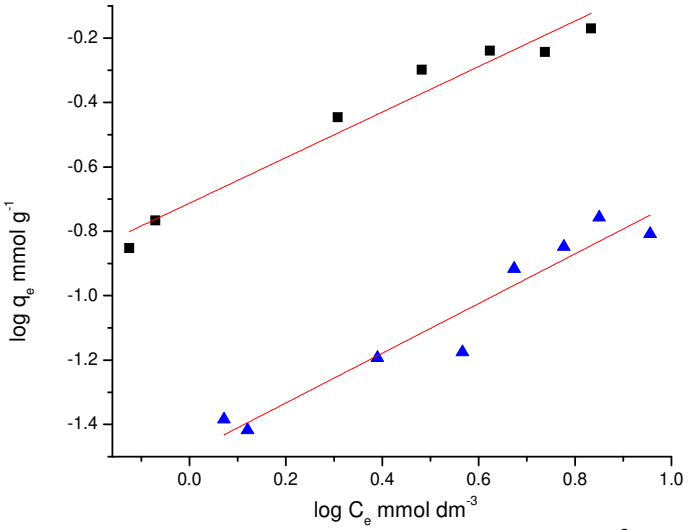


**Figure B 14. Fruendlich's linearlization of sorption isotherm for $Pb^{2+}$(●), $Cd^{2+}$(▲)**

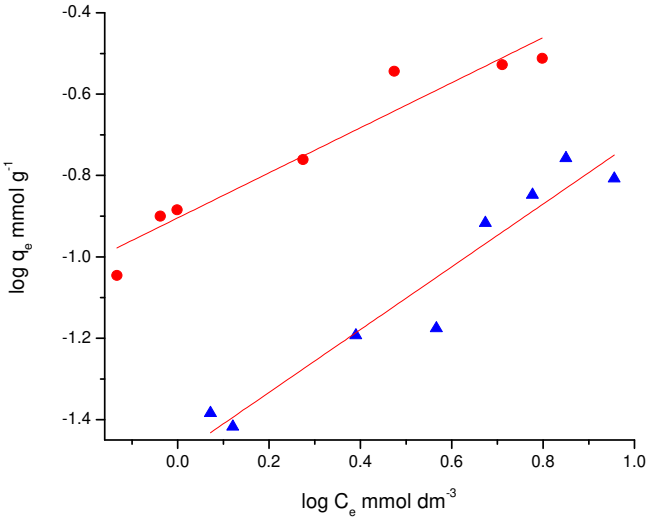


**Figure B 15. Temin's linearlization of sorption isotherm for $Cu^{2+}$(■), $Pb^{2+}$(●),**

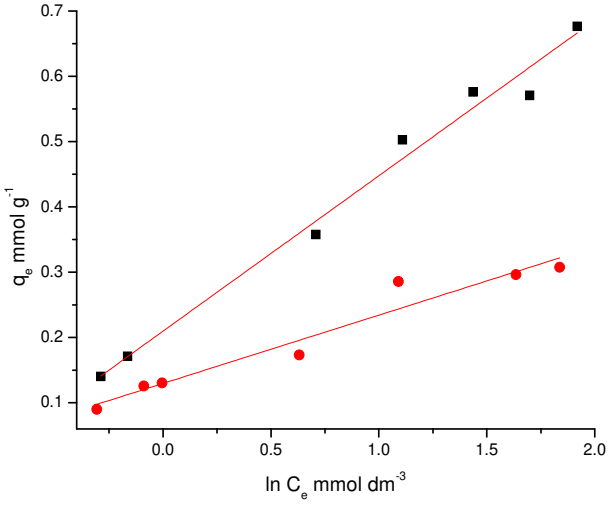

**Figure B 16. Temkin's linearlization of sorption isotherm for $Cu^{2+}$(■), $Cd^{2+}$(▲)**

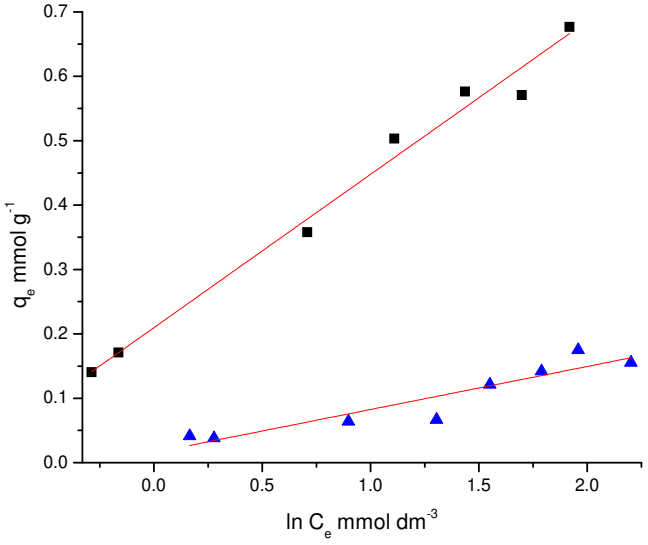


**Figure B 17. Temkin's linearlization of sorption isotherm for $Pb^{2+}$(●), $Cd^{2+}$(▲)**